NASA Contractor Report 159312

Research on Graphite Reinforced Glass Matrix Composites

K.M. Prewo
E.R. Thompson

UNITED TECHNOLOGIES RESEARCH CENTER
East Hartford, Ct. 06108

Contract NAS1-14346
February 1980

National Aeronautics and
Space Administration

Langley Research Center
Hampton, Virginia 23665

UNITED TECHNOLOGIES
RESEARCH CENTER

East Hartford, Connecticut 06108

NASA CR-159312

Research on Graphite Reinforced Glass Matrix Composites

K. M. Prewo
E. R. Thompson

INTERIM REPORT
Contract NAS1-14346

February 1980

Page intentionally left blank

Research on Graphite Reinforced Glass Matrix Composites

TABLE OF CONTENTS

TABLE OF CONTENTS (Cont'd)

LIST OF TABLES

LIST OF ILLUSTRATIONS

LIST OF ILLUSTRATIONS (Cont'd)

LIST OF ILLUSTRATIONS (Cont'd)

LIST OF ILLUSTRATIONS (Cont'd)

LIST OF ILLUSTRATIONS (Cont'd)

I. INTRODUCTION

Fiber reinforced resin and metal matrix composite materials are finding wide application due to their unique performance advantages over more traditional monolithic engineering materials. High levels of stiffness and strength have been achieved in combination with low composite material density. In addition, other advantages such as thermal stability and wear resistance have added to the range of engineering designs which can use composites to good advantage. The herein described program, which has succeeded in developing a fiber strengthened glass matrix composite system, provides yet another alternative for consideration. By placing graphite fibers in a glass matrix, it has been possible to achieve a unique material which is distinct from the resin and metal matrix composites which precede it. It combines the attributes of low density, high strength and stiffness, high toughness, mechanical and thermal fatigue resistance, and exceptional dimensional stability over a temperature range well beyond that of resin matrix composites. In addition, its combination of low density and environmental stability cannot be achieved by any metal matrix composite system.

The use of glass as a matrix for fiber reinforcement is a consequence of the increasing need for higher temperature, stable, low density composites. This constitutes a direct outgrowth from the already well developed technology of resin matrix composites in that the matrix can be caused to flow and encapsulate the reinforcing fibers without damage to fiber integrity. Also, as in the case of resin and metal matrix composites, the elastic modulus of the fibers exceeds that of the matrix sufficiently to provide an effective reinforcement. The development of the fabrication procedures and technology which have led to the herein reported data can be traced through the previous two interim technical reports of this program (Refs. 1,2) and several summary publications (Refs. 3,4). The current report will deal in much greater detail with the mechanical properties of the developed composite and also secondary processing procedures which could eventually lead to engineering articles having complex shapes.

Use of commercial products or names of manufacturers in this report does not constitute official endorsement of such products or manufacturers, either expressed or implied, by the National Aeronautics and Space Administration.

II. EXPERIMENTAL

A. Composite Fabrication Procedures

1. Fibers and Glasses Used

Six different types of graphite fibers were used, Table I. They varied in character from a very low elastic modulus pitch based carbon (Kureha) to an extremely high elastic modulus (Thornel pitch based) fiber and thus provided a wide variation of fiber properties for composite performance assessment. Five of the six fibers (not the Kureha) were utilized in their continuous strand form while the Kureha fiber was examined only in the form of a chopped fiber paper consisting of 3×10^{-3} m long fibers in a 2-D planar array. The Celion 6000 fiber was also used in a chopped fiber paper form with an average fiber length of 2×10^{-2} m.

The Corning Glass Works borosilicate glass 7740 was used throughout the program. Its properties, Table I, have been shown in the past (Refs. 1,2) to be compatible with the fabrication procedures and graphite fibers used. Its properties are compared in the table with two other glasses which have been used less successfully in that their use resulted in HMS graphite fiber reinforced composites with inferior flexural strength.

2. Primary Composite Fabrication Procedures

Primary composite fabrication consisted, in all cases, of first making a precursor tape consisting of fiber and dispersed glass powder. This tape was then cut into segments and placed in graphite dies for hot press consolidation into composite panels. The various stages of this overall process are described below while greater background to the overall process can be found in Ref. 2.

a. Precursor Tape Fabrication

Two types of precursor tape have been fabricated, one containing the continuous fibers and the other consisting of the chopped fiber paper. In the former case the fiber is unwound from its spool and pulled through an agitated slurry of glass particles and wound onto a mandrel at a controlled spacing to produce a tape which can be cut from the mandrel after drying.

The precursor tapes fabricated using only the chopped fiber paper were prepared using the same type of agitated slurry, however, in this case strips of paper were dipped into the slurry and then dried. The chopped Celion 6000 fiber paper was used with an areal density of 0.027 kg/m^2.

Table I

Graphite Fiber Properties

	Kureha	Celion 6000	Thornel 300	Thornel Pitch Type VS0054-0	HMS	GY-70
Fiber Diameter (microns)	12.5	7.1	7.0	11.0	7.3	8.4
Filaments Per Tow	-	6000	1000	2000	10,000	384
Density, kg/m^3	1550	1760	1760	2100	1800	1960
Elastic Modulus, GPa	41	234	234	654	350	516
Tensile Strength, MPa	827	2758	2930	2070	2700	1860

Glass Properties

	CGW 7740	CGW 1723	CGW 7940
Glass Type	Borosilicate	Aluminosilicate	Pure Silica
Density, kg/m^3	2230	2640	2200
Elastic Modulus, GPa	63	88	72
Coeff. Thermal Expansion, 10^{-7} m/mK	32.5	46	3.5
Strain Point K	783	938	1229
Anneal Point K	833	983	1357
Softening Point K	1093	1181	1853

The slurry composition used in all cases was the same. It consisted of 85 grams of glass in 0.26 liters of isopropyl alcohol with 24 grams of polyethylene glycol, 6 grams of DuPont Ludox H.S. 30 plus 5 drops of wetting agent. After composite hot press consolidation was completed, this mixture results in a matrix of 7740 glass that contains an additional 2% SiO_2 obtained from the Ludox. For the remainder of this report this matrix will simply be referred to as 7740 glass; however, it is understood that this includes the 2% SiO_2 addition.

b. Composite Hot Press Consolidation

(1) Fabrication of Flat Plates

After drying in air, the precursor tapes were cut into segments of the desired size and orientation and placed in graphite dies. Most frequently, composite panels measuring 7.5 cm square were fabricated; however, in some cases 10 cm square panels were also produced. The loaded dies were then placed in the hot press which was subsequently evacuated to achieve an initial vacuum atmosphere. Thereafter, if desired, controlled gases could be flowed through the press or a vacuum maintained for heat-up and hot pressing. In general, composites were consolidated using the conditions found to be superior in the previous phase of this program (Ref. 2), i.e. at a temperature of 1723 K, with a pressure of 6.89 MPa maintained for 1 hr, and an atmosphere of argon. After consolidation the pressure was held during cool down until the temperature dropped below 973 K.

(2) Fabrication of Hat Sections

One of the objectives of this program is to demonstrate that simple shapes can be fabricated using the current state of the art glass matrix composite technology. The recent fabrication of several composite hat section beam segments using two different techniques is an example of this technology. The hat section beam shape was chosen because of its applicability to many structural elements as well as the fact that it represents a three dimensional structure, as compared to the essentially two dimensional flat plates produced to date.

A matched set of graphite tools was designed which could produce a hat section with a uniform section thickness of 0.38 cm, a total length of 10 cm, and a total span of 7.5 cm. The two fabrication procedures used to fabricate composite articles are described below. In each case the material used consisted of HMS fibers in a 7740 glass matrix. Composite plys were oriented in a 0/90 alternating ply sequence.

Process #1 - Hot Press Consolidation Directly to Final Shape

In this process the starting material is unconsolidated fiber plus glass powder tape plys which are laid directly into the die cavity in a $0^{\circ}/90^{\circ}$ sequence. The overall ply dimensions are 10 cm x 10 cm which correspond to the dimensions of the total surface area of the hat section. The total ply lay-up is then hot pressed using standard procedures already developed in this program. A resultant hat section (GC 514), pressed at 1623 K, is shown in Fig. 1. The surface discolorations are due to the BN die release coating. During pressing, one portion of the hot pressing die fractured causing a nonuniformity in resultant hat section thickness; however, this was the only major imperfection resulting from this procedure. One additional, less important, problem was that the molybdenum foil on the convex side of the hat section wrinkled during pressing causing imprints of these wrinkles along the length of the top surface.

Process #2 - Hot Forming of a Preconsolidated Composite Plate

The second procedure utilized preconsolidated 0/90 reinforced flat plates of composite which have been fully processed using standard bonding procedures. These flat plates were cut to a dimension of 10 cm x 7.5 cm so that they would fit into the open die cavity. It was recognized that this would not permit the fabrication of specimens with full flange width ; a wider die opening would have to be used to achieve the same size flange as resulted from Process #1 above. Each flat plate was individually formed to final shape by placing it between the matched die halves, heating to a desired temperature, and then applying pressure. Several pressings were made and it was soon found that component shaping could take place rapidly and at relatively low pressure. The details of three such hot forming operations are given in Table II and the resultant hat sections are shown in Fig. 2 along with the component made by Process #1. The most important point to be noted in Table II is that it was possible to complete a forming operation in 1 min. This is the time during which pressure was applied and material deformation took place. It was not determined whether forming could have taken place even faster; however, this is quite likely and points to the possibility of developing a very low cost fabrication procedure which utilizes flat plate stock as the starting material. In addition, the maximum pressure required to achieve this rapid rate of deformation was only 1.6 MPa.

Two significant problems were uncovered during these secondary forming operations. One was that the molybdenum foil wrinkled on the convex sides of the formed parts. These wrinkles consisted of two longitudinal folds that ran the length of each of the completed hat sections and left their imprints in the composite surfaces. This problem could be overcome by finding a die surfacing

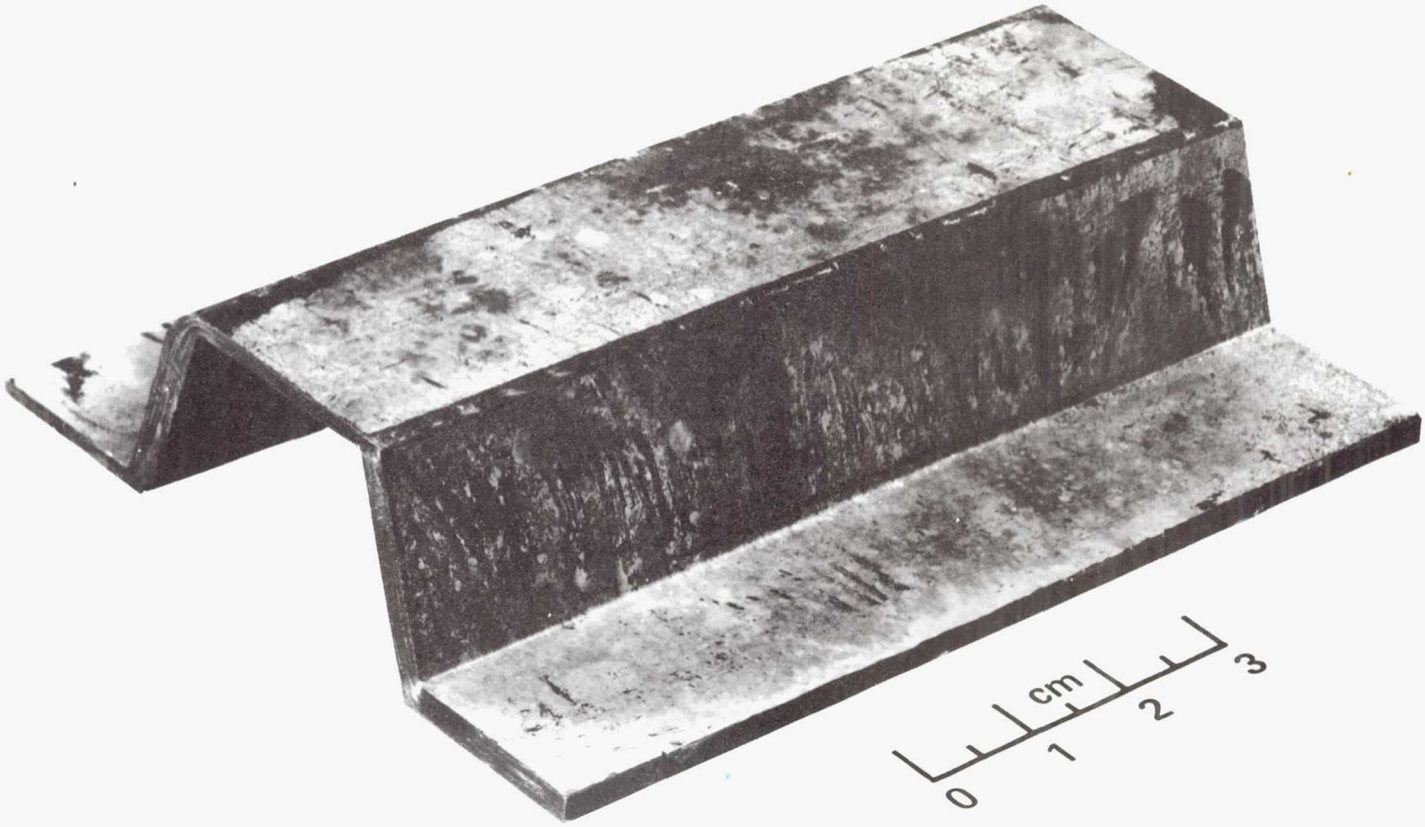

Fig. 1 0/90 — HMS Reinforced 7740 Hat Section Fabricated Using Process No. 1

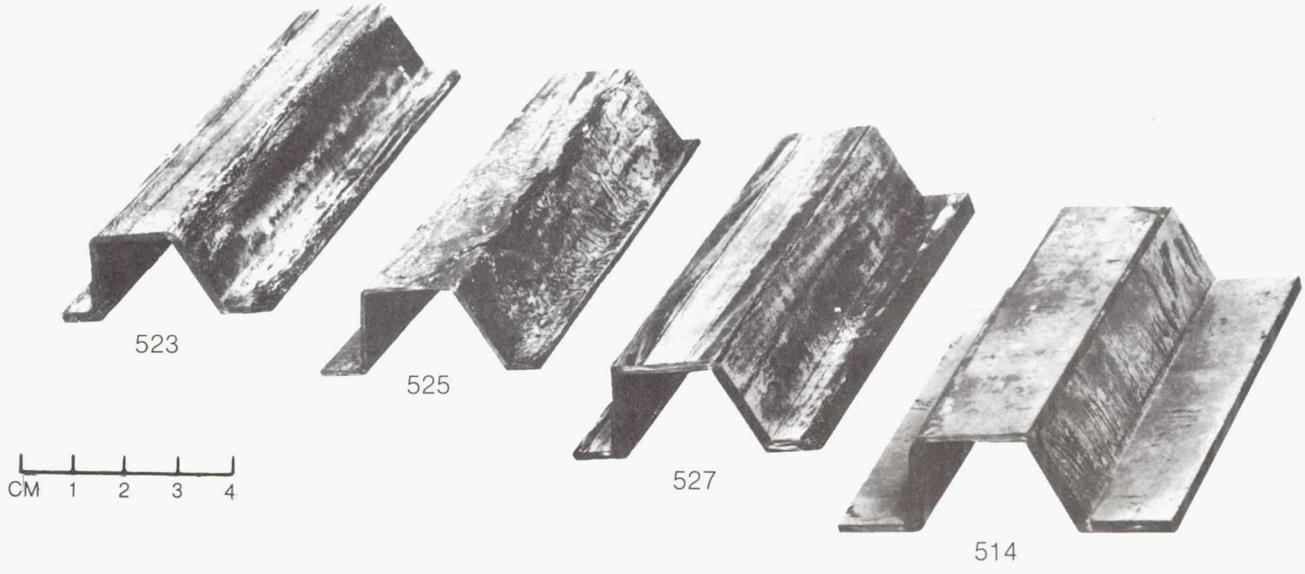

Fig. 2 0/90 — HMS Reinforced 7740 Hat Sections Fabricated Using a Variety of Conditions

Table II

Hot Forming of Preconsolidated Composite Plates

Forming Operation Number	Maximum Temp(K)	Maximum Pressure(MPa)	Total Forming Time(min)	Comments
GC 523	1173	3.35	10	•Cracks formed at the bend radii •Moly foil wrinkled on convex side •Free edges became ragged
GC 525	1473	3.35	5	•Basic shape excellent •No cracks •Moly foil wrinkled on convex side •Free edges became ragged
GC 527	1473	1.6	1	•Basic shape excellent •No cracks •Moly foil wrinkled on convex side •Free edges became ragged

material that would act as a debonding agent and remain integral with the die itself. The second problem was that the free edges of the formed sections became rather ragged due to the fact that they were not fully contained in the final stages of pressing. This is because the flat plate used initially was only 10 cm x 7.5 cm in size so that it could fit into the die cavity. This problem can be overcome by changing the die configuration to meet the particular requirements of secondary forming and also by providing a simple edge trimming operation after forming.

(3) Improved Graphite Die Material

As in all previous portions of this program, the tooling used in composite fabrication consisted of ATJ graphite which, on the primary surface of contact with the glass matrix composite, is covered with molybdenum foils which are in turn coated with a BN powder. Without the use of these coated metal foils the glass bonds to the graphite tooling mainly by impregnating the graphite surfaces which are somewhat rough and porous. It has been shown, however, that this problem can be overcome through the use of vitreous carbon tooling. Composite GC 670, which consisted of a 0/90 HMS fiber reinforced 7740, was hot pressed at 1723 K, 6.89 MPa, for 60 min with one of the die plungers consisting of a vitreous carbon plate. The resultant composite did not bond to the vitreous carbon, but instead separated cleanly without any force required to cause the separation. This demonstration is important since, as was shown above, particularly for complex shapes, the use of metal foil die liners is inconvenient, costly, and can cause composite surface imperfections due to wrinkles in the metal foils.

3. Secondary Composite Fabrication Procedures

Several experiments were performed to ascertain whether graphite fiber reinforced glass matrix composites can be joined using secondary bonding procedures. The following three different techniques were used to join composite plates consisting of 0/90 HMS reinforced 7740 and also chopped Celion 6000 fiber reinforced 7740.

- Metallic soldering in which both composite plate faces to be joined were coated, by sputtering, with layers of first chromium and then gold. The solder consisted of an 80% Au-20% Sn alloy foil.

- Glass soldering in which various slurry compositions were synthesized by mixing glass powders in isopropyl alcohol and painting them onto the surfaces to be bonded.

- Field assisted bonding in which highly polished surfaces of composite were sandwiched together with either thin molybdenum or glass foils between them. Application of a very large electric potential across the bond line and simultaneously raising the temperature to 773 K proved insufficient to form any sort of bond.

The experimental details of the above procedures are summarized in Table III along with an enumeration of the composite specimens and equipment used. After bonding, each of the composite plates was sectioned for microscopic analysis and mechanical testing. All tests were performed in three point bending with the specimen span-to-depth ratio of 4.0 or smaller and with the bond line located on the specimen central plane (neutral axis) to induce shear failure within the bond. The results of these tests are listed in Table IV, where it can be seen that, at least in two cases, shear strengths in excess of 45 MPa were achieved and in fact several measured values approached 65 MPa with the specimens failing first in regions removed from the bond line. The microstructure of the strongest glass solder bonded composite is shown in Fig. 3 where the starting glass was a slurry comprised of 25 grams of Drakenfold E-1576, 25 grams of Al-95 or beta-spodumene, and 25 grams of Ludox in 200 ml of isopropyl alcohol. While this single experiment gave good results, it was not definitive since the best ratio of Drakenfold E-1576 and beta-spodumene has not been determined. Also this single successful bonding experiment was carried out at 1023 K and some slightly different temperature might be better. Finally, the experiment was carried out in the vacuum hot press and might be more suitably carried out in the large vacuum furance so larger pieces could be bonded together.

The metallic solder bond is shown in Fig. 4. Again this single experiment is far from definitive. It should be possible to obtain similar or superior results by sputtering other metals and by using higher-temperature metal solders.

B. Composite Characterization Procedures

1. Analysis of Fiber Content

A procedure was developed and verified for the determination of composite fiber content, matrix content and porosity.

The procedure consists of the following steps.

(1) Measure the density of the total composite specimen (ρ_c). This is done either on the full composite plate after hot pressing, or by using a smaller mechanical test specimen.

(2) Weigh the composite specimen prior to oxidation and obtain its total weight (W_c).

(3) Expose the specimen to 1073 K for 12 hrs in air. The graphite fiber is oxidized completely by this procedure, leaving no char or residue.

Table III

Experiments in Joining Two Graphite Fiber Reinforced Glass Matrix Composites

Composite*		Slurry or Solder	Atmosphere	Applied Pressure	Axiliary Apparatus
GC 669	(A)	25 gms, Drakenfeld E-1576 W.G. in 100 ml isopropyl alcohol	Air 910 K	0.02 MPa	Thermolyne Furance
GC 669	(B)	25 gms, Drakenfeld E-1576 W.G. 25 gms C.G.H. 79.13 2 gms Ludox 200 ml isopropyl alcohol	Argon 1023 K	2 MPa	Vacuum Hot Press
GC 658	(C)	25 gms of Drakenfeld E-1576 25 gms Al-95 lithium metasilicate 2 gms Ludox 200 ml isopropyl alcohol	Argon 1023 K	2 MPa	Vacuum Hot Press
GC 671	(D)	25 gms of PEMCO Pb-461 25 gms Al-95 lithium metasilicate 2 gms Ludox 200 ml isopropyl alcohol	Argon 1073 K	2 MPa	Vacuum Hot Press
GC 671	(E)	25 gms of C.G.W. 7740 2 gms of Ludox 100 ml isopropyl alcohol	Argon 1273 K	2 MPa	Vacuum Hot Press
GC 658	(F)	Sputtered gold, chromium 80 Au-20Sn Solder	Air 598 K	None	Sputtering Apparatus
GC 670	(G)	Molybdenum Sheet Field Assisted Sealing	Air 773 K	0.01 MPa	High voltage source & Thermolyne Furnace
GC 670	(H)	Glass Foil Field Assisted Sealing	Air 773 K	0.01 MPa	High voltage source & Thermolyne Furnace

*Composites 669, 670 and 671 are 0/90 HMS reinforced and 671 and 658 are chopped Celion 6000 reinforced

Table IV

Results of Short-Beam Shear Tests on Two Composite Samples Bonded Together - All Tests 2.5 cm Span

Specimen Identity	Span to Depth Ratio	Max. Shear Stress MPa	Nature of Break
Glass Solder Slurry A, GC 669	3.6	9.7	Bond shear
	3.6	9.7	Bond shear
Glass Solder Slurry B, GC 669	4.0	14.1	Bond shear
	4.0	17.4	Bond shear
	4.0	16.0	Bond shear
Glass Solder Slurry C, GC 658	1.8	58.8	Compression & flexural
	1.8	48.7	Compression & flexural
	1.8	66.3	Compression & flexural
Glass Solder Slurry D, GC 671	2.3	20.9	Shear-slip
	2.3	19.9	Shear-slip
	2.3	17.8	Shear-slip
Metal Solder Solder, GC 658	1.9	44.9	Shear in material
	1.9	61.3	Flexural & compression
	1.9	63.4	Flexural & compression

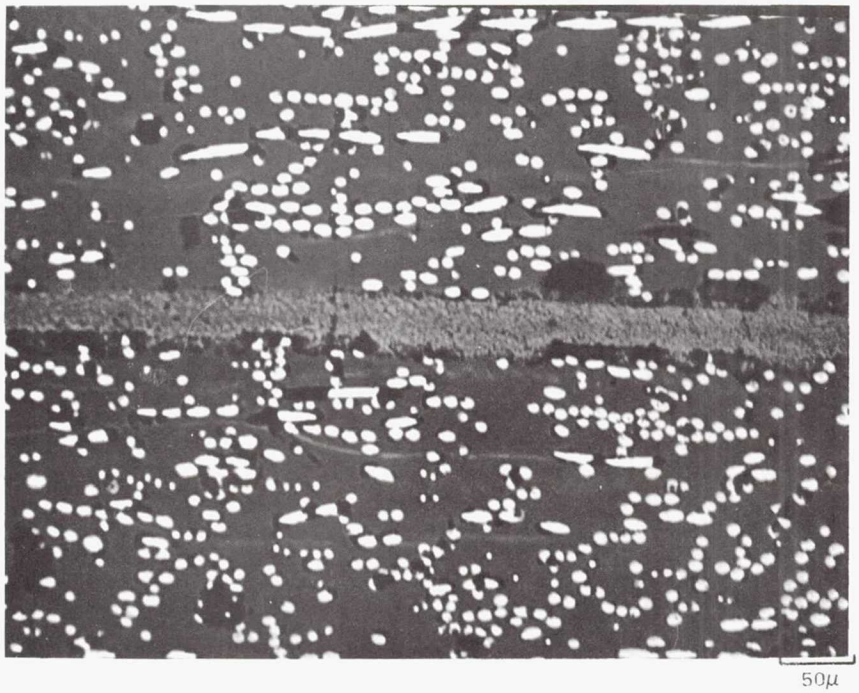

Fig. 3 Bond Region for Glass Soldered Composite GC658 (Glass Slurry C Used)

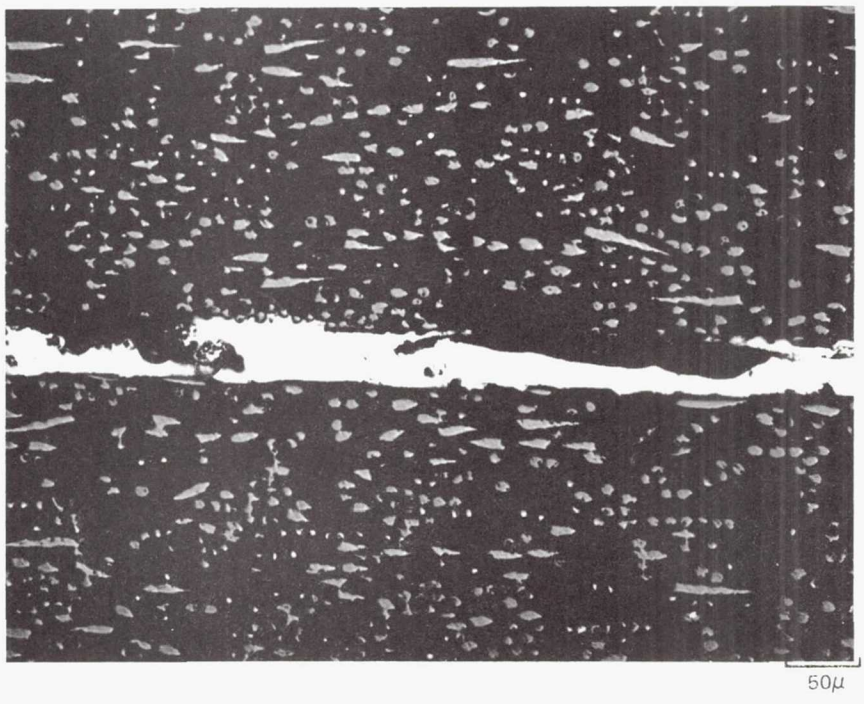

Fig. 4 Bond Region for Metal Soldered Composite GC658

(4) Weigh the specimen after oxidation to obtain the weight of the remaining glass (W_g).

(5) Using the known quantities

density of glass - ρ_g
density of fiber - ρ_f

calculate the following:

(a) Weight of fibers in specimen	$W_f = W_c - W_g$
(b) Volume of composite specimen	$V_c = W_c/\rho_c$
(c) Volume of glass in specimen	$V_g = W_g/\rho_g$
(d) Volume of fiber in specimen	$V_f = W_f/\rho_f$
(e) Volume of porosity in specimen	$V_p = V_c - V_f - V_g$
(f) Volume percent glass in specimen	$v/o\ G = V_g/V_c \times 100\%$
(g) Volume percent fiber in specimen	$v/o\ F = V_f/V_c \times 100\%$
(h) Volume percent porosity in specimen	$v/o\ P = V_p/V_c \times 100\%$

A confirmation of the procedure's accuracy was obtained by determining the fiber content of an HMS/7740 composite by two methods, i.e. oxidation and dissolution of the matrix in acid. The comparative data, Table V, indicate that both methods provide equivalent values.

2. Three Point Flexural Strength

Three-point bend tests were performed on specimens of several thicknesses using a range of testing spans to provide a wide spectrum of span-to-depth ratios. In each case the specimens were 0.5 cm wide and 7.7 cm in overall length with all surfaces ground prior to testing. The majority of tests were performed in air with applied load vs mid-span deflection traces taken using a deflectometer attached to the crosshead of the loading machine. Tests were performed over the temperature range of 300 K to 973 K.

3. Three Point Flexural Creep

Standard three-point bend specimens (0.2 cm x 0.5 cm x 7.7 cm) were cut and surface ground in preparation for test. All tests were performed in three-point bend with a span of 5 cm and in an air atmosphere. In each case the mid-span deflection of the specimen was monitored continuously with an LVDT to provide a recording of deformation vs time. Tests were halted either due to specimen fracture or when the time of test exceeded 200 hrs.

Table V

Determination of Composite Fiber Content

Specimen	Method		Glass v/o G	Fiber v/o F	Porosity v/o P
GC 414A-1	Oxidation		36.8	62.2	1.0
-4	"		38.0	61.6	0.3
-6	"		36.7	62.2	1.1
-8	"		35.9	63.8	0.3
		Avg	36.9	62.5	0.7
-3	Acid Leach		37.1	62.1	0.8
-7	"		37.8	61.3	0.9
-9	"		36.4	62.9	0.7
		Avg	37.1	62.1	0.8

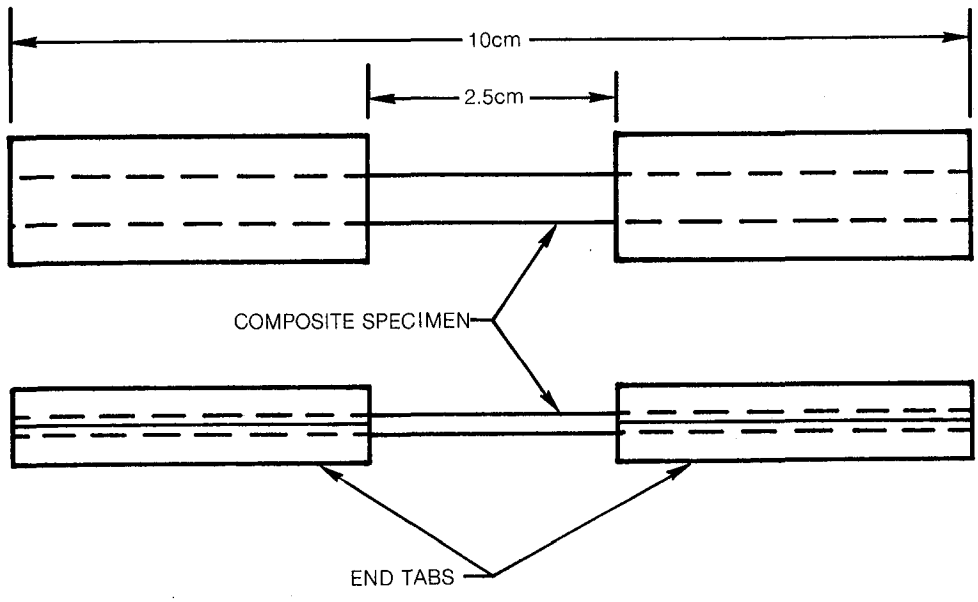

Fig. 5 Tensile Specimen Configuration

4. Three Point Flexural Fatigue

Standard three-point bend specimens (0.2 cm x 0.5 cm x 7.7 cm) were cut and surface ground in preparation for test. All testing was performed in three-point bend with a span-to-depth ratio of 25 at a frequency of three cycles per second in an atmosphere of air. Tests were run at 300 K and 703 K with several unfatigued quality control specimens tested to fracture at 300 K from each test group. All fatigue tests were run with a ratio of minimum to maximum applied flexural stress of 0.1 (R = 0.1).

5. Tension Test

The tensile testing of seven different types of graphite fiber reinforced glass composites was performed. Specimens with a total length of 10 cm were cut from 10 cm x 10 cm panels fabricated in the standard manner. The specimens were parallel sided and bonded into glass fiber reinforced resin tabs leaving a 2.5 cm free gauge length, Fig. 5. The specimen thickness and width were approximately 0.18 cm and 0.5 cm respectively. The doublers were slotted to accept these specimen dimensions, and all specimens were strain gauged prior to test. Tensile testing was performed at a crosshead rate of 0.25 mm per minute.

6. Thermal Exposure and Thermal Fatigue

Samples were machined for air oxidation in the dimensions 0.2 cm x 0.5 cm x 7.7 cm. All specimens had their major flat surfaces ground to expose the graphite fibers and several specimens, to be exposed at each temperature, were trimmed at the ends to remove excess glass. This was done to ensure uniformity of structure throughout the specimens and remove any protective layer which might inhibit oxidation. Mass and dimensional measurements were made prior to and after exposure and cycling. Stainless steel wire baskets vertically supported the samples to prevent contact with the center of the sample and ensure that the samples remained in a relatively unstressed condition.

7. Thermal Expansion

Thermal expansion measurements were made in a Theta Industries differential dilatometer which was operated in a horizontal mode. The composite specimens consisted of 0.62 cm x 0.62 cm x 2.5 cm long parallel sided blocks of material which were individually placed in series with instrument silica push rods and holders. The comparative specimen consisted of a Corning 7971 (SiO_2-TiO_2) glass sample of nearly the same dimensions which was located in a similar arrangement, but in parallel with, the graphite reinforced glass specimen. The 7971 standard had previously been calibrated by both the University of Arizona and Corning Glass over a temperature range of 73 K to 873 K. The actual operative procedure consisted of thermally stabilizing the specimen in the instrument, by holding at room temperature for 5 hrs, followed by heating at a rate of 2 K per minute to the maximum desired temperature. Thereafter the specimen was cooled at a rate

determined by the rate of heat loss of the instrument, which was somewhat less than the 2 K per minute heating rate. The differential length change (difference between standard and composite) was then analyzed by computer and plotted as a change in length of the composite. Thus, the thermal strain was taken to be the change in length divided by the original length, referred back to the starting room temperature condition. Testing was performed in air.

III. RESULTS AND DISCUSSION

A. Flexural Strength of New Fiber Reinforced Composites

1. Continuous Fibers

The flexural strengths of the composites fabricated from the new continuous fibers incorporated into the program are presented in Table VI. For each case the composite fiber content, glass content, and porosity are also given. It can be seen that both the Thornel 300 and Celion 6000 fiber reinforced composites exhibited a very strong dependence of flexural strength on volume percent fiber with the Thornel 300 fiber composite also exhibiting a considerable variation in strength (composites 611 and 631) even for a nearly constant composition. This points up one of the problems still existent in the program, which is the sometime lack of reproducibility in composite performance. These composites were made using identical fabrication procedures yet their flexural strength varied substantially. Also of interest is the very high strength (1167 MPa) obtained with a fiber obtained from Fiber Materials Inc. (FMI) of Biddeford, Maine. FMI provided this boride coated fiber with the expectation that it might exhibit superior oxidative stability during composite exposure to air at elevated temperature. This, however, was not the case. Oxidative exposure caused as much degradation as had been experienced with standard uncoated HM graphite fiber reinforced composites.

2. Chopped Fiber Papers

The hot press consolidation of composites reinforced with chopped Celion 6000 fiber was performed using a variety of hot pressing conditions, Table VII. It was found that the highest value of strength was associated with the lowest fiber content obtained in the series. Despite the low fiber contents, these values of strength are nearly equal to those obtained previously in the program for 0/90 cross ply continuous fiber reinforced 7740 composites (Ref. 2). In addition, the strengths obtained with the chopped fiber reinforcement should be nearly isotropic in the fiber plane.

The procedure used to fabricate the above composites involved a preheat treatment at 600 K for 2 hrs in air to remove approximately 10% by weight of polyester binder. Although not difficult, this process was not felt to be desirable and a request was made of the International Paper Company, suppliers of the paper, to provide a binder that was more easily removed and that would not result in undesirable by-products. In response to this request, International Paper Co. supplied several sheets of graphite fiber with a carbohydrate binder

Table VI

0^{o} Three Point Flexural Strength of
Continuous Graphite Reinforced 7740

Composite	Fiber Type	v/o F	v/o G	v/o P	Avg. Flex. Strength MPa
630	Thornel Pitch VS0054-0	54	46	0	683
731	Thornel 300	60	40	0	1046
631	Thornel 300	39	60	1	711
611	Thornel 300	37	63	0.5	407
608	Celion 6000	70	30	0.6	872
613	Celion 6000	45	54	0.7	313
395	Borided HM	65	35	-	1167

Table VII

Effect of Hot Pressing Conditions on the Structure and Properties of Celion 6000 Paper/7740 (polyester binder removed prior to pressing)

Composite Number	Hot Pressing Conditions			ρ_c	v/o G	v/o F	v/o P	Avg Three Point Flex. Strength	Std. Dev.
	Temp. K	Pressure MPa	Time min	gm/cc				MPa	MPa
GC 481	1723	6.89	60	2.01	63.9	33.3	2.9	308	19
				2.02	64.6	33.0	2.5		
GC 485	1723	6.89	60	2.01	63.1	34.3	2.6	270	15
					63.0	34.4	2.6		
GC 497	1723	13.8	60	1.97	56.4	40.5	3.2	243	42
					56.2	40.2	3.5		
GC 498	1773	13.8	60	1.92	53.3	42.6	4.2	192	18
					52.3	42.8	4.8		
GC 500	1873	13.8	60	1.94	51.7	44.1	4.1	190	24
					51.7	44.7	3.6		
GC 503*	1723	6.89	60	2.07	71	29	0	315	17
				2.07	70	29	1		

*Carbohydrate binder removal prior to hot pressing

which they had been developing. The removal of this binder was accomplished simply by lighting, with a match, one edge of a piece of paper and observing the rapid progression of the flame across the entire paper surface. This appeared to completely remove the binder and still left the remaining paper in a handleable form that could be easily dipped in a glass containing slurry and used for composite fabrication. The resultant composite data, Table VII, demonstrate that this procedure resulted in a superior product with flexural strengths equivalent to or greater than those of previous specimens.

Kureha carbon fiber paper was obtained from the Mitsubishi International Corp. This pitch based carbon fiber paper is anticipated to eventually be very inexpensive and for this reason was examined as a possible means of achieving a low cost composite. The grade papers E 704 and E 715 were used. They are classified by Mitsubishi as graphite paper with areal weights of 0.04 Kg/m^2 and 0.15 Kg/m^2 respectively. According to the Kureha data sheets, the graphitic form of fiber provided should be characterized by a tensile strength of 827 MPa and a density of 1.55 gm/cm^3. Two 7740 glass matrix composites (GC 672 and 673) were fabricated using this paper and standard bonding conditions. Resultant composite appearance was excellent and an overall composite density of 1.8 to 1.9 gm/cm^3 was obtained. Resultant composite strength, however, was quite low with an average value of 54 MPa being well below that typical of the other graphite paper reinforced glasses described above.

B. Three Point Flexural Strength as a Function of Temperature and Specimen Geometry

The three-point flexural strengths obtained by testing 0°-HMS/7740 over the temperature range of 300 to 973 K (in argon) are presented in Fig. 6. The specimens were tested at a span-to-depth ratio of 32 to 1 and the resultant strengths are compared in the figure with those reported previously on this program. The average 300 K strength of 930 MPa agrees well with the high levels of strength we have been obtaining from the current system which consists of a matrix of 7740 glass plus 2% SiO_2 and has been fabricated at 1723 K. The current fabrication procedures are described in section IIA of this report. Analysis of this composite indicated that it contained 71% by volume fiber, 27% matrix glass and approximately 1-2% voids. The flexural strength increased with increasing temperature to a maximum average of 1324 MPa at 873 K and then decreased with increasing test temperature. At 973 K the specimens deformed without any sign of fracture. Thus, in general, it has been found that the more recently fabricated composite material is improved in strength over the entire temperature range when compared with 1976 vintage composites.

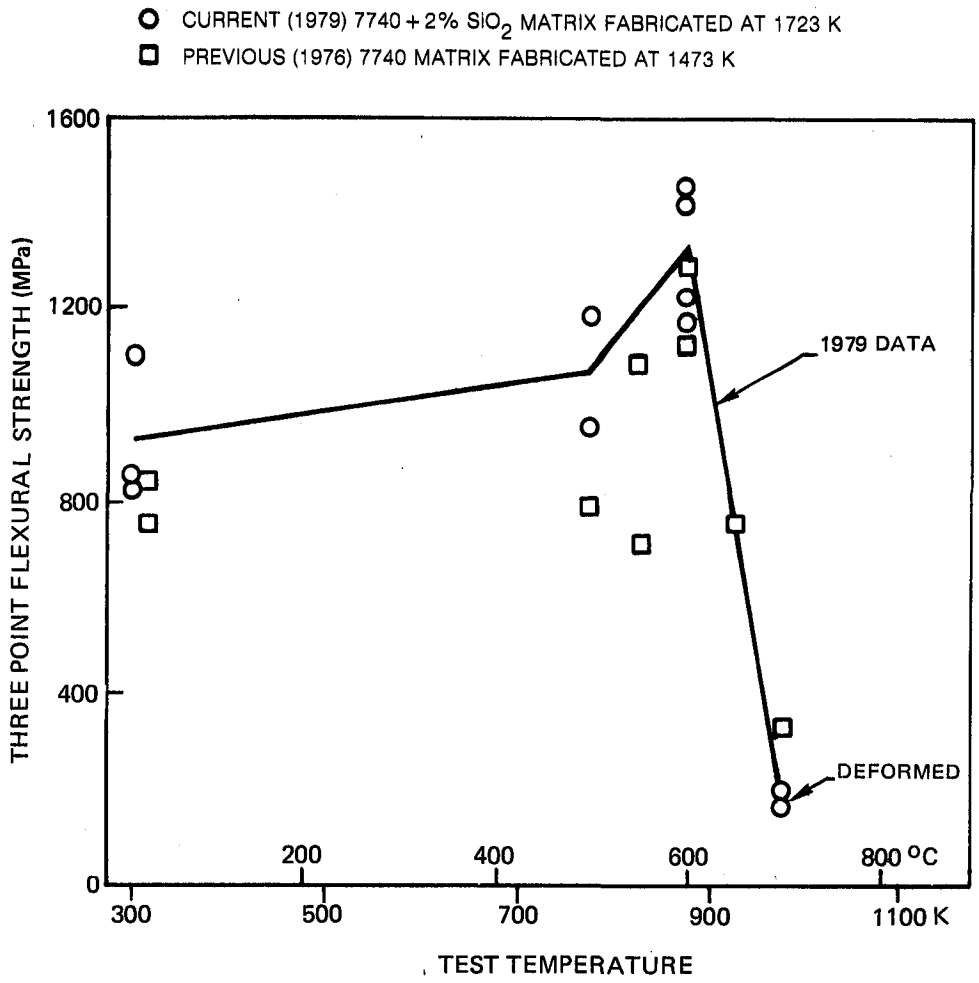

Fig. 6 Three Point Longitudinal Flexural Strength for HMS Reinforced 7740 as a Function of Test Temperature

79-01-171-1

Composite three-point bend test data were obtained over a wide range of span-to-depth ratios to better examine composite behavior. Because of both the complex stress state generated in a three-point bend test, and also because of multiple composite failure modes possible, the resultant test data are presented both as flexural strength and also shear strength values. In both cases the strength calculations were made using the following simple beam equations which determine the maximum flexural stress (σ_{max}) on the beam tensile surface, and the maximum shear stress (τ_{max}) which occurs at the beam mid plane.

$$\sigma_{max} = \frac{3}{2}\frac{PL}{bh^2} \qquad \tau_{max} = \frac{3}{4}\frac{P}{bh}$$

In these expressions P represents the load applied to the specimen mid span, L is the span, b and h are the specimen width and depth respectively. Thus, during any given test the ratio of maximum applied shear to flexural stresses depends on the specimen span-to-depth ratio (L/h). Since a given material can fail by either shear or tension, one of these failure modes will occur first depending on test configuration. For high longitudinal strength composites, the large ratio of tensile to shear strength causes these materials to deform by shear for test configurations having low values of (L/h) and to fracture in tension for high values of (L/h). In the figures to be described below, composite flexural and shear strengths are calculated for all specimens tested. It should be noted that actual composite strength does not vary with span-to-depth ratio. It is only the calculated values which vary due to the fact that an inappropriate failure mode is assumed. The first example below for 0^{o}-GY70/7740 demonstrates this point clearly where it will be shown that the test data provide an accurate assessment of material flexural strength and an underestimate of material shear strength.

The data obtained for 0^{o}-GY70/7740 are presented in Figs. 7 and 8 as a function of test span-to-depth ratio. The flexural strength data, Fig. 7, exhibit little or no dependence on test geometry over the range of (L/h) investigated. For all specimens tested, the average strength is 630 MPa. In contrast, the calculated shear strength data, Fig. 8, show a continuous decrease in strength with increasing (L/h). The line drawn through the data was obtained, not by fitting the data points, but by calculating an effective shear strength for each value of (L/h), based on the average 300 K flexural strength of 600 MPa. This correlation suggests that failure of all of the specimens was controlled by the flexural strength of the material and that true shear failure did not occur. Thus, the data plotted in Fig. 8 are simply the calculated maximum shear stresses acting on the beam mid-plane during test. The true shear strength of the material was not reached and thus it must exceed a value of 55-60 MPa as determined by this test technique. On the other hand, the true flexural strength appears to have been determined at 600 MPa.

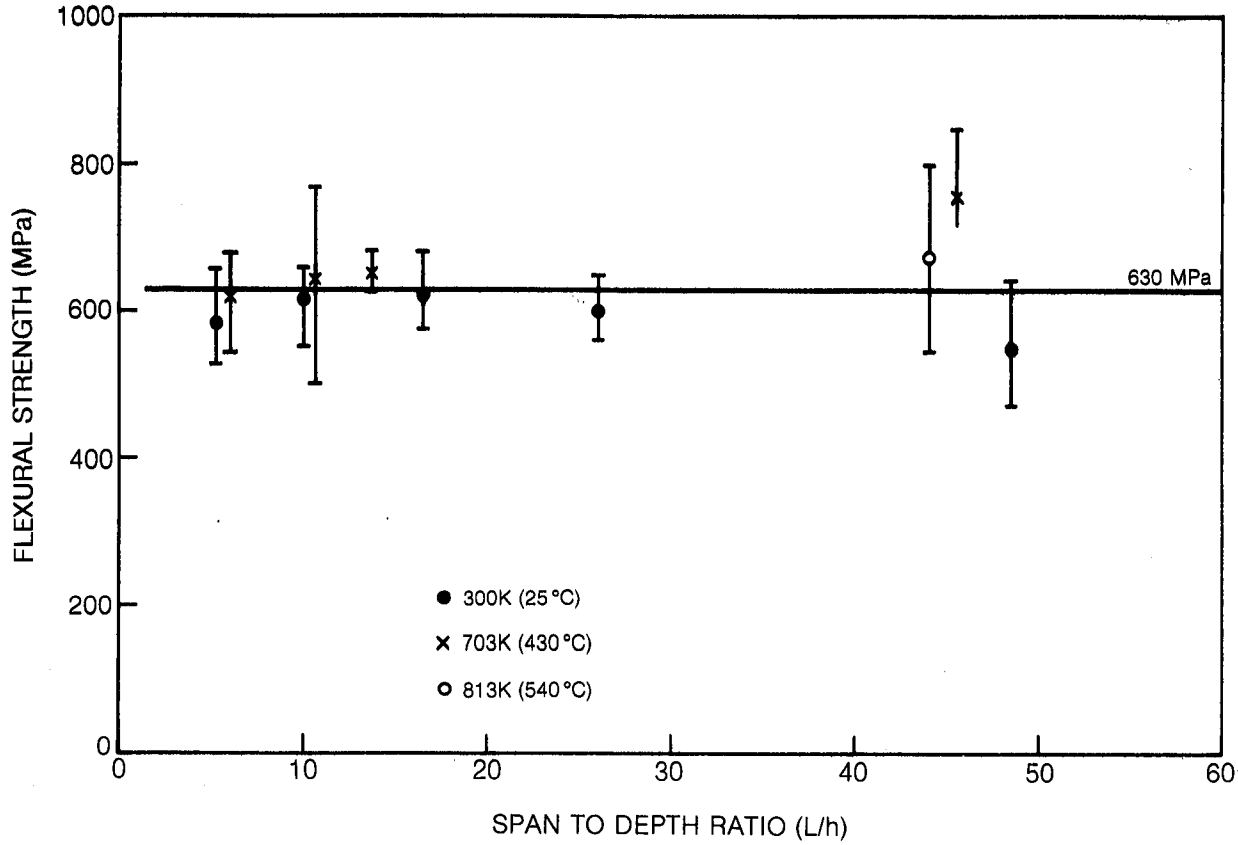

Fig. 7 Observed Flexural Strength as a Function of Span to Depth Ratio for 0° — GY70/7740

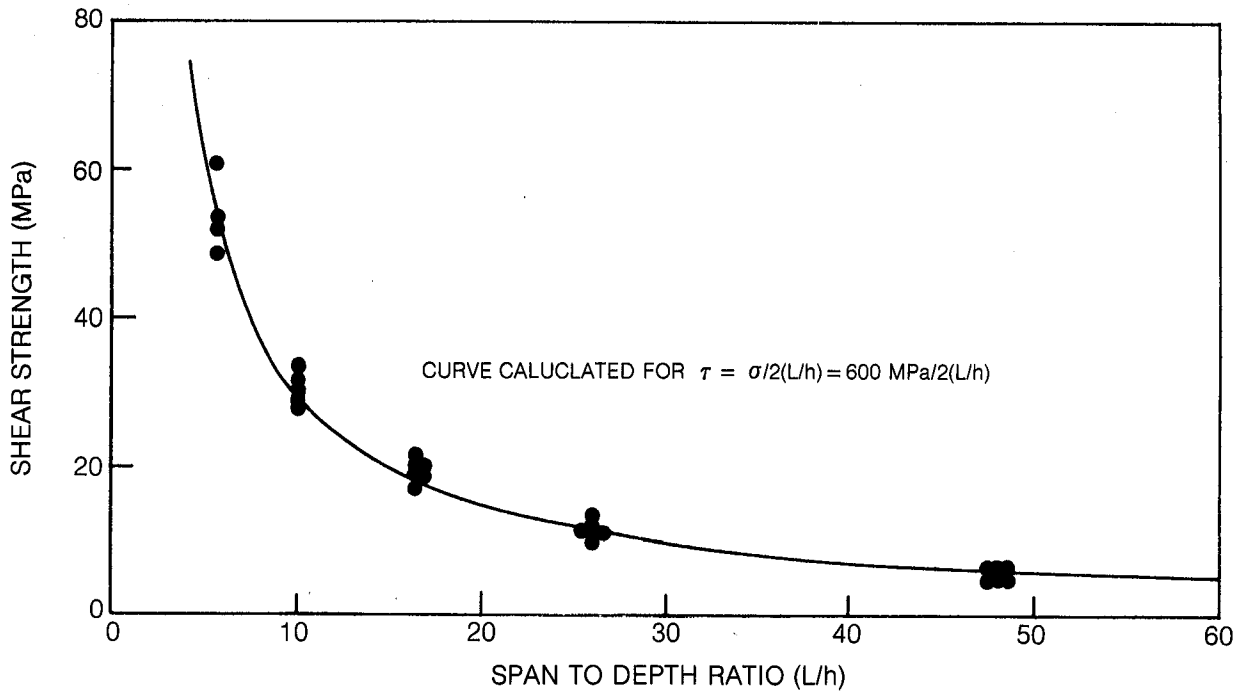

Fig. 8 Observed Shear Strength as a Function of Span to Depth Ratio for 0° — GY70/7740 at 300K

80-5-82-3

Examination of the fractured bend specimens confirms the above. Even at the smallest value of L/h tested (5.4), the specimens failed without any sign of shear deformation. Instead, fracture propagated across the specimen after initiating on the tension side of each beam. This is characteristic of the GY70/7740 system in which the fiber-matrix bond appears to be quite strong.

Another interesting aspect of this test is the value of elastic modulus obtained as a function of (L/h), Fig. 9. The modulus calculation was performed based on the assumption of no deformation due to shear taking place; however, as can be seen from the figure, it is likely that this assumption is only true for very large (L/h) values. For small values of span-to-depth ratio, elastic shear deformation can be substantial because of the much lower shear modulus of the material, as compared to the true axial elastic modulus of approximately 325 GPa.

The similarly obtained data for 0^{o}-HMS/7740 composites are presented in Figs. 10 and 11. Unlike the GY70 reinforced composites, the flexural strength was found to vary substantially with span-to-depth ratio. The significant decrease in calculated flexural strength in the low (L/h) region implies that some shear failure is taking place. This is in agreement with the observation that the specimens passed through the maximum in the load-deflection trace without the appearance of any visible cracking on the specimen tensile surfaces. The specimens were not, however, severely bent after testing; only a slight overall change in specimen shape was detected after test. The shear strength data, Fig. 11, do not indicate unambiguously that the value of approximately 60 MPa can be taken as the effective material shear strength. However, by virtue of the observed failure mode described above, it is highly probable that this is fairly close to the actual material value.

The data for 0/90 cross ply specimens of both GY70 and HMS fiber reinforced 7740 are presented in Figs. 12-15. In these cases both the calculated composite flexural strengths and shear strengths were considerably less than those of the unidirectionally reinforced specimens described above. All of the GY70 fiber reinforced specimens tested in the 0/90 lay-up failed by the formation of visible cracks on their tensile surfaces, while in the case of the HMS fiber reinforced specimens, no evidence of tensile failure could be found at a span-to-depth ratio of 10. It is also interesting to note that, for the HMS/7740 composites, the calculated shear strength decreased with increasing test temperature. In all cases the observed shear strength was significantly lower in the case of the 0/90 composites than their unidirectionally reinforced counterparts.

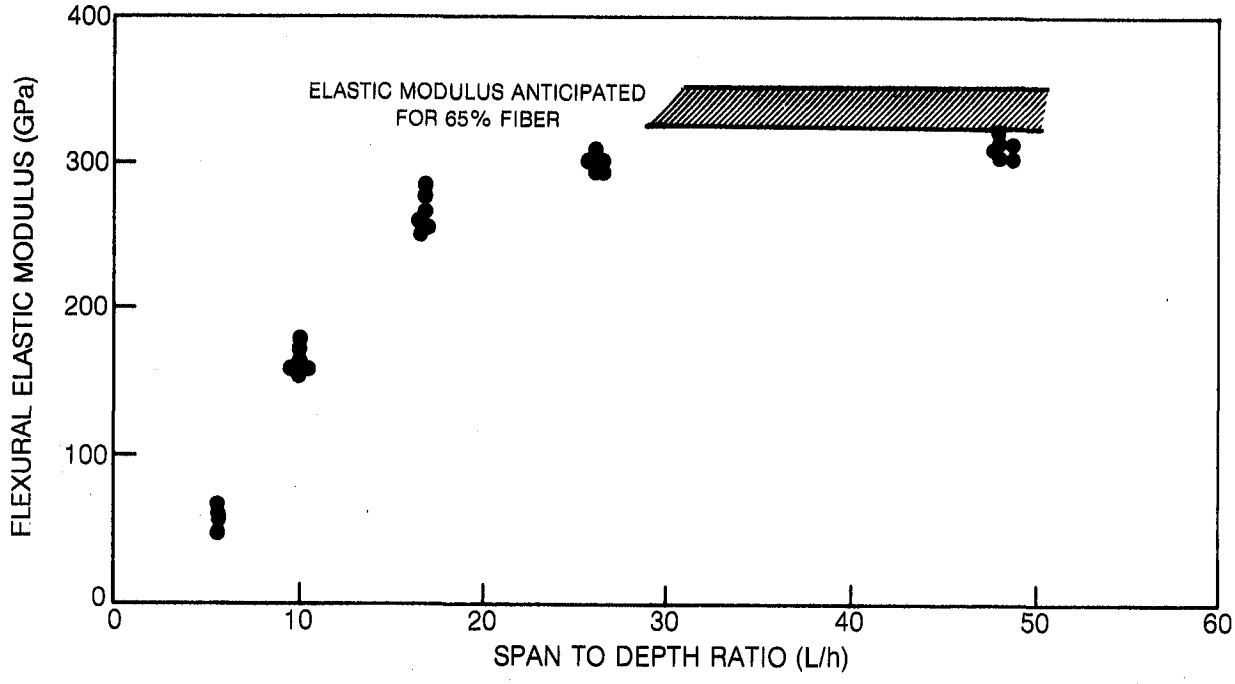

Fig. 9 Observed Flexural Elastic Modulus as a Function of Span to Depth Ratio for 0° — GY70/7740 at 300K

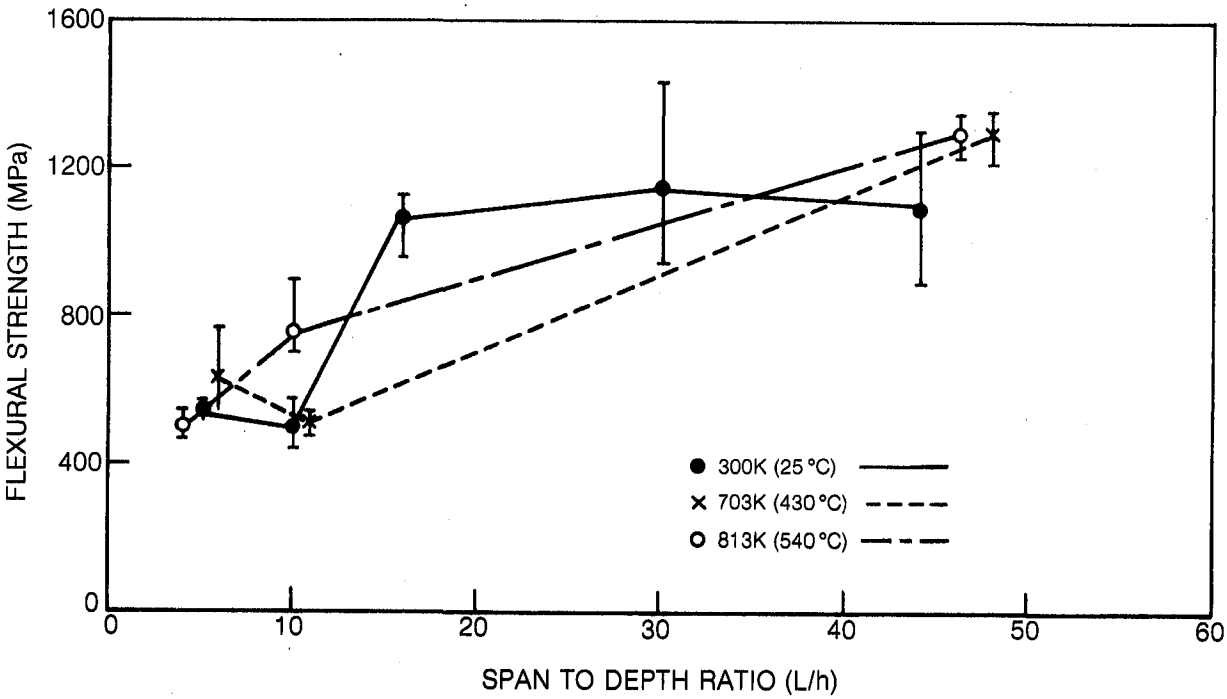

Fig. 10 Observed Flexural Strength as a Function of Span to Depth Ratio for 0° HMS/7740

80-5-82-4

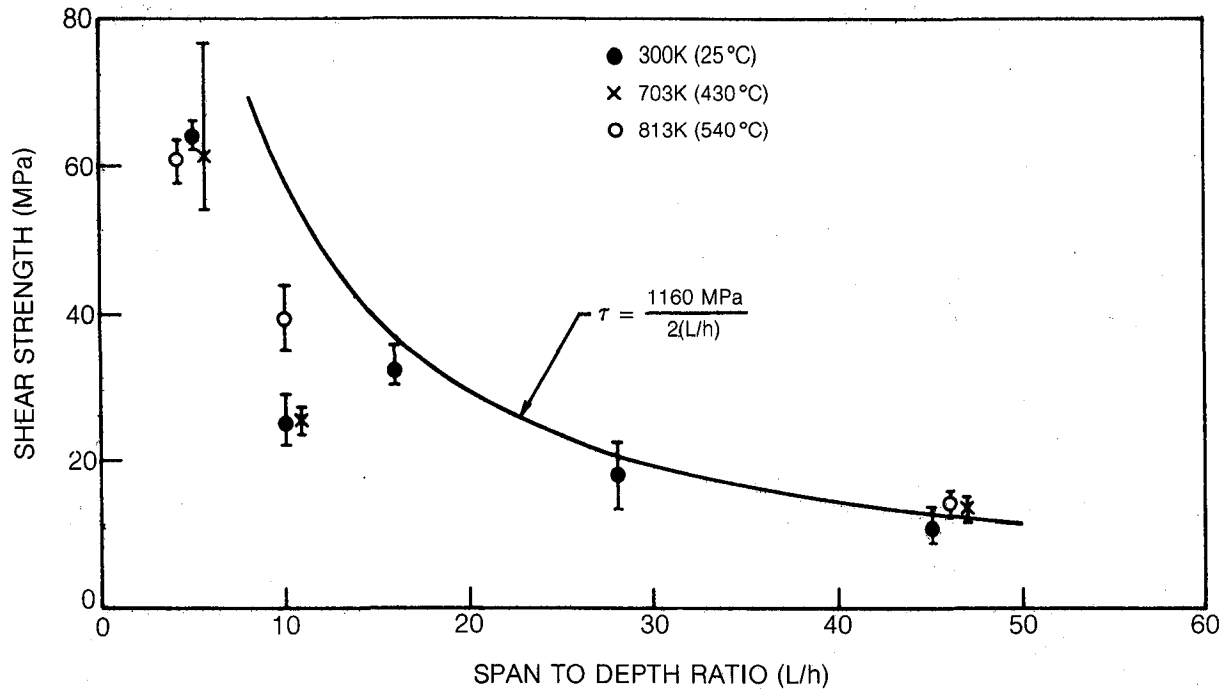

Fig. 11 Observed Shear Strength as a Function of Span to Depth Ratio for 0° HMS/7740

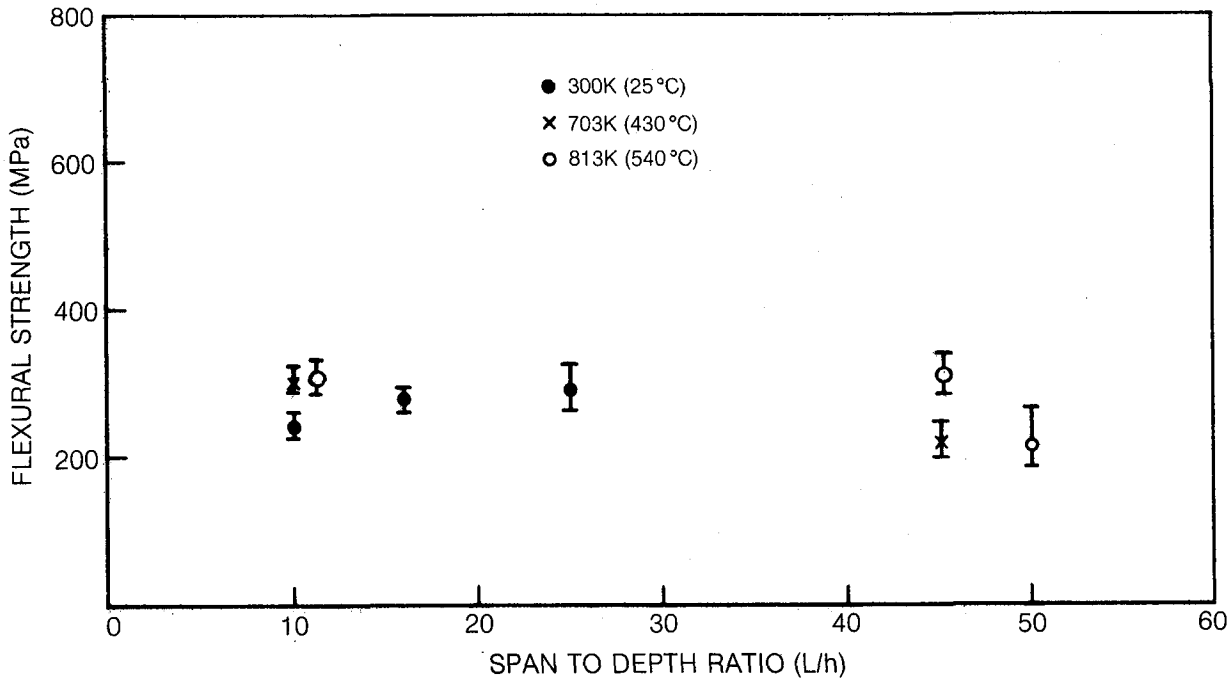

Fig. 12 Observed Flexural Strength as a Function of Span to Depth Ratio for 0/90 GY70/7740

80-5-82-5

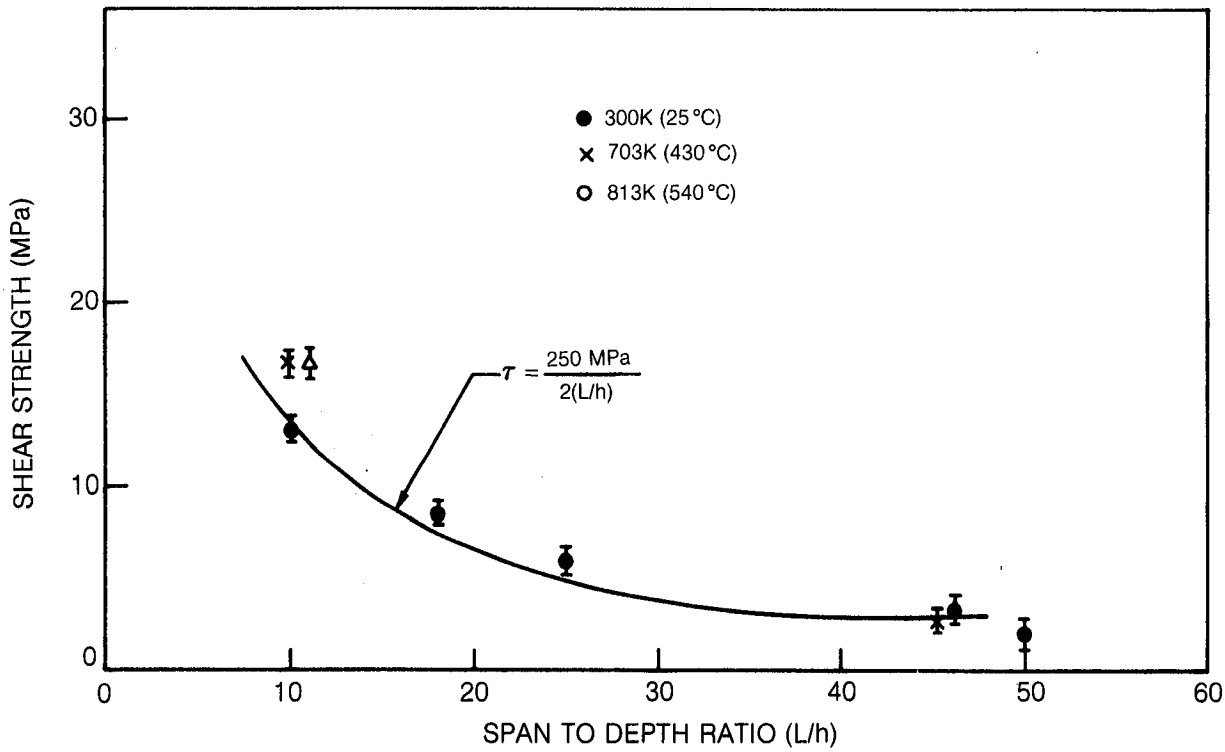

Fig. 13 Observed Shear Strength as a Function of Span to Depth Ratio for 0/90 GY70/7740

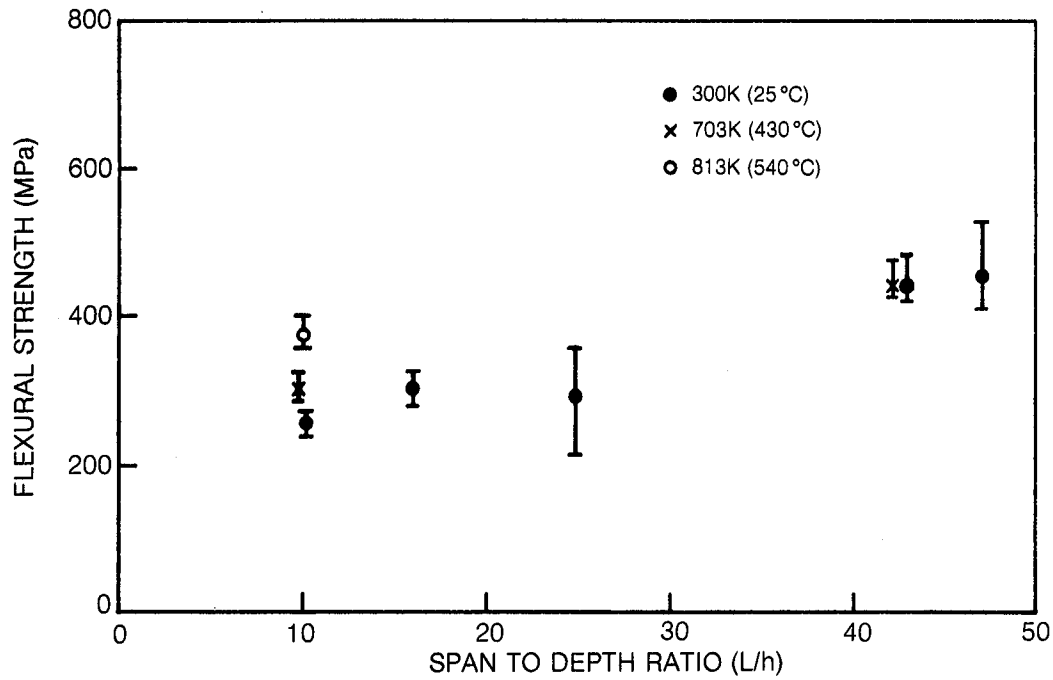

Fig. 14 Observed Flexural Strength as a Function of Span to Depth Ratio for 0/90 HMS/7740

80-5-82-6

C. Three Point Flexural Creep

The times to rupture vs the applied maximum flexural stress for unidirectionally reinforced HMS and GY70 fiber reinforced 7740 glass are presented in Figs. 16 and 17. The three-point flexural strengths of as-fabricated specimens are also shown at the zero hour position. In both fiber cases it was found that all specimens tested at 813 K failed prior to the 200 hr time used as a "run out" condition. In contrast, at 703 K almost all specimens survived for the full 200 hrs even though some of the applied maximum flexural stresses were within the range of the original composite strength.

To aid in interpretation of the stress rupture data, both figures also include data which indicate the residual composite strength obtained from specimens that were exposed to the temperatures indicated without any applied stress. Thus, at 813 K it would appear that the application of stress accelerated composite degradation and that specimen failures occurred at times and stress levels less than anticipated simply on an oxidative basis. At 703 K, however, the stress rupture times extend into the residual strength band indicating that the continuous application of stress was not important in degrading composite strength.

The residual strengths of the specimens which survived 200 hrs exposure at 703 K are presented in Table VIII. The data include the values of strength obtained from unexposed specimens for comparison. The residual strengths fall well within the range expected for specimens exposed to unstressed oxidation (refer again to bands in Figs. 16 and 17) and in the case of the HMS fiber reinforced composite, the residual strength is within the range characteristic of unexposed specimens.

Specimen deformation, as measured by changes in mid-span deflection, was found to be quite small for the 703 K test condition and very large for 813 K. The data in Fig. 18 are for a specimen loaded at 703 K to 490 MPa, which is approximately 70% of the average room temperature flexural strength of this material. The initial deflection, recorded at the onset of loading, is a purely elastic response of the specimen while the increase in deflection with time implies gradual creep of the material. After 230 hrs the total extent of this deflection is equal to approximately 38% of the total initial elastic deflection of the specimen. Although most of this deformation occurred at a nearly constant rate, there are three instances noted on the chart where small discontinuous increases in deflection were recorded. The sum total of these displacement increments can account for approximately 50% of the total creep deflection recorded.

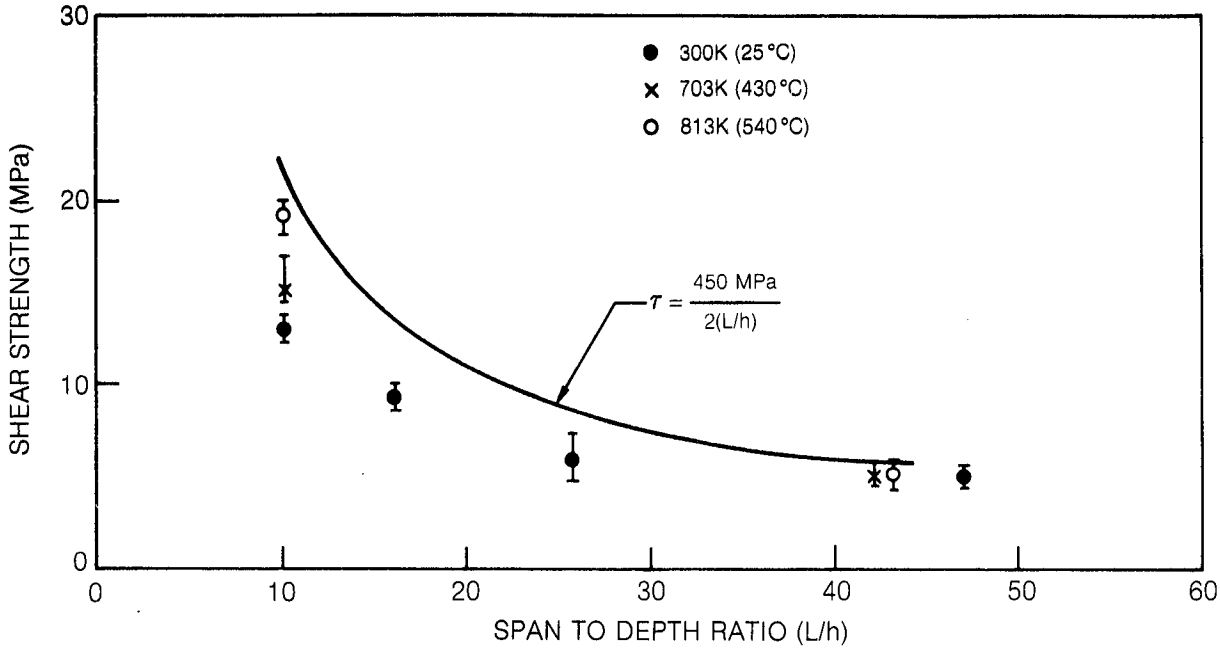

Fig. 15 Observed Shear Strength as a Function of Span to Depth Ratio for 0/90 HMS/7740

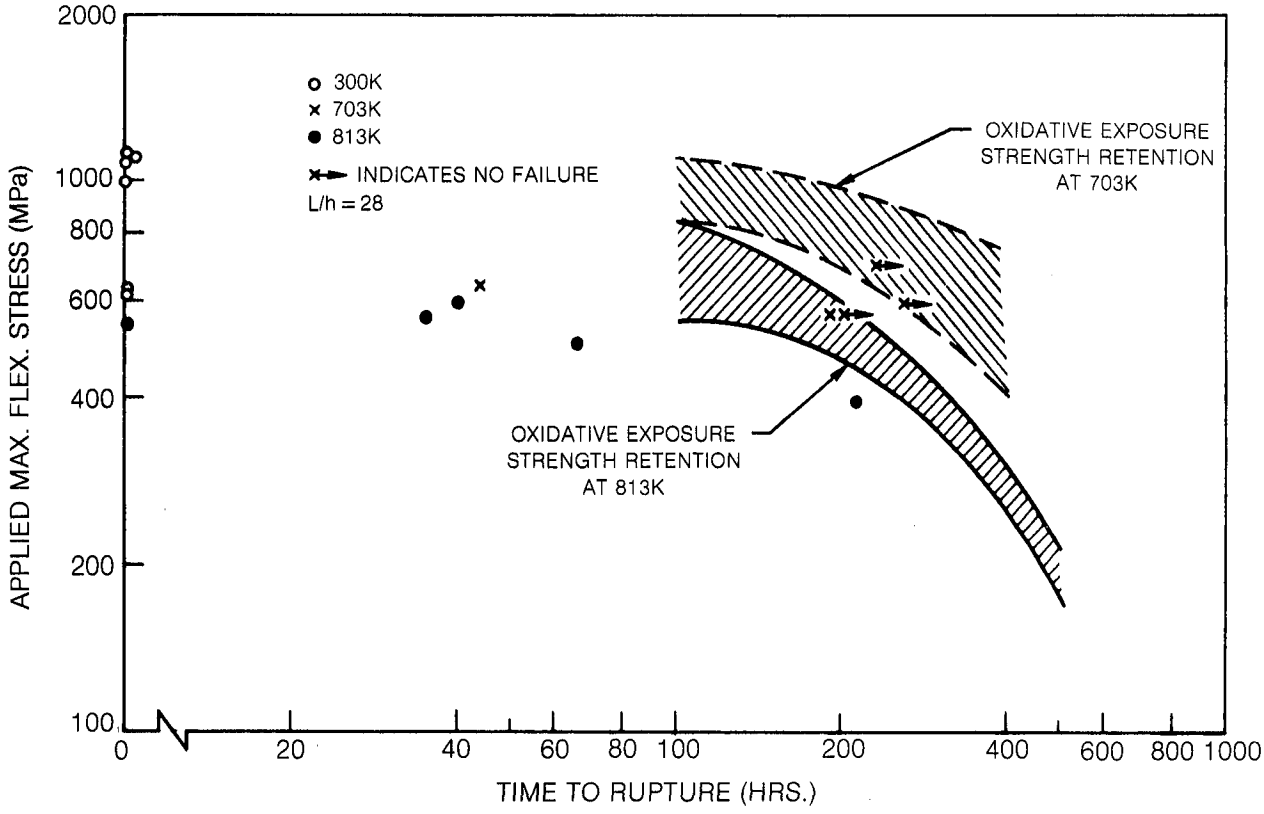

Fig. 16 Applied Maximum Flexural Stress vs. Time to Rupture for 0° — HMS/7740

80-5-82-7

Table VIII

Residual Strength of Specimens Which
Survived Stress-Rupture Testing at 703 K

Spec.	Fiber	Exposure Condition (Hrs)	Exposure Condition (Stress-MPa)	Residual Flex. Strength (MPa)
GC 404C-1,6,12	HMS	-	-	638, 1081, 634
GC 424A-1,6,12	"	-	-	1102, 992, 1085
404C-4	"	255	597	795
404C-5	"	200	498/636	799
424A-3	"	200	560	943
GC 436A-1,6,12	GY 70	-	-	544, 560, 580
436A-2	"	209	290	506
436A-3	"	200	362	488
436A-10	"	200	362	499

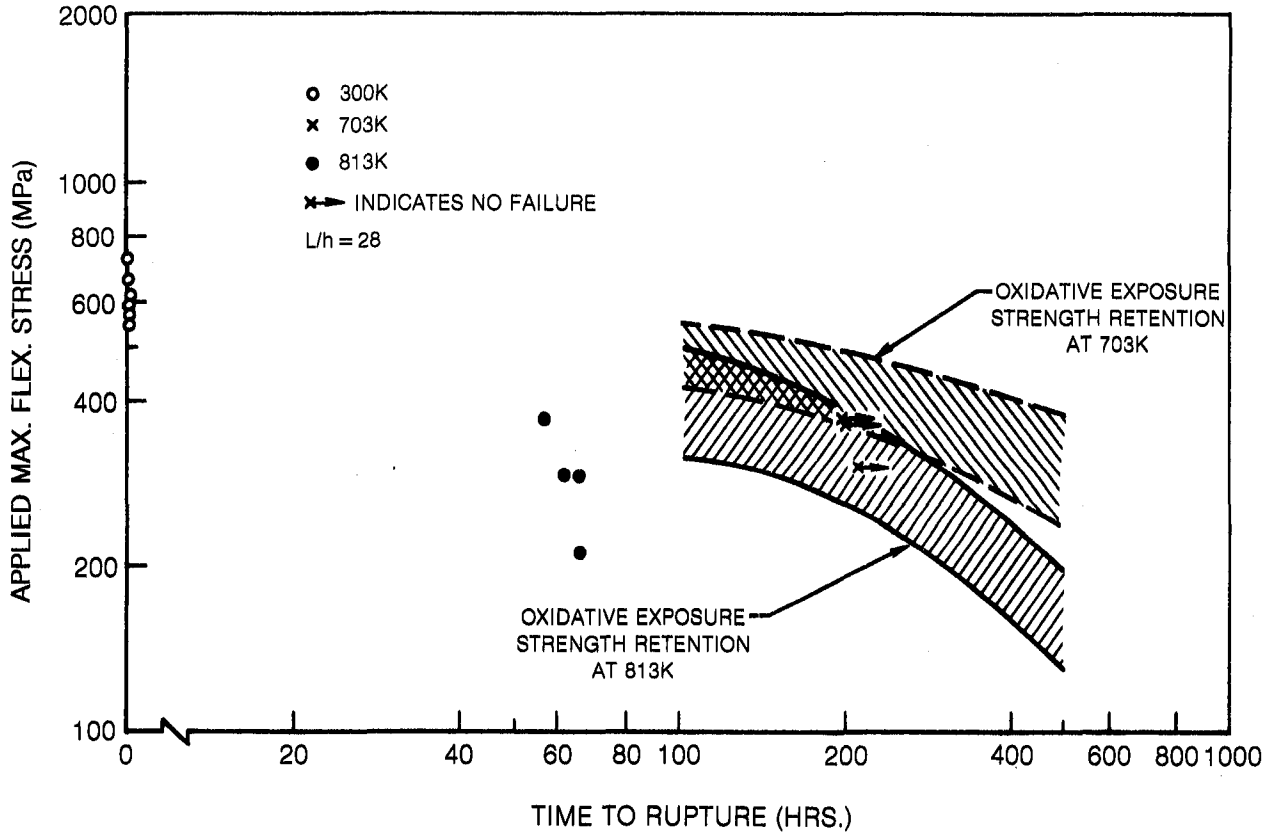

Fig. 17 Applied Maximum Flexural Stress vs. Time to Rupture for 0° — GY 70/7740

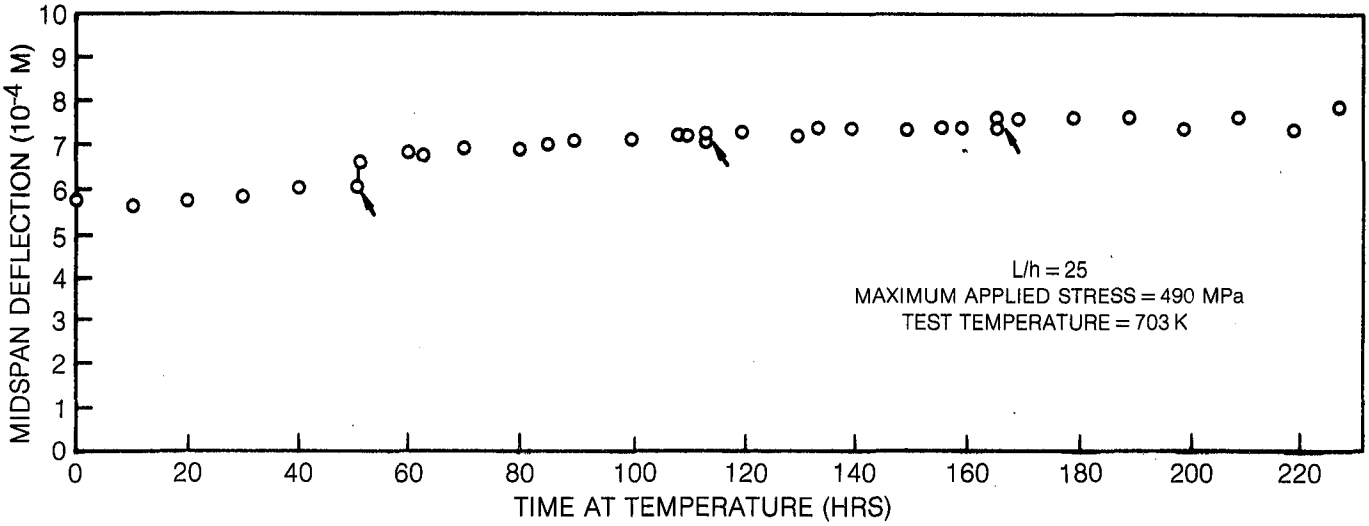

Fig. 18 Flexural Creep of 0° — HMS/7740 at 703K

80-5-82-8

The second creep curve, Fig. 19, was obtained by first loading (at 703 K) a specimen to 500 MPa and the, after 138 hrs, increasing that stress to 640 MPa. The latter stress level is approximately 90% of the average room temperature flexural strength of this material; however, no extensive specimen creep was noted after an additional 60 hr exposure.

At 813 K specimen deformation occurred much more rapidly, Fig. 20, with the rate of deformation increasing with increasing time. This is undoubtedly due to the degradation and progressive fracture of graphite fibers due to oxidation. In addition, the fractured composites did not appear to be bent, indicating the absence of any major matrix deformation controlled mode of failure.

D. Three Point Flexural Fatigue

The fatigue data are presented in Figs. 21-24 where the maximum applied flexural stress is plotted vs the number of cycles to failure. Those specimens which did not fail after 10^6 cycles were then monotonically loaded in three-point bend to determine their residual strength. The 300 K data for 0^o-GY70/7740 composites are presented in Fig. 21 where it can be seen that maximum applied fatigue stresses well into the range of the monotonic composite strength were sustained for 10^6 cycles. Only one specimen failed prior to the run out level and the applied maximum stress on that specimen was well within the unfatigued strength range. In addition, the residual strengths of all of the fatigued specimens were also well into this range indicating that the fatigue process had not degraded overall composite performance. The 703 K data, Fig. 22, also indicated excellent composite fatigue strength; however, in this case more premature failures were noted. The high residual strength of the specimens that survived 10^6 cycles at 703 K also indicates that the oxidative degradation process was not accelerated by fatigue testing. A 10^6 cycle run out required air exposure at temperature for 93 hrs. The unstressed static exposure of GY70/7740 specimens to this condition will be shown to have only a minor effect on composite properties. In the description of thermal exposure results it will be shown that a mass loss of approximately 0.6% takes place and no significant strength loss is measured.

The data for 0°-HMS/7740 are presented for both test temperatures in Fig. 23. As in the case of the GY70/7740, fatigue resistance was excellent at 300 K. A departure from the standard fatigue testing format can also be noted in the figure in that one specimen was subjected to 276,000 fatigue cycles at a maximum applied stress of 689 MPa. This "preconditioning" at this low stress level was then followed by additional fatigue at a higher stress level to ascertain whether the earlier low stress cycles caused any improvement or degradation in performance. An improvement would indicate the possible presence of a flaw blunting mechanism while degradation could relate to a deterioration of the microstructure. Final fatigue testing to failure at a stress of 940 MPa caused ultimate specimen fracture after an additional 2,820 cycles which was very similar in lifetime to other specimens tested without prefatigue exposure. Thus,

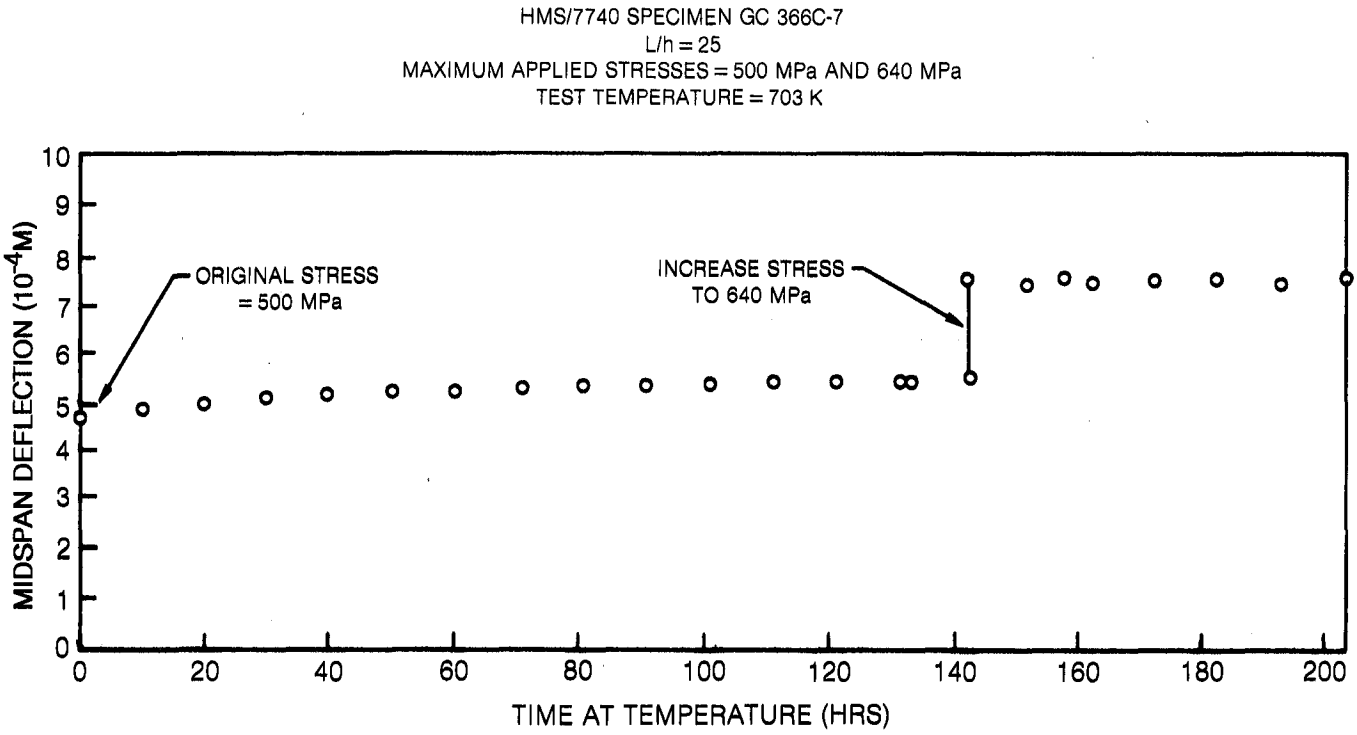

Fig. 19 Flexural Creep of 0° — HMS/7740 at 703K

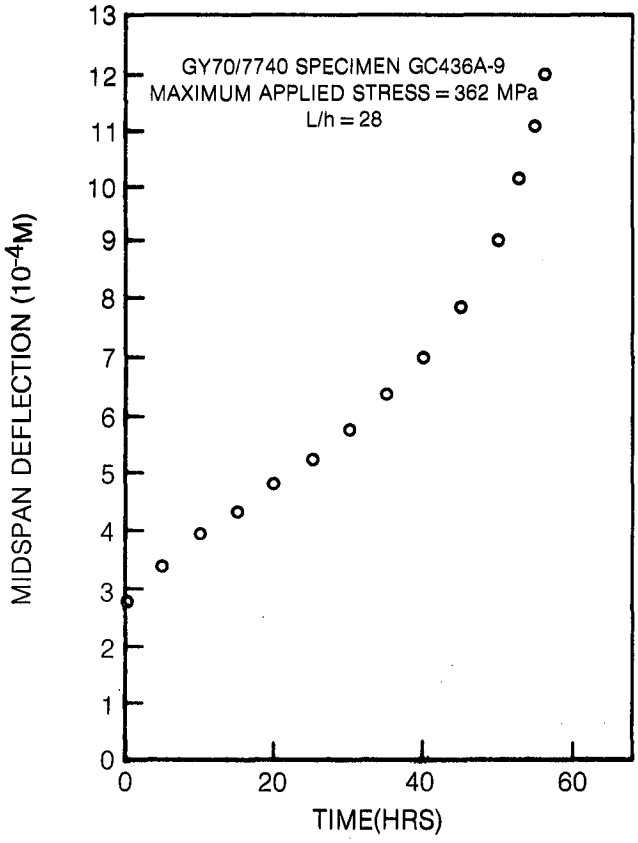

Fig. 20 Flexural Creep of 0° GY70/7740 at 813K

80-5-82-9

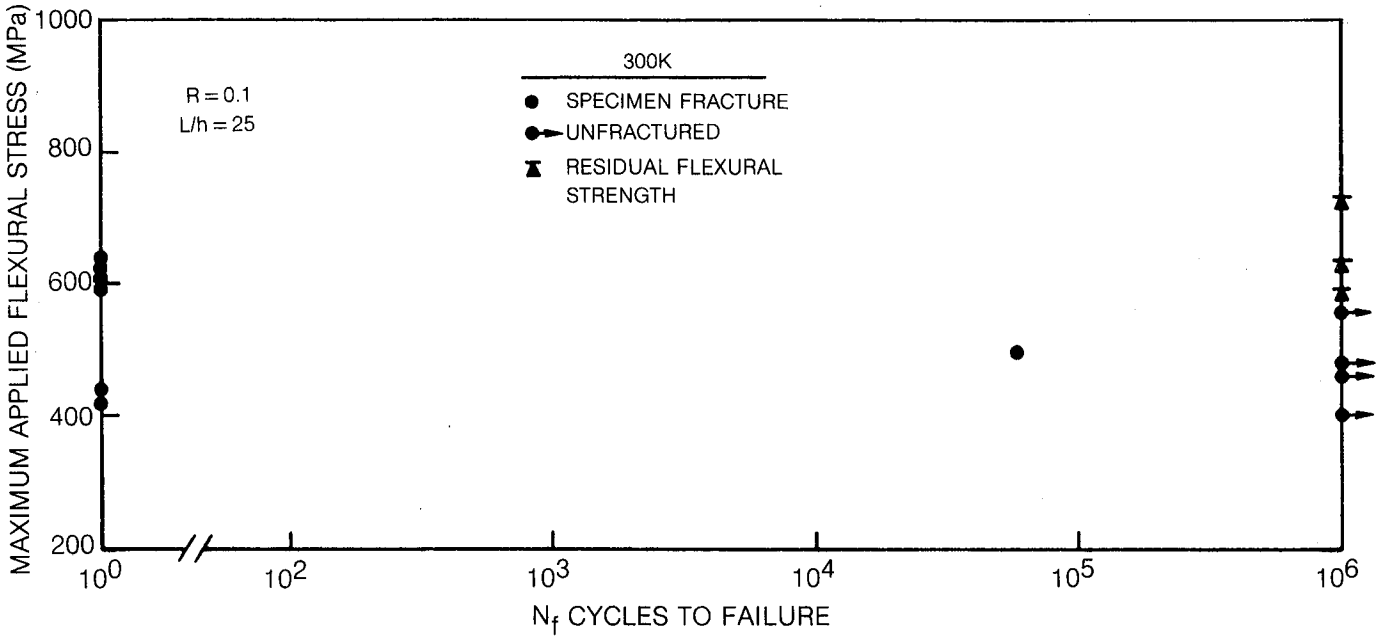

Fig. 21 Three Point Flexural Fatigue of 0° — GY70/7740

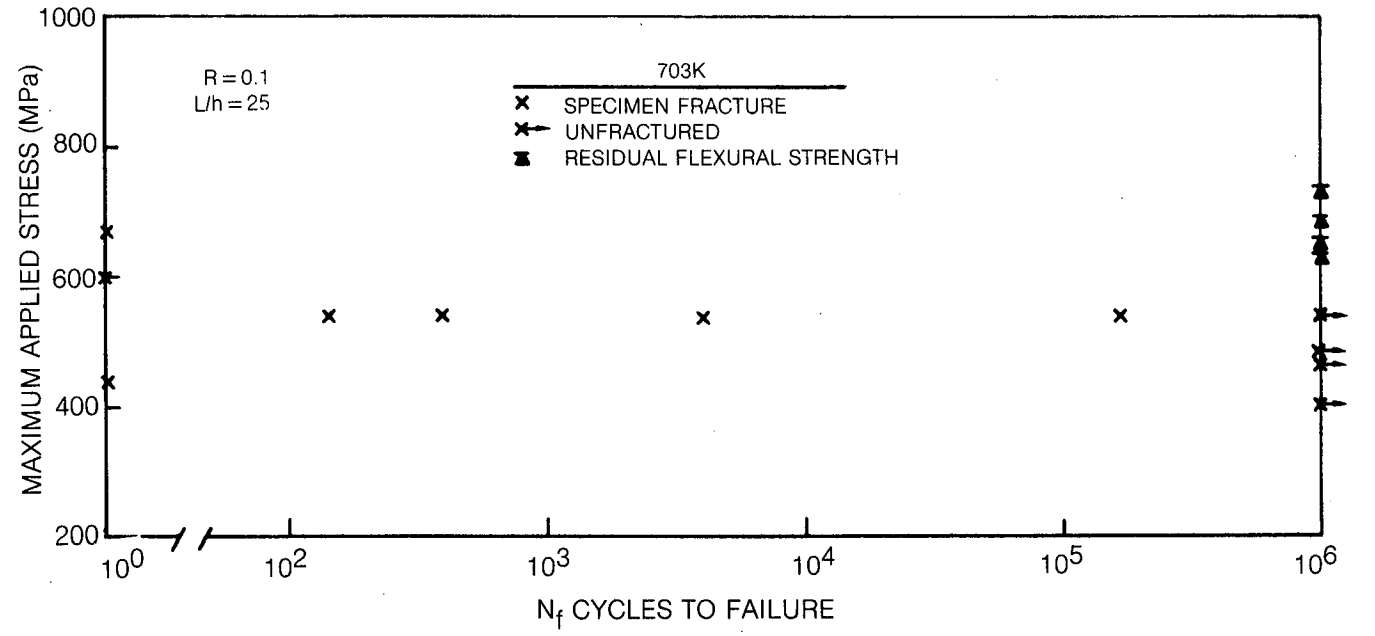

Fig. 22 Three Point Flexural Fatigue of 0° — GY70/7740

80-5-82-10

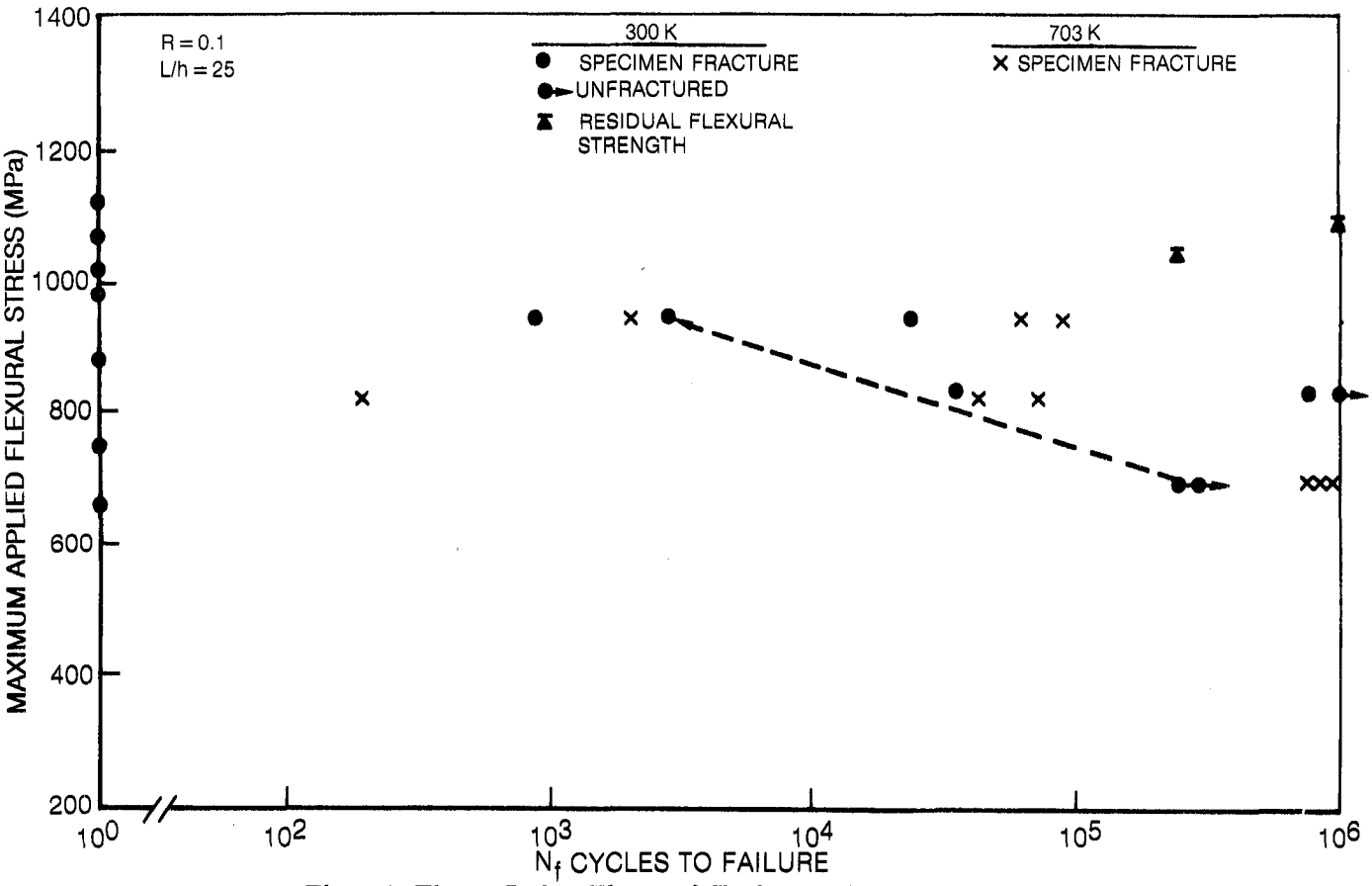

Fig. 23 Three Point Flexural Fatigue of 0° — HMS/7740

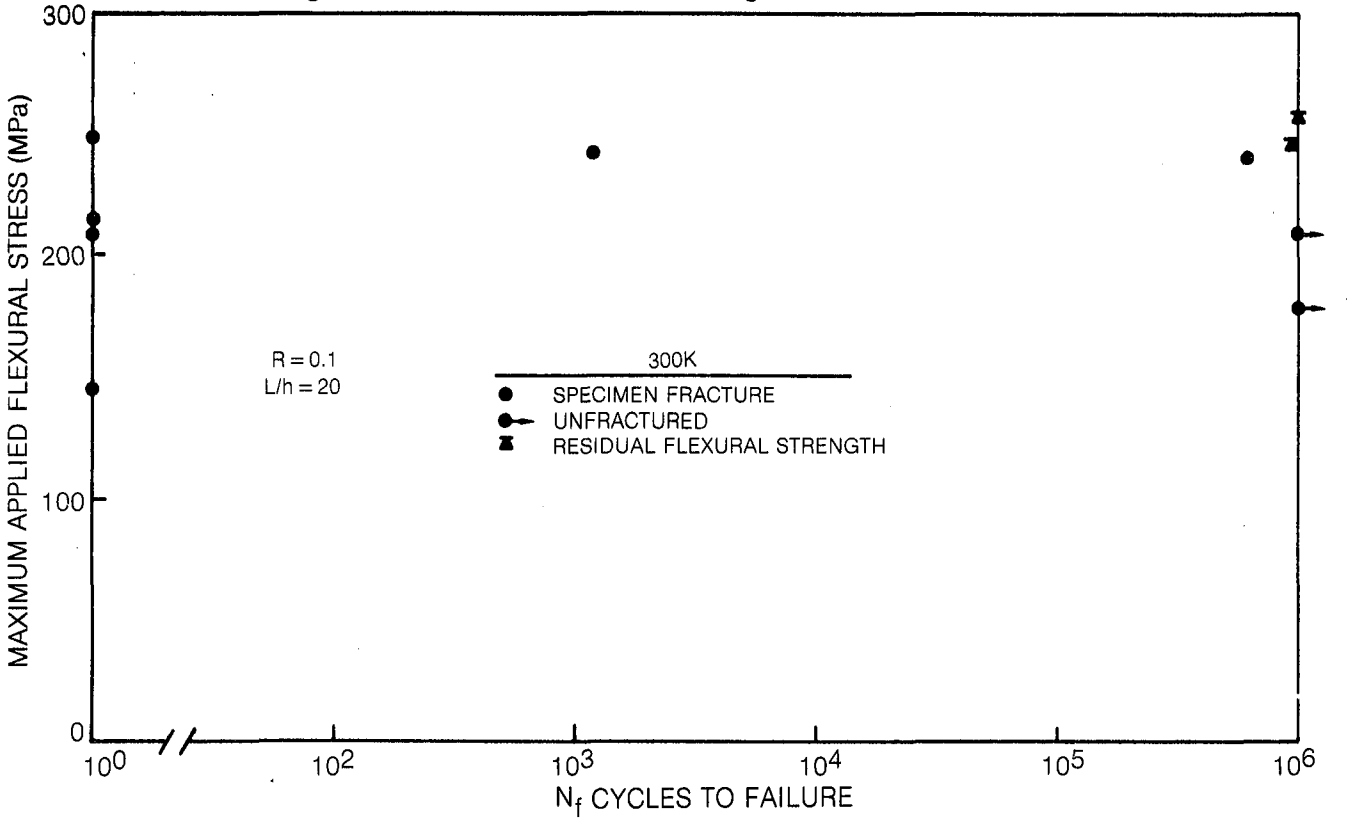

Fig. 24 Three Point Flexural Fatigue of 0/90 — GY70/7740

80-5-82-11

the test result showed no effect of the lower stress preconditioning. At 703 K it was not possible to achieve a full 10^6 cycle run out at even the lowest stress level of 689 MPa. However, three specimens tested approached this number of cycles, with one reaching 916,690 cycles prior to fracture.

Several 0/90 GY70/7740 cross ply specimens of 0.25 cm thickness were tested in fatigue at 300 K, Fig. 24. The span-to-depth ratio of these test specimens was only 20 because they were not surface ground to the usual specimen thickness prior to testing. Grinding was avoided to prevent damage of the 0° surface plys of the specimens. As in the case of the 0° specimens described above, the cross ply material exhibited excellent fatigue resistance with 10^6 run out occurring at relatively high stress levels and residual strength being equal to or greater than that of the unfatigued material.

E. Tension Test

The tensile strength, elastic modulus and strain to failure data obtained are summarized in Table IX. Each of the systems tested will be considered in turn.

1. HMS Fiber Reinforced 7740 - Composites GC 628, GC 594 and GC 593

The tensile stress vs strain curve for one of the 0° specimens is shown in Fig. 25. Although the curve appears to be quite linear, it actually is composed of two nearly linear portions that transition at a stress level of approximately 75 MPa. The specimen fracture surface is quite flat with no signs of fiber pull out or gross delamination.

The 0/90 cross ply reinforced specimens were considerably weaker than their all 0^o counterparts and fracture occurred in only one case completely within the test gauge length. The overall composite failure strain, Fig. 26, however, was similar to that achieved with the 0^o material.

2. HTS Fiber Reinforced 7740 - Composite GC 629

The stress-strain curve for this 0^o composite, Fig. 27, was essentially linear to the point of failure. This system exhibited the highest strength and failure strain combination of any of those tested. It also contained the highest percentage of fiber reinforcement. The composite fracture surface was markedly different from that of the HMS specimen. In this case it was very fibrous with the entire gage length of the specimen taking on a brush-like appearance after fracture.

Table IX

Tensile Test Data (300 K Test)
for 7740 Matrix Composites

Specimen	Fiber	v/o G	v/o F	v/o P	Orientation	UTS MPa	E GPa	ε_f (%)	Fracture Location
GC 594-14	HMS	46	54	0	0°	412	195	0.20	Gage
-15	HMS	-	-	-	0°	398	193	0.20	Gage
GC 628-4	HMS	52	48	0	0°	342	195	0.17	Dbl. Edge
-6	HMS				0°	354	173	0.20	Dbl. Edge
-8	HMS				0°	349	-		Dbl. Edge
GC 593-3	HMS	56	46	-	$0^\circ/90^\circ$	137	60.1	0.27	Gage*
-4	HMS	-	-	-	$0^\circ/90^\circ$	126	67.8	0.20	Dbl. Edge*
GC 629-4	HTS	32	67	1	0°	572	151	0.36	Gage
-6	HTS				0°	658	153	0.41	Gage
-8	HTS				0°	613	-	-	Gage
GC 630-4	Pitch	46	54	0	0°	616	338	0.22	Gage
-6	Pitch				0°	511	329	0.16	Gage
-8	Pitch				0°	534	-	-	Gage
GC 631-4	Th 300	60	39	1	0°	359	126	0.32	Gage + Dbl.
-6	Th 300				0°	460	121	0.40	Gage + Dbl.
-8	Th 300				0°	386	-	-	Dbl. Edge
GC 632-4	GY-70	42	58	0	0°	424	293	0.14	Gage
-6	GY-70				0°	362	273	0.12	Gage
-8	GY-70				0°	Failed prior to loading			
GC 633-4	Cel				0°	447	117	0.32	Gage
-6	6000				0°	395	110	0.40	Gage
-8	"				0°	432	-	-	Gage
GC 576-2	Cel	67	27	6	Paper	157	55.2	0.65	In Dbl.
	6000	-	-	-	0°	142	48.4	0.61	In Dbl.
	Paper								

*Specimens were not surface ground prior to test. All other specimens were surface ground prior to test.

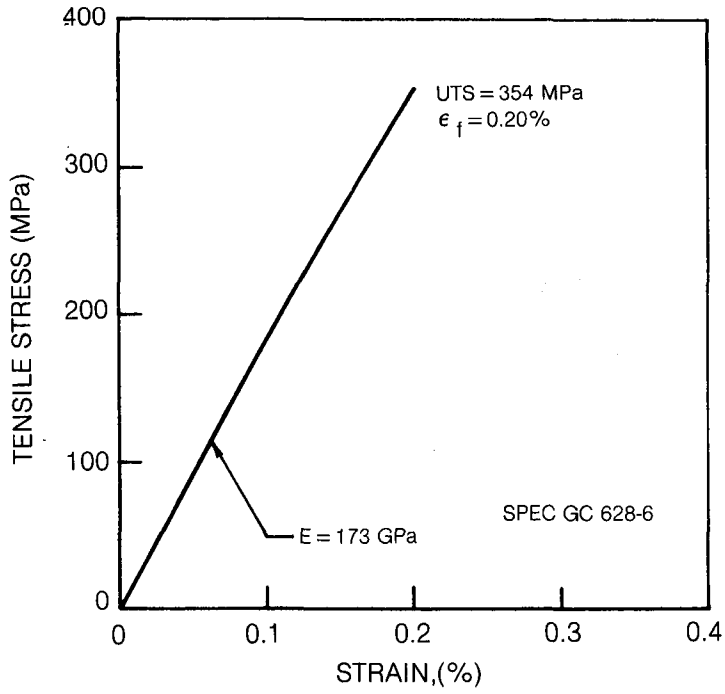

Fig. 25 Axial Tensile Stress — Strain Curve for 0° — HMS/7740 at 300K

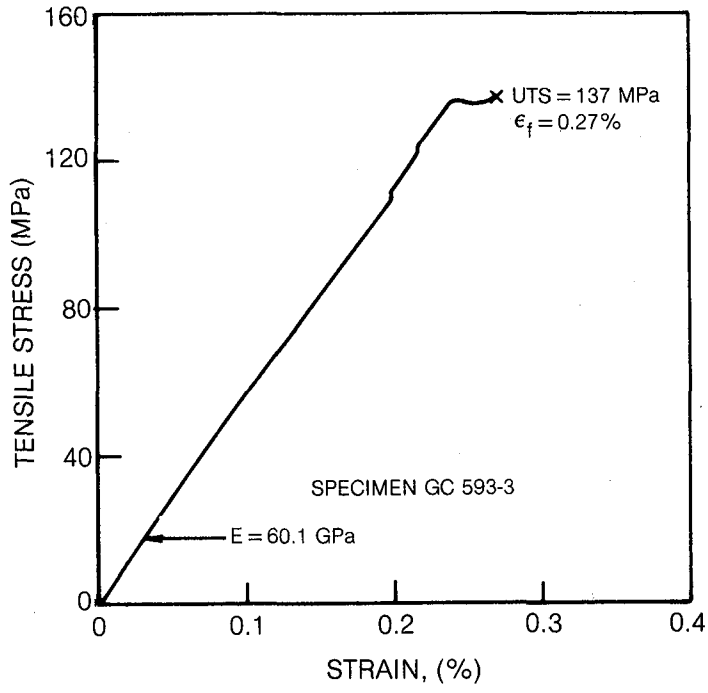

Fig. 26 Transverse Tensile Stress — Strain Curve for 0/90 — HMS/7740 at 300K

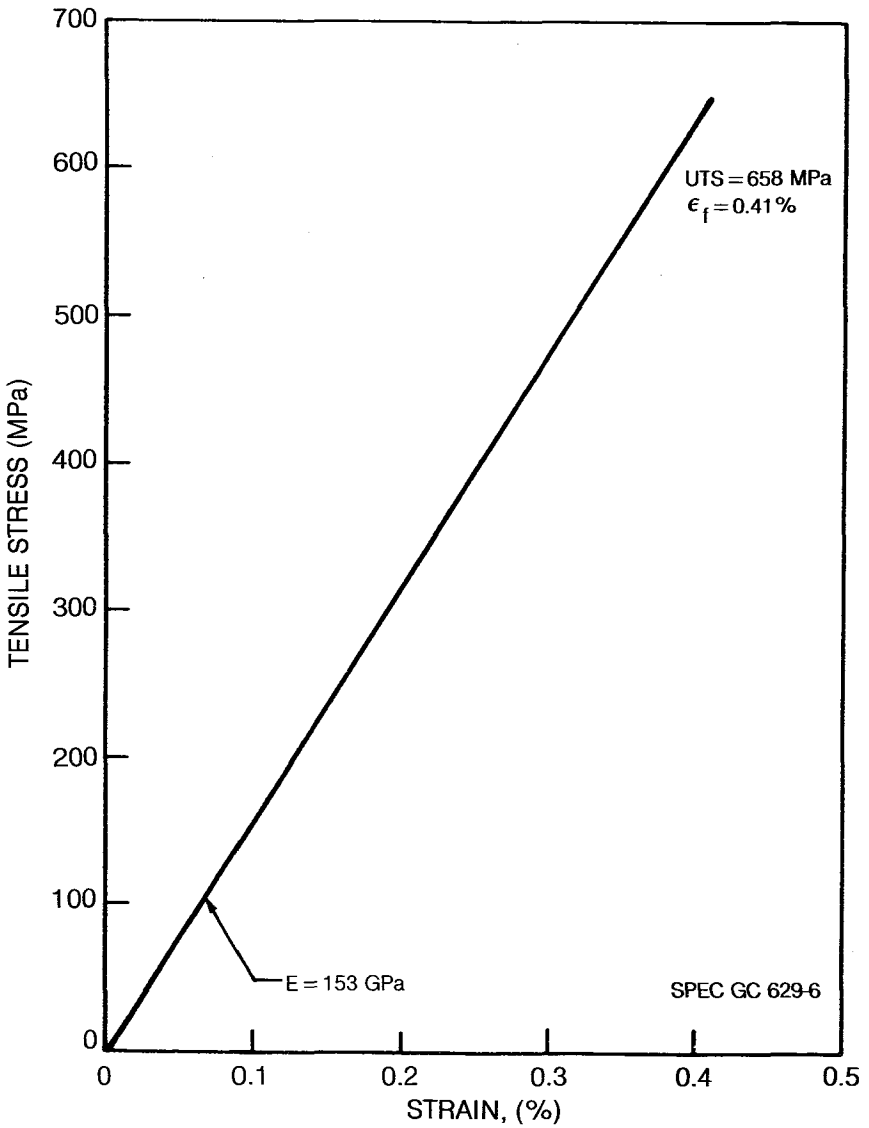

Fig. 27 Axial Tensile Stress — Strain Curve for 0° — HTS/7740 at 300K

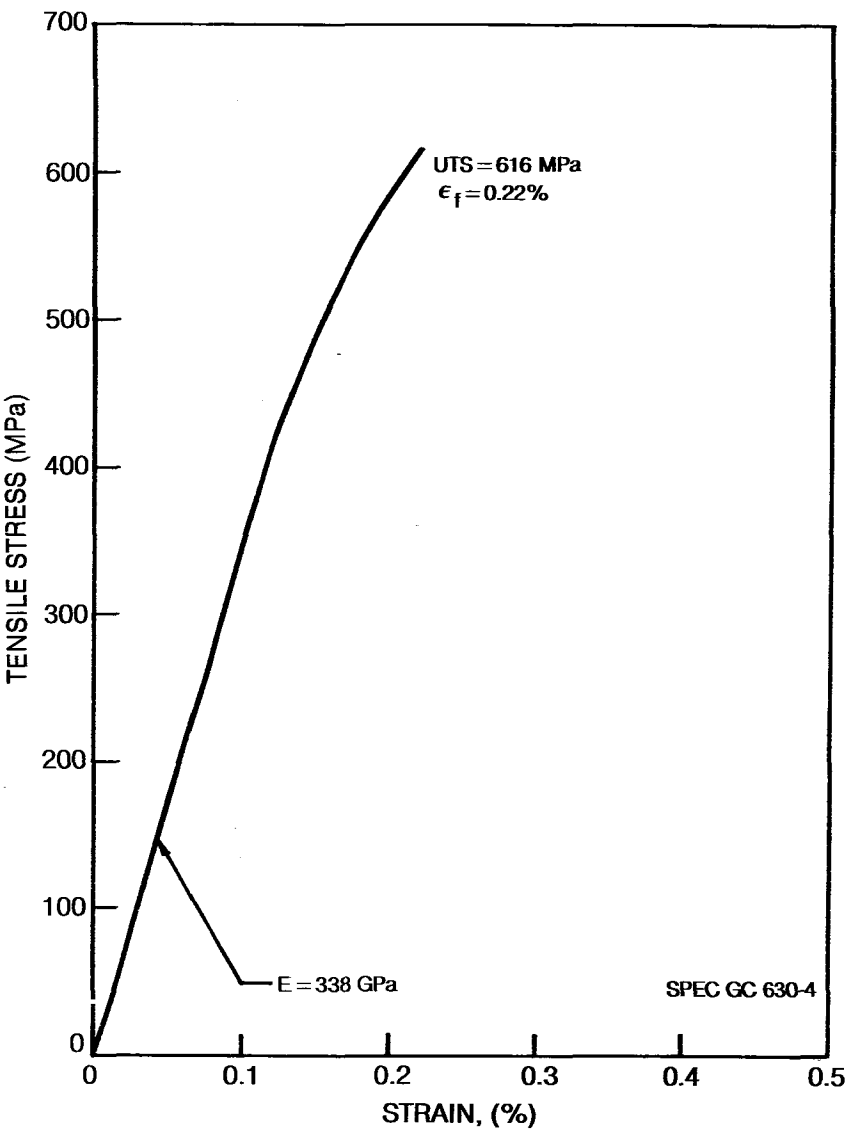

Fig. 28 Axial Tensile Stress-Strain Curve for 0° — Thornel Pitch (VS0054-0)/7740 at 300K

80-5-82-16

3. Thornel Pitch Fiber Reinforced 7740 - Composite GC 630

The 0° stress vs strain curve, Fig. 28, was linear up to about 65% of the UTS, after which it became very nonlinear. This latter behavior was probably due to the formation of large longitudinal shear cracks which were a prominent feature of the fractured specimens. No fiber-matrix debonding or pullout, however, accompanied these cracks. The very high elastic modulus obtained is a major aspect of this composite and hence, even though the composite tensile strength was relatively high, the final failure strain was low.

4. Thornel 300 Fiber Reinforced 7740 - Composite GC 631

The 0° stress vs strain curve, Fig. 29, is bi-linear with the decrease in slope occurring at approximately 100 MPa. Although the composite tensile strength is relatively low, the failure strain is quite high due to the low elastic modulus of both fiber and composite. The slight nonlinearity in the curve near the UTS is probably associable with the formation of large longitudinal shear cracks, some of which followed an interlaminar path. Again, as in the case of the Pitch based fiber, no fiber-matrix debonding or pullout occurred.

5. GY70 Fiber Reinforced 7740 - Composite GC 632

The stress vs strain curve for this composite, Fig. 30, was totally linear to the point of fracture and the resultant composite fracture surface appeared relatively featureless. The fracture plane was flat and no signs of pullout or shear cracking were evident.

6. Continuous Celion 6000 Fiber Reinforced 7740 - Composite GC 633

The stress vs strain curve for this 0^{o} material was the most nonlinear of all the 0^{o} specimens measured, Fig. 31. An initial decrease in slope occurred at about 100 MPa followed by a major nonlinear portion of the curve at approximately 85% of the UTS. This latter feature contributed to raising the ultimate composite failure strain to approximately 0.50% and is probably associated with the extensive fiber-matrix debonding characteristic of the final fracture. The entire gage section turned into a "brush" of graphite fibers after fracture.

7. Chopped Celion 6000 Fiber Paper Reinforced 7740 - Composite GC 576

The stress-strain behavior, Fig. 32, of the Celion 6000 paper reinforced glass matrix composites differed significantly from that of the above materials. In this case the specimen exhibited a significant decrease in slope at an applied stress of 40 MPa, which was then followed by an increase in slope and final failure at approximately 0.6% strain. This unique behavior is probably related to the occurrence of matrix cracking at the 40 MPa stress level and the extreme difficulty for crack propagation through the specimen cross section. The resultant high level of failure strain is highly desirable for most applications; however, the low level of overall strength, compared to the unidirectionally reinforced material, would be unsatisfactory for many high performance situations.

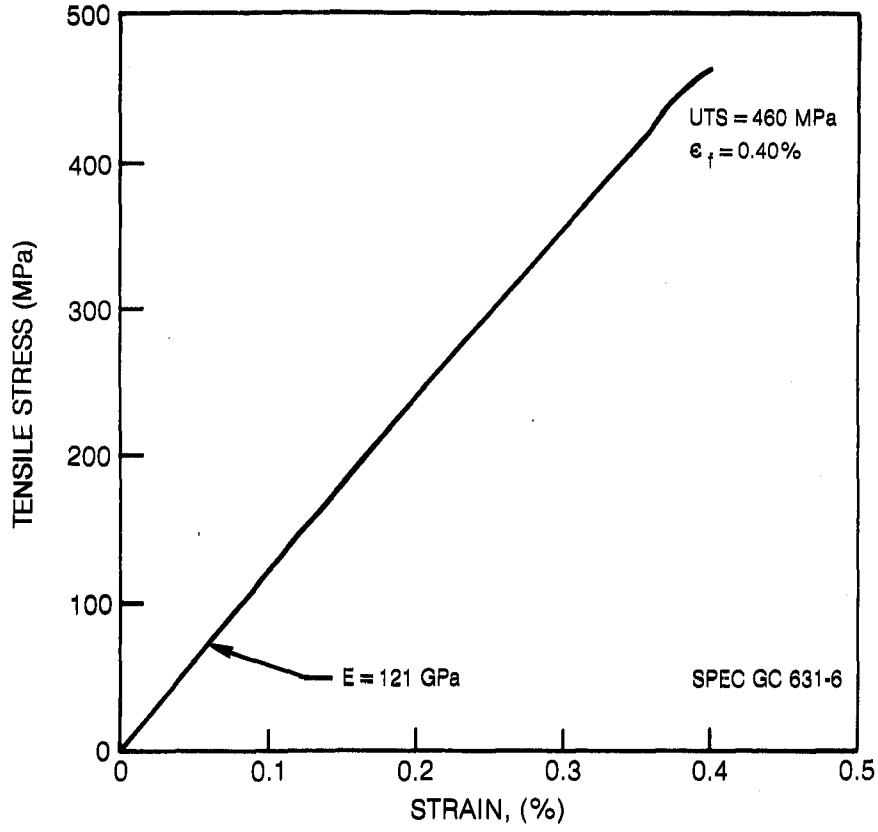

Fig. 29 Axial Tensile Stress — Strain Curve for 0° — Thornel 300/7740 at 300K

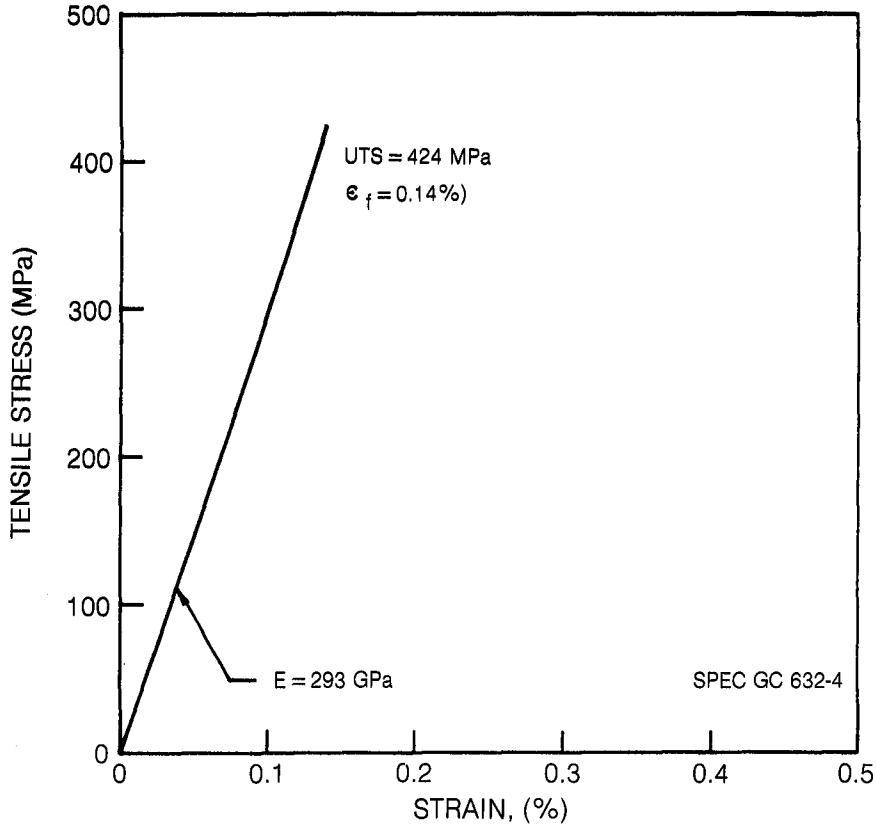

Fig. 30 Axial Tensile Stress — Strain Curve for 0° — GY70/7740 at 300K

80-5-82-13

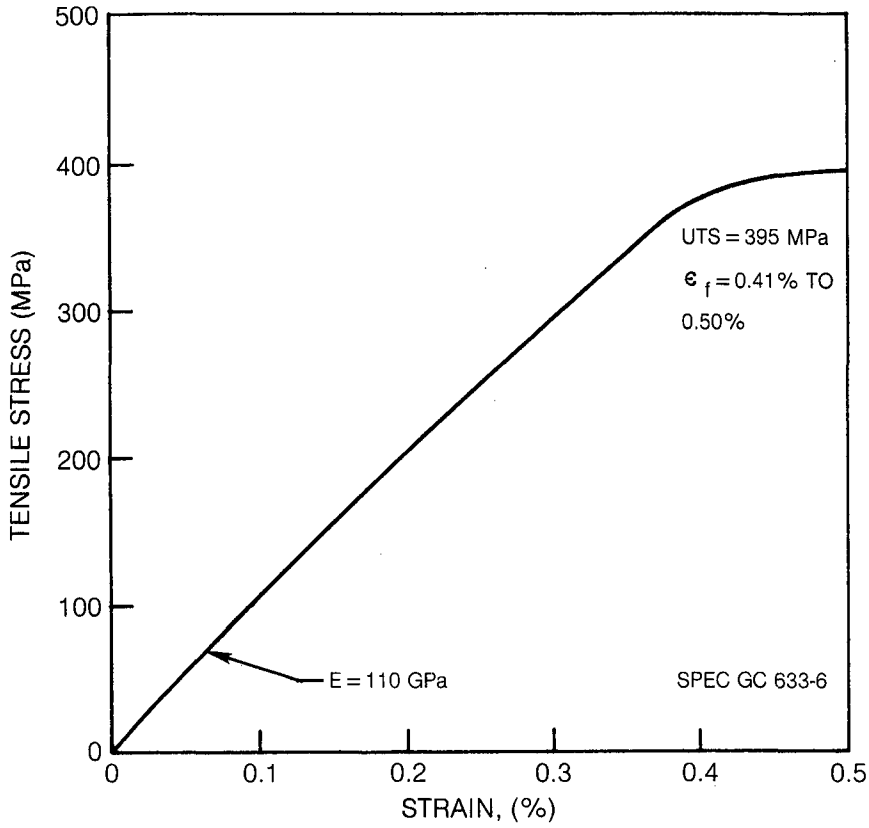

Fig. 31 Axial Tensile Stress — Strain Curve for 0° — Celion 6000/7740 at 300K

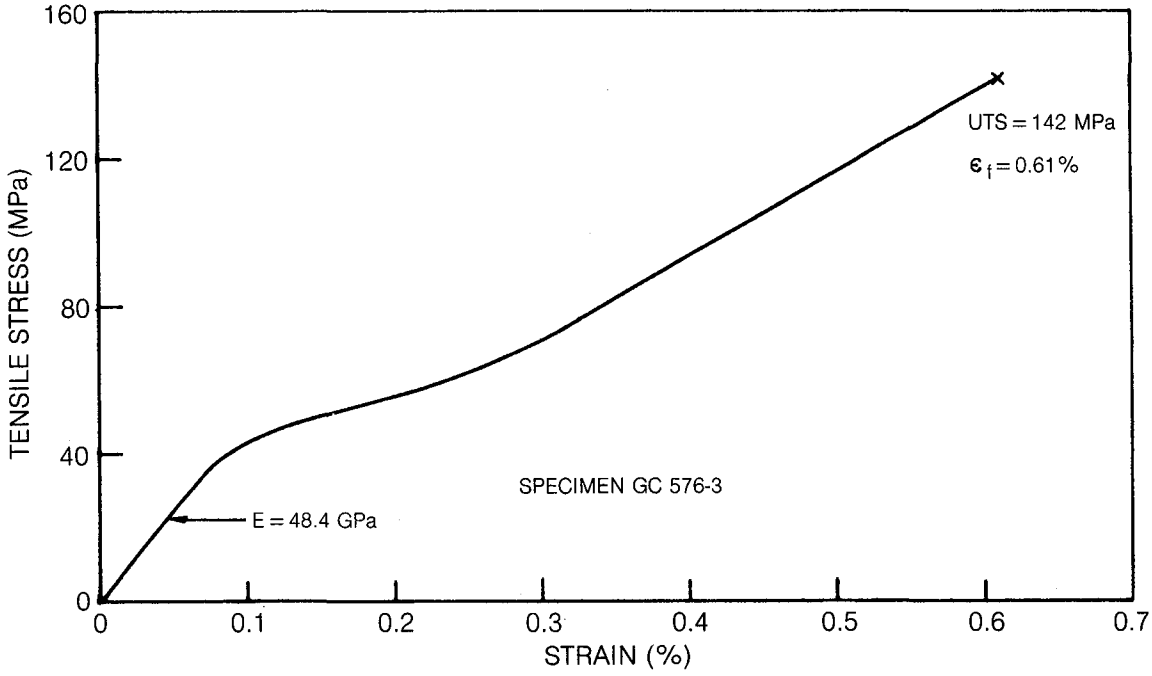

Fig. 32 Tensile Stress — Strain Curve for Celion 6000 Paper — 7740 Tested at 300K

80-5-82-14

A further comparison of composite properties is presented in Table X where manufacturer's claimed fiber properties of strength and elastic modulus are used as a baseline. A simple rule-of-mixtures calculation of composite elastic modulus, using the tabulated values for fiber and 7740 glass matrix properties, indicates that all of the measured axial moduli fall below those expected. The level of agreement ranges from between 79% and 95%. Some of the inaccuracy may be related to the fact that the manufacturer's "typical" data are used rather than those for a particular spool. In addition, the use of the full matrix elastic modulus of 63 MPa may overestimate the matrix contribution. Matrix cracking may lower this value significantly.

Although it was expected that a "rule-of-mixtures" approach should yield relatively good agreement for the elastic modulus comparison, no such agreement should be expected for composite tensile strength. Even a simplified calculation, used in the table, which completely neglects any matrix contribution term, would not be expected to be very accurate since, at the very least, an effective bundle strength should be used for the fiber strength. However, the statistical data needed to determine the bundle strength are not available. The calculation presented in Table X is used simply in a relative sense. The Pitch fiber reinforced composite came closest to achieving a large fraction of the fiber average strength, 49%, while all of the other composites were at a 27-36% level of achievement. Because of the relatively linear shapes of the stress vs strain curves, the levels of agreement in composite failure strain resemble those based on strength.

Three point flexural bend strengths were also determined for specimens taken from the same composite panels used to obtain the above described tensile data. A comparison between the average tensile and flexural strengths and elastic moduli is presented in Table XI. It can be noted that composite elastic modulus is nearly identical as measured by either test while the composite flexural strength is substantially higher than the tensile strength in four out of eight cases. In the case of the HMS fiber reinforced specimens, the flexural strengths in this table are lower than those reported earlier in this report, Fig. 5. This is parimarily due to the lower percentage of fiber reinforcement present in the current specimens but may also relate to variations in starting fiber properties.

The superiority of flexural strength was expected for several reasons. First, on a statistical basis it is expected that a higher flexural strength would result due to the smaller volume of material undergoing the maximum calculated beam stress. Second, the problems of alignment and gripping induced failure should be less for the flexural test. On the other hand, it is possible to measure a low flexural strength due to the occurrence of other failure modes such as shear or compression. Examination of the fractured three point bend specimens did indeed fail by an interlaminar shear mode rather than in tension. A very poor fiber-matrix bond existed and this was also reflected in the

Table X

Comparison of Measured and Simplified Rule of Mixtures 0° Properties
for Uniaxially Reinforced Specimens

Specimen	Type	Fiber			Composite Elastic Modulus			Composite UTS			Composite Failure Strain		
		E_f (GPa)	UTS_f (MPa)	v/o F	Calc* (GPa)	Meas (GPa)	Meas/Calc	Calc** (MPa)	Meas (MPa)	Meas/Calc	Calc*** %	Meas %	Meas/Calc
594	HMS	350	2700	54	218	194	0.89	1460	405	0.28	0.77	0.20	0.26
628	HMS	350	2700	48	200	184	0.92	1300	348	0.27	0.77	0.18	0.23
629	HTS	256	2830	67	192	152	0.79	1900	614	0.32	1.1	0.38	0.35
630	Th Pitch	654	2070	54	382	334	0.87	1120	554	0.49	0.32	0.19	0.60
631	Th 300	234	2930	39	130	124	0.95	1142	400	0.35	1.25	0.36	0.29
632	GY 70	537	1860	58	338	283	0.84	1080	395	0.36	0.35	0.13	0.37
633	Cel 6000	234	2760	-	-	113	-	-	425	-	1.18	0.36	0.30

*calculated using $E_c = (v/oF)\ E_f + (v/oG)\ (63\ GPa)$

**calculated using $UTS_c = (v/oF)\ (UTS_f)$

***calculated using $\varepsilon_f = UTS_f/E_f$

Table XI

Comparison of Tensile and Flexure Data

Specimen	Fiber Type	Composite Flexural Properties		Composite Tensile Properties		Flex Strength/ Tensile Strength
		Strength (MPa)	Elastic Modulus (GPa)	Strength (MPa)	Elastic Modulus (GPa)	
594	0° HMS	620*	-	405	194	1.53
628	0° HMS	527**	180	348	184	1.51
593	0/90 HMS	325*	-	132	64	2.46
629	0° HTS	806**	155	614	152	1.31
630	0° Th. Pitch	683**	332	554	334	1.23
631	0° Th. 300	711**	127	400	124	1.78
632	0° GY70	432**	275	395	283	1.09
633	0° Cel 6000	388**	94	425	113	0.91
576	0° Cel 6000 paper	433*	85	150	52	2.88

* 5 specimens tested to obtain an average flexural strength
** 4 specimens tested to obtain an average flexural strength

fractured tensile specimen character where the specimens appeared brush-like after testing. In the case of specimen set GC 632 consisting of GY70 reinforced glass, it was not possible to ascertain whether specimens failed in tension or compression by simply looking at the fractured specimens. Therefore, three additional specimens were tested from the same panels and again it was not possible to ascertain the exact mode of failure because of its very sudden nature and the rather brittle appearance of the fracture surfaces. In the cases of both the Thornel Pitch (GC 630) and HTS (GC 629) fiber reinforced specimens it was possible to note evidence for compression, rather than tensile, failure in the flexural test. This was particularly true for the Thornel Pitch reinforced composites which exhibited only compression failure.

The fracture surfaces of three types of tensile specimens were examined in the scanning electron microscope. The fracture surface of a 0° HMS fiber reinforced 7740 specimen, Fig. 33, is characterized by the presence of almost no fiber pull out from the matrix. However, large axial splits are observed which appear to occur primarily along fiber rich zones. These may correspond to regions of low transverse strength which, upon the sudden release of energy during tensile failure, fracture. The fracture of a $0^{\circ}/90^{\circ}$ HMS reinforced 7740 composite, Fig. 34, includes the same above-mentioned features as well as transverse ply fracture which occurs primarily along fiber-matrix interfaces. Finally, the tensile fracture of chopped Celion 6000 fiber reinforced glass, Fig. 35, is characterized by extensive fiber pull out on a microscale. Fiber lengths of 300-500 microns in length are readily observed completely free of any surrounding matrix.

F. Thermal Exposure and Thermal Cycling

The change in mass of unidirectionally reinforced 7740 glass matrix composites is given in Figs. 36 and 37 as a function of their exposure time to air at the indicated temperatures. For both the HMS and GY70 reinforced materials it was found that the total loss of mass after even 500 hrs at 703 K was less than 5% while a similar length of exposure to 813 K resulted in between 30 to 50% mass reduction. As shown in Fig. 36, there was very little dependence of performance on whether the specimen ends were glass rich (untrimmed ends) or whether the ends were trimmed to remove any excess glass.

After measurement of their residual mass the specimens were tested to failure in three point bend to measure their flexural strength, Figs. 38 and 39. As would be expected from the change in mass data, the composite strength was significantly reduced after exposure at 813 K. Significant strength loss, however, was also observed for those specimens exposed to 703 K, particularly in the case of the GY70 fiber reinforced composites. To get a better understanding of this and the mechanisms which control composite mass and strength loss, several specimens were sectioned and polished. The examination of both transverse and longitudinal sections taken from exposed composites revealed two distinctly different rate processes taking place, one from the specimen ends

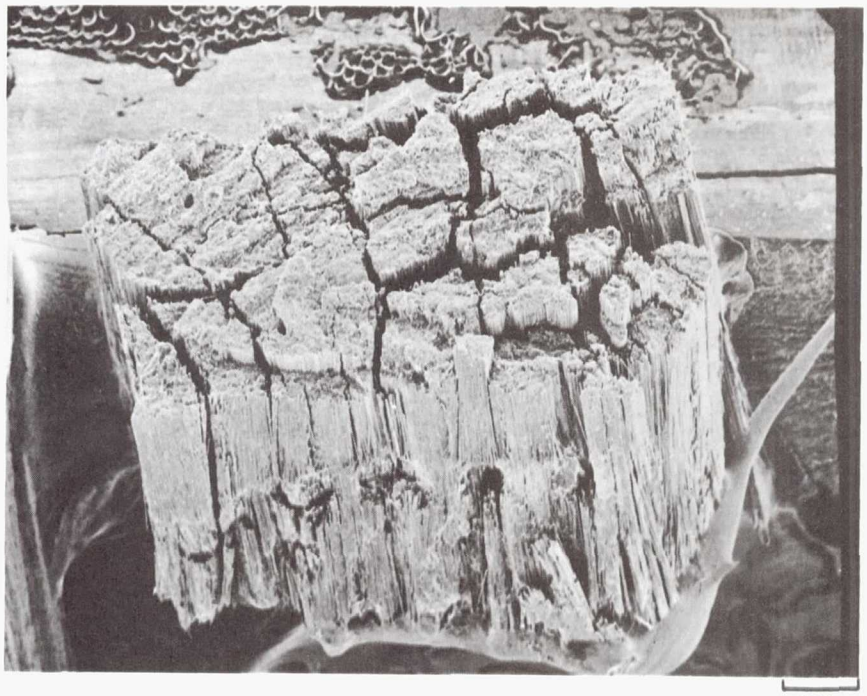

Fig. 33 Fracture Surface of 0° — HMS/7740 Tensile Specimen GC 594-14

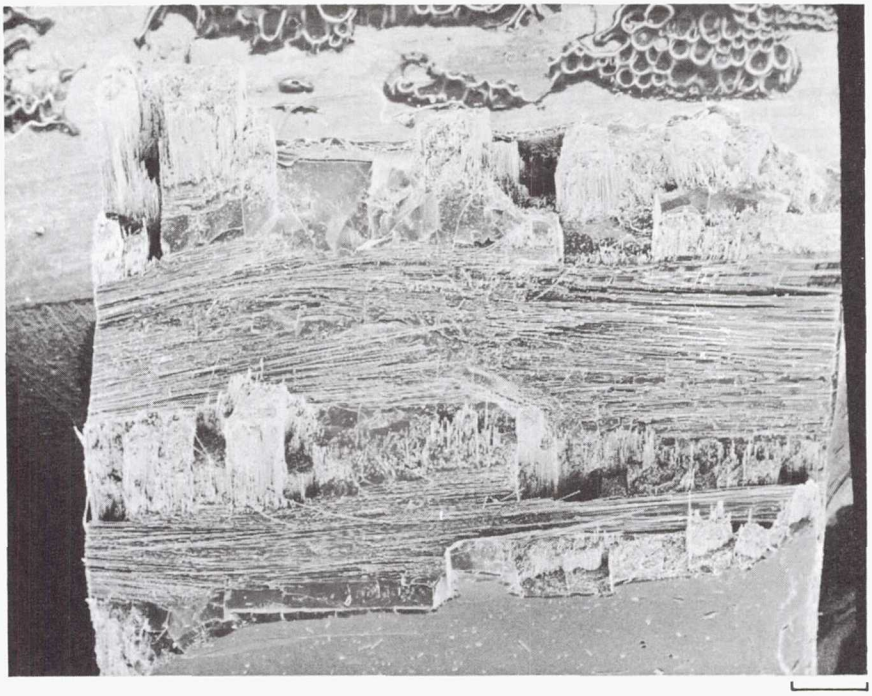

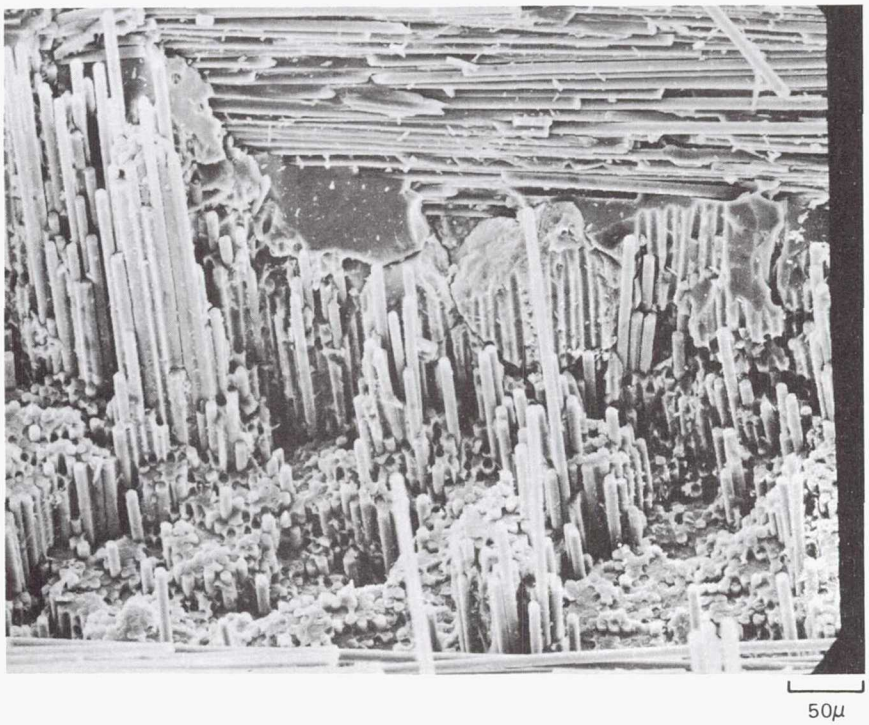

Fig. 34 Fracture Surface of 0/90 — HMS/7740 Tensile Specimen GC 593-3

79-07-69-8

Fig. 35 Fracture Surface of Celion 6000 Paper/7740 Tensile Specimen GC 594-14

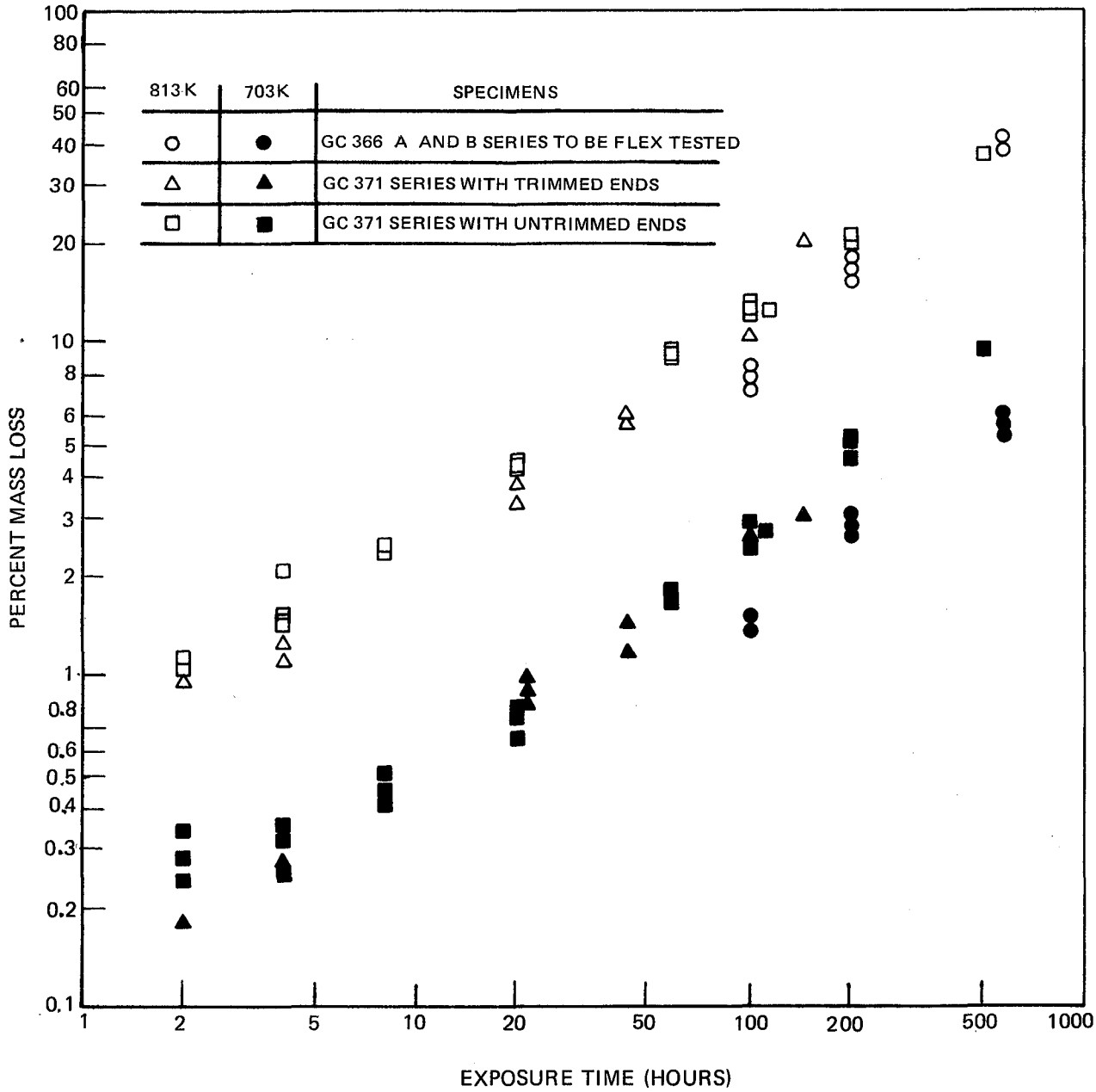

Fig. 36 Change in Mass of HMS Fiber Reinforced 7740 Glass as a Function of Exposure Time in Air at 703 K and 813 K

78-08-67-2

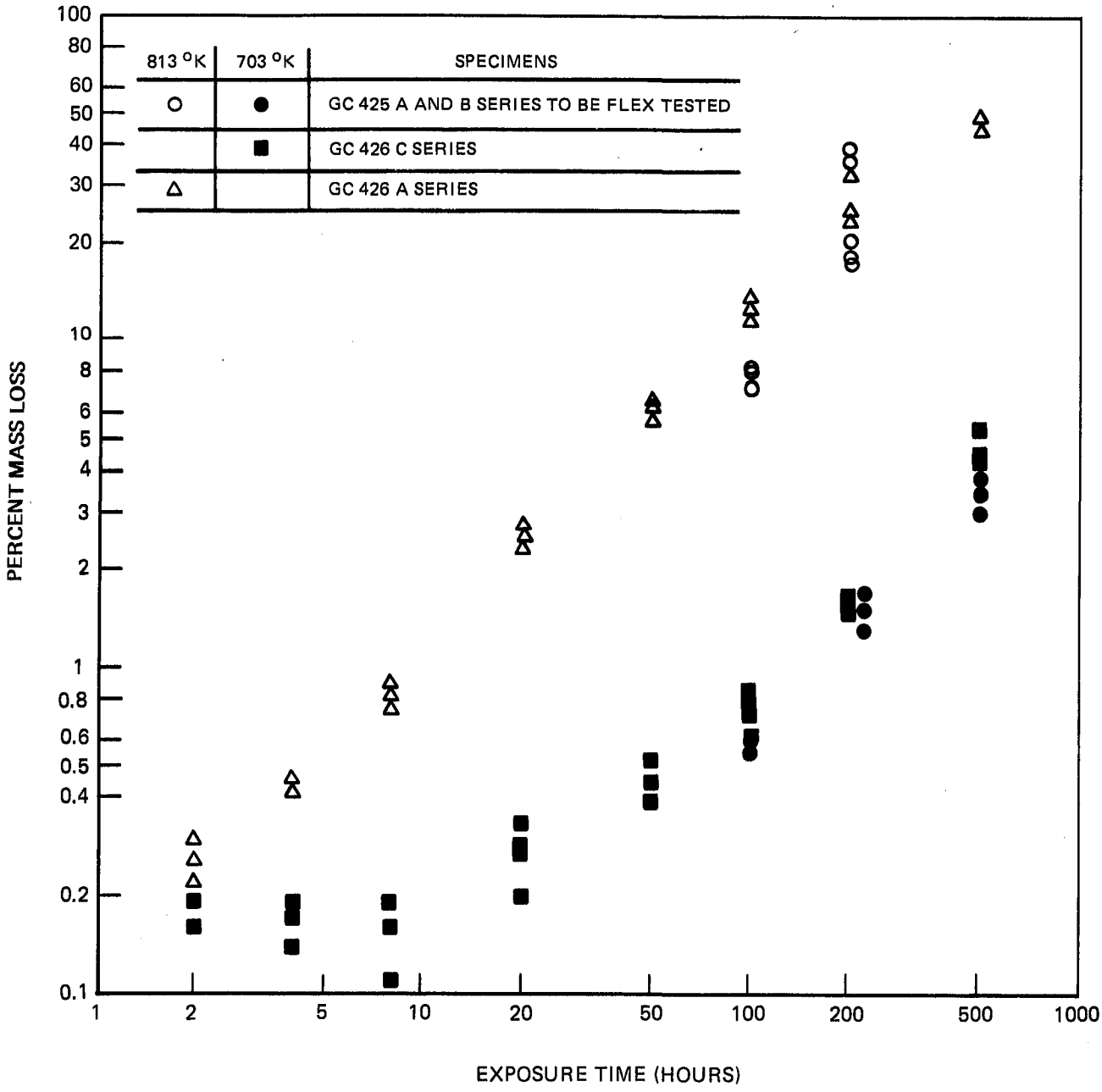

Fig. 37 Change in Mass of GY70 Fiber Reinforced 7740 Glass as a Function of Exposure Time in Air at 703 K and 813 K

78-10-61-2

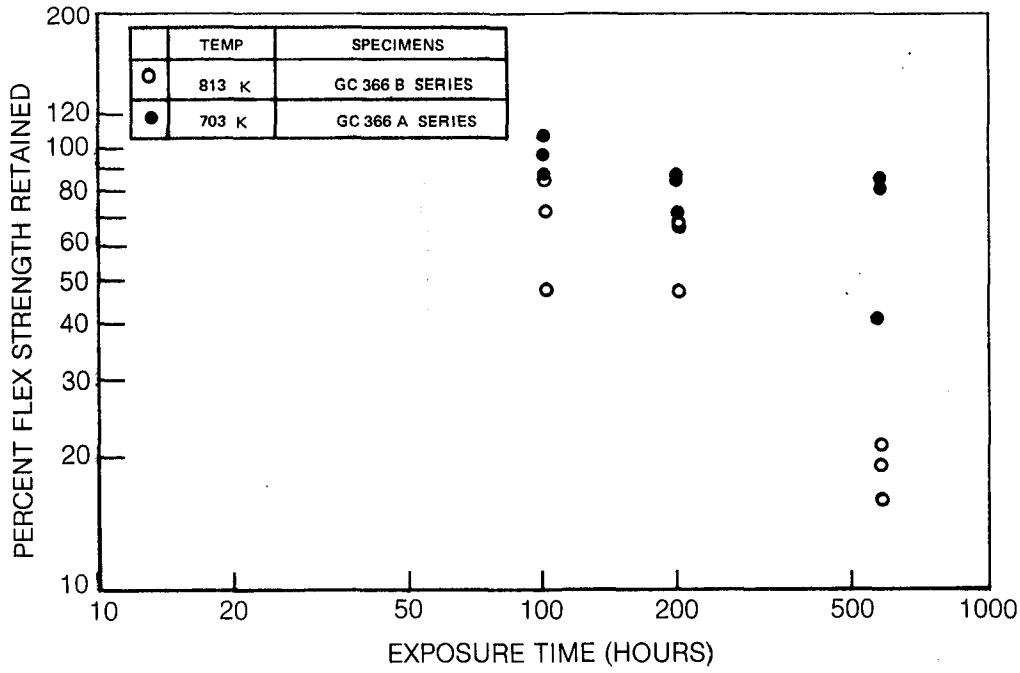

Fig. 38 Change in Flex Strength of HMS Fiber Reinforced 7740 Glass as a Function of Exposure Time in Air at 703 K and 813 K

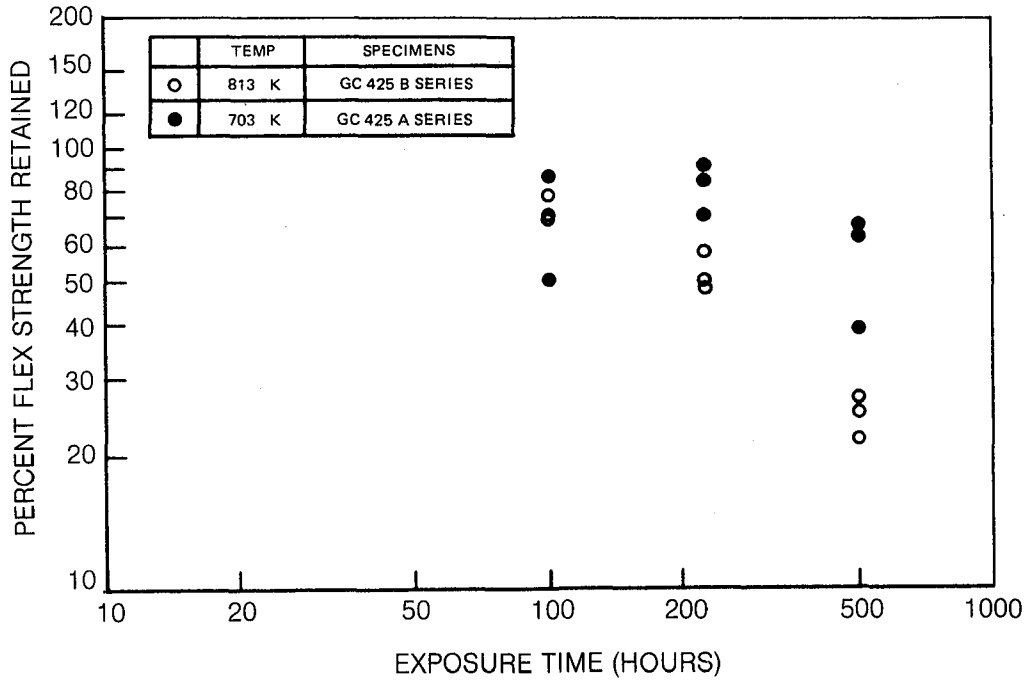

Fig. 39 Change in Flex Strength of GY70 Reinforced 7740 Glass as a Function of Exposure Time in Air at 703 K and 813 K

and one from the transverse sides inward. Figures 40 and 41 can be used to examine the process of fiber oxidation which occurs from the composite specimen sides. As described previously in the experimental procedure, these surfaces were ground prior to exposure to fully expose fibers and remove any excess glass. The transverse section in Fig. 40 is typical of an unexposed specimen which has already been tested to failure in three point bend, while Fig. 41 is the cross section of a specimen which had been exposed at 813 K for 500 hrs. The photograph on the left in this figure illustrates the actual composite structure while the drawing on the right represents the outline of the oxidized portions of material. This transverse section was taken from the center of the exposed specimen so that any end effects, to be discussed below, were not operative in this vicinity. The dark areas in both the photo and the outline are those which have exhibited oxidation of the fibers. As can be seen, the oxidative process proceeds on both a broad front, and also along preferred paths. The latter are frequently, but not always, associated with glass rich regions which exist between adjacent tows of fibers. The fibers adjacent to these glass rich areas appear to be oxidized more rapidly than those within the tows themselves. The drawn outline outer boundary represents the original unoxidized specimen outer surface.

As would be expected, the extent of transverse oxidation increased with increasing time at temperature, Fig. 42. The outlined areas indicate the general progress of fiber oxidation. (Note, the transverse section of specimen GC 371-C-1 in this figure was taken from another portion of the specimen shown in Fig. 41). By taking several sections of oxidized specimens, and measuring the average depth of oxidation penetration, it has been possible to make a plot of transverse penetration depth versus time of exposure, Fig. 45. The average depth was arrived at by measuring the total area of oxidized material and dividing by the original specimen surface length, i.e. twice the thickness plus width.

It was found that the rate of oxidation in the longitudinal direction was much more rapid than that in the transverse direction. This can be seen in Fig. 43 where both the original longitudinal section and the representative outline are presented. In this case the specimen end had been trimmed prior to oxidation to remove any excess glass. As in the case of transverse oxidation, the extent of observable degradation increased with increasing exposure time, Fig. 44, and consisted of paths of preferential attack. The nature of these paths, i.e. glass rich or other, was not resolvable. The average depth of longitudinal oxidation penetration is given in Fig. 45 as a function of exposure time for specimens with both trimmed and untrimmed ends. No discernable difference was noted in penetration of oxidation due to end condition. Note, for the glass rich or untrimmed end specimens, the depth of penetration is taken from the ends of the fibers inward, and not from the outside glass end surface of the specimen.

Fig. 40 Transverse Section of HMS/7740 (Unexposed)

78–08–159–1

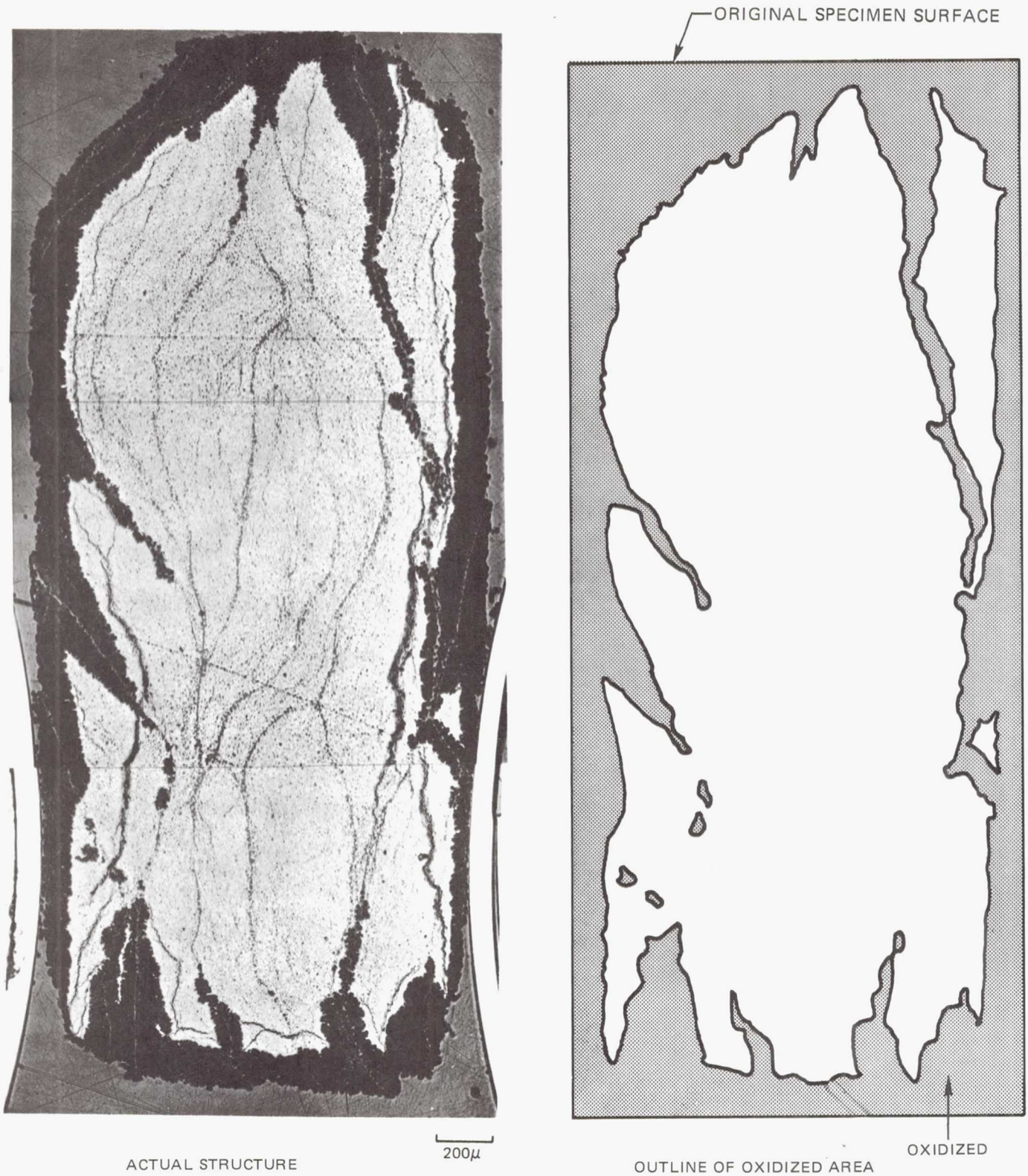

Fig. 41 Transverse Section of HMS/7740 Specimen GC 371-C-1 Oxidized at 813K for 500 Hours

78–08–159–6

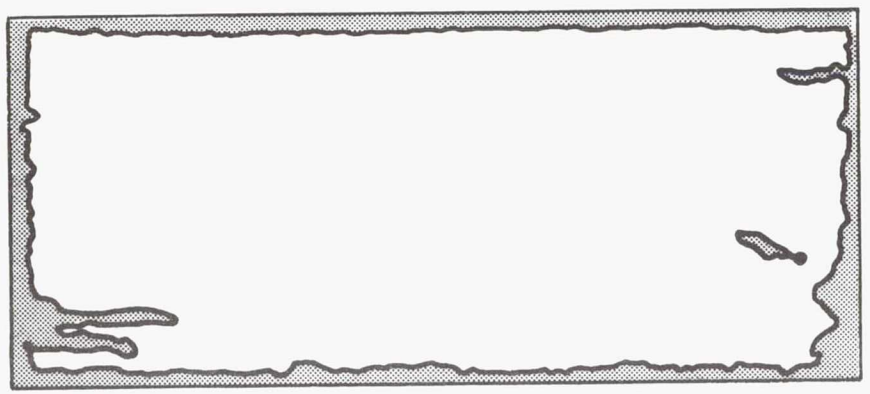

GC 371–C–6
100 HRS

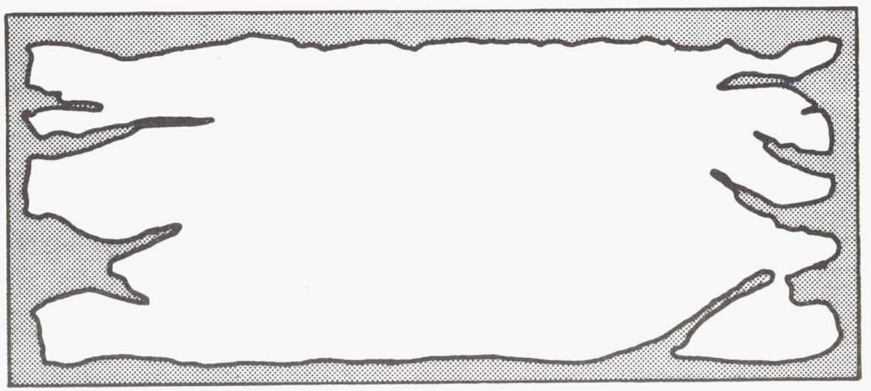

GC 371–C–12
147 HRS

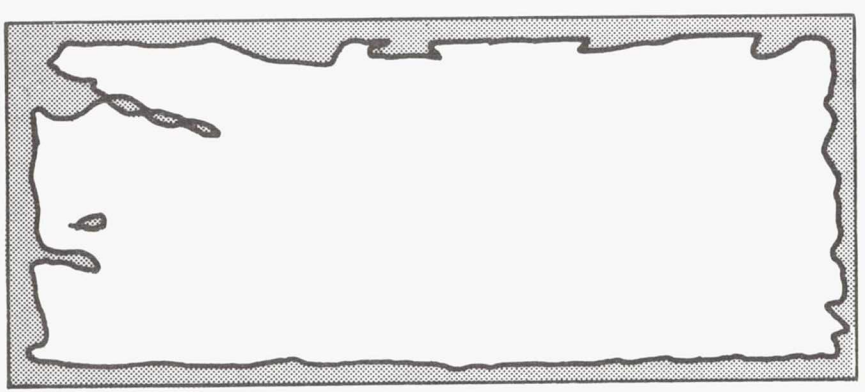

GC 371–C–7
200 HRS

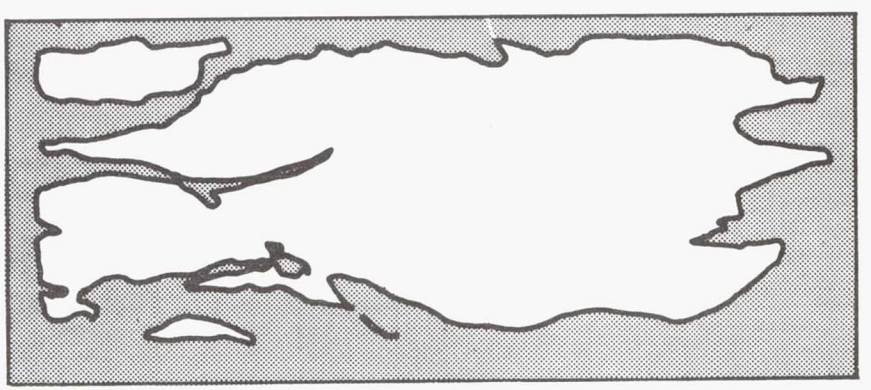

GC 371–C–1
500 HRS

Fig. 42 Transverse Sections of HMS/7740 Specimens Oxidized at 813K

78–08–159–4

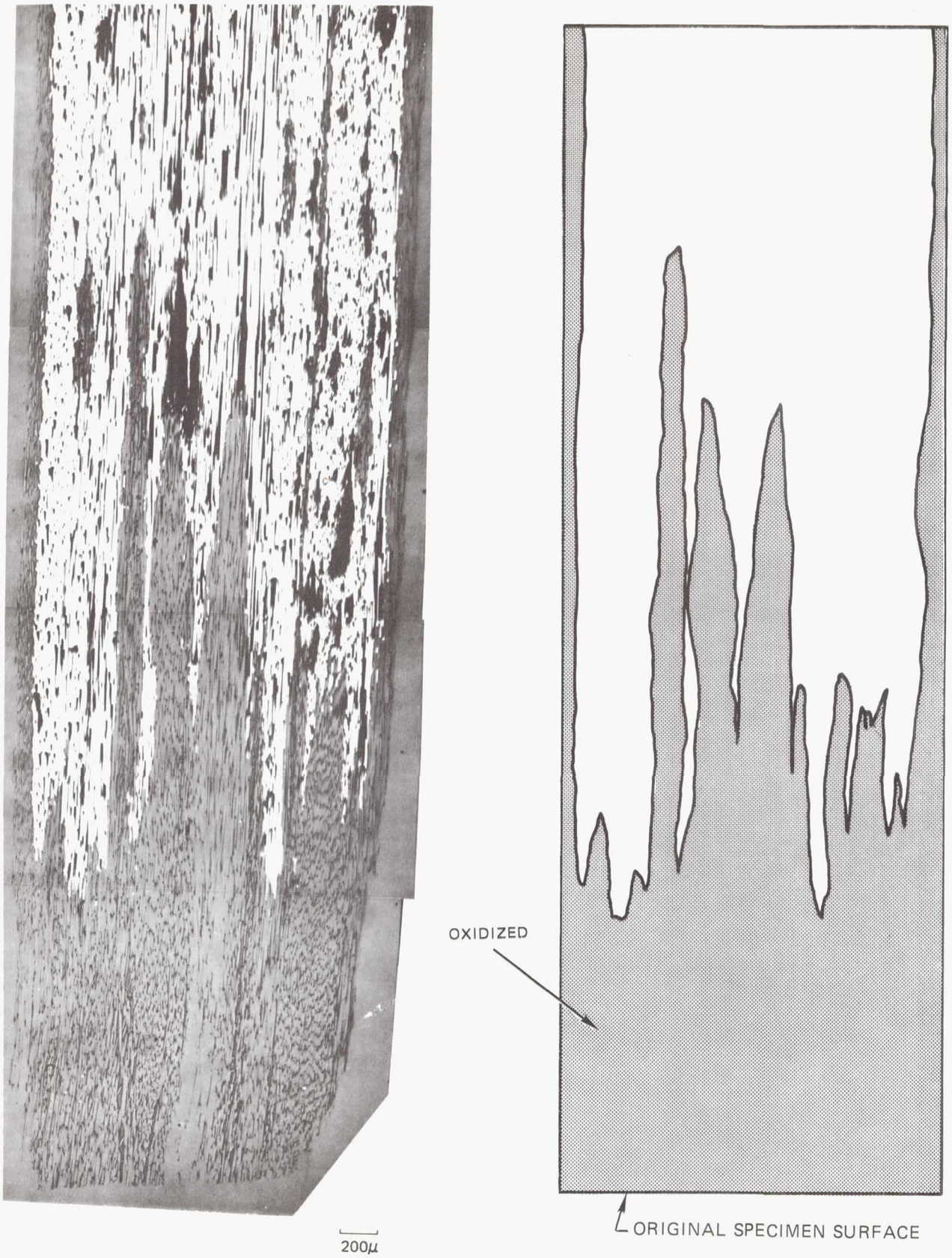

Fig. 43 Longitudinal Section of HMS/7740 Specimen GC371-C-12 Oxidized at 813K for 147 Hrs (Trimmed Specimen End)

78-08-159-3

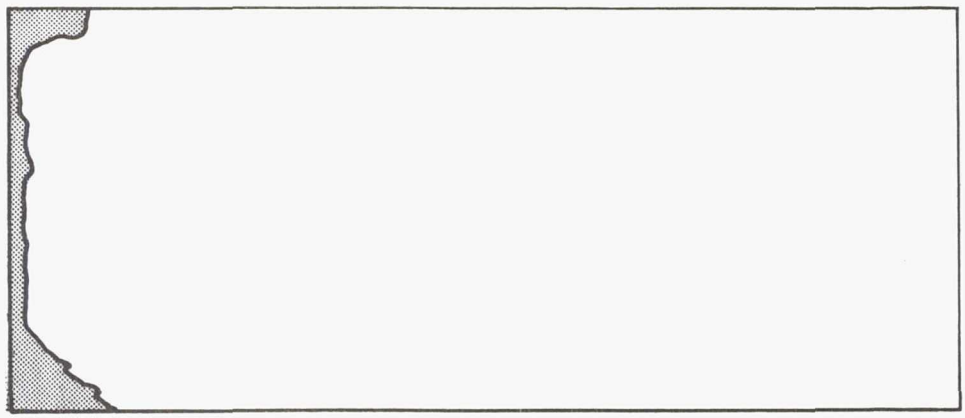

GC 371–C–11
20 HRS

GC 371–C–9
40 HRS

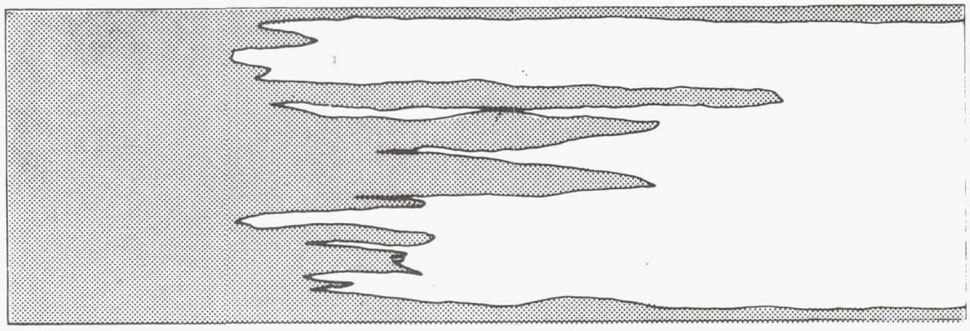

GC 371–C–12
147 HRS

Fig. 44 Longitudinal Sections of HMS/7740 Specimens Oxidized at 813K

78–08–159–5

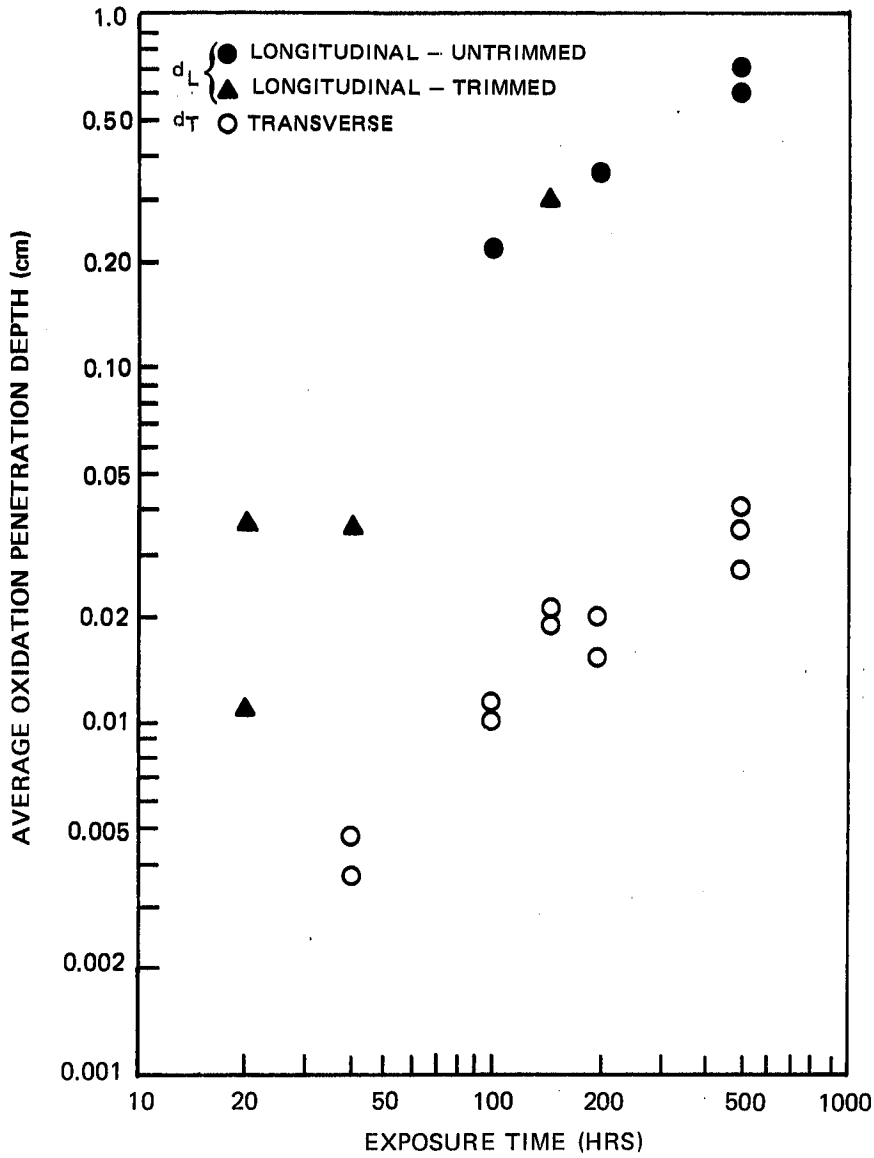

Fig. 45 Average Depth of Oxidation Penetration in HMS/7740 as a Function of Exposure Time at 813K in Air

78-09-10-3

By use of the data in Fig. 46 it was possible to calculate the contributions to specimen mass loss due to both transverse and longitudinal penetration. The total percent mass loss can be calculated using the formula

$$\% \text{ Mass Loss} = \frac{(\rho_F)(v/o\ F)(d_L\ A_L + d_T\ A_T)}{W_c}$$

where ρ_F = density of the fiber
$v/o\ F$ = the volume percent of fiber
d_L, d_T = longitudinal and transverse depth of penetration respectively
A_L, A_T = longitudinal and transverse original specimen surface areas respectively
W_c = original unoxidized mass of the composite.

The resultant total calculated mass loss, as well as the individual longitudinal and transverse contributions, are presented in Fig. 46. The range of originally measured mass loss is also plotted in the figure and it can be seen that the calculated and measured values agree quite well. It is also interesting to note that, although the rate of oxidation is much more rapid from the specimen ends, the relatively small specimen end surface area causes this path to be the minor contributor to total specimen mass loss.

An attempt has also been made to calculate the expected rate of composite flexural strength loss due to oxidation. This has been accomplished by assuming that strength loss is due to a simple reduction in composite beam transverse cross section and that the effects of nonuniform transverse attack are unimportant. The calculation was put in the following form to result in a measure of percent flexural strength retained

$$\% \text{ Flexural Strength Retained} = \frac{(b-2d_T)(h-2d_T)^2}{bh^2} \times 100\%$$

where b,h = the original unexposed specimen width and depth.

This formula stems from the ratio of three point bend flexural strengths of exposed and unexposed specimens. The calculated level of strength retention is presented in Fig. 47 along with the originally measured data reported previously. The level of agreement substantiates the postulated mechanism and indicates that there are no major additional degrading effects due to a notch sensitivity or the occasional deeply penetrating regions of degradation.

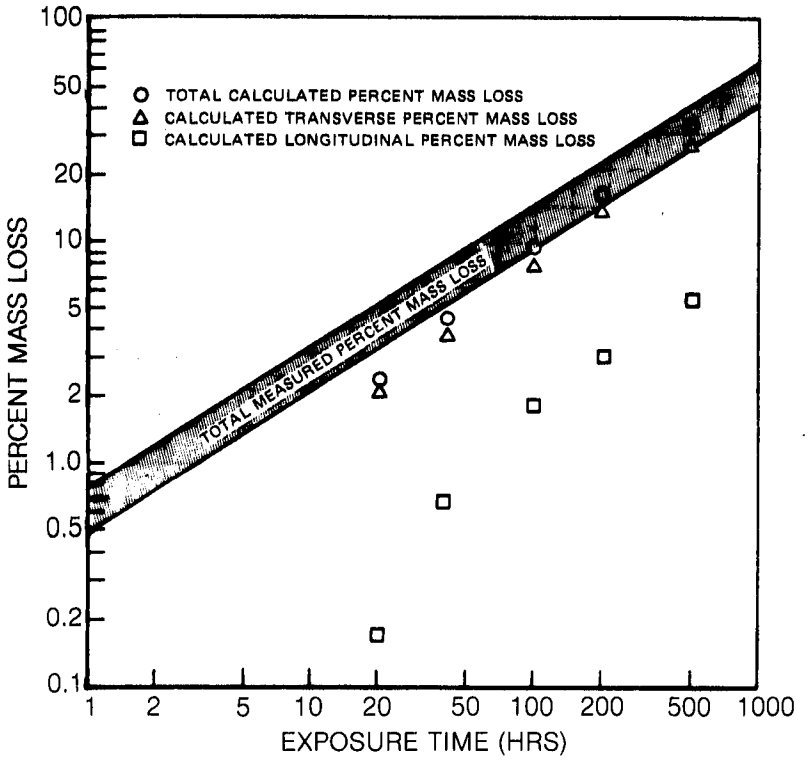

Fig. 46 Comparison of Calculated and Measured Mass Loss of HMS/7740 Specimens Oxidized at 813K in Air

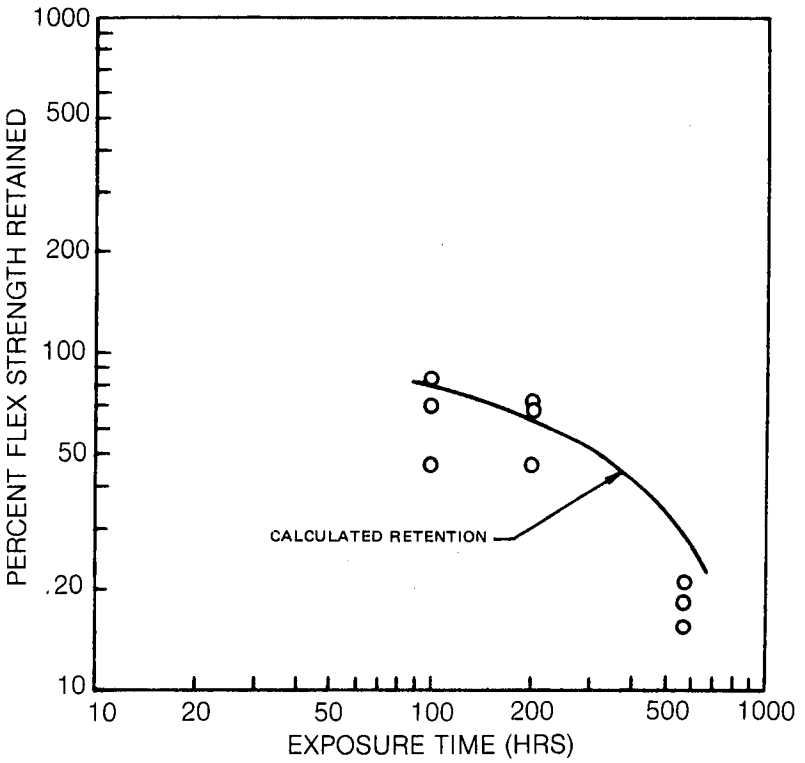

Fig. 47 Comparison of Calculated and Measured Flex Strength Retention for HMS/7740 Oxidized at 813K in Air

80-5-82-17

The results obtained by thermally cycling specimens were rather similar in form to those obtained by static thermal exposure. Both the HMS and GY70 fiber reinforced composites exhibited gradual mass loss with increasing number of cycles and this mass loss caused a measurable decrease in composite flexural strength, Figs. 48 and 49. In the case of thermal cycling to 813 K, examination of the thermal history which took place during each cycle, Fig. 50, it can be judged that 1000 cycles corresponds to approximately 117 hrs at temperatures above 573 K and nearly 75 hrs at 813 K. The 70 to 85% strength retention after 1000 cycles, Fig. 48, is in good agreement with the level of strength retained after 100 hrs of constant temperature exposure, Fig. 38.

Several thermal cycling experiments were also performed on 0/90 cross plied composite material to ascertain whether the degradation mechanism is accelerated by a complex lay-up pattern. The data, Table XII, indicate no degradation after 500 thermal cycles which is, in fact, superior to the data presented in Fig. 49 for unidirectionally reinforced material.

G. Thermal Expansion

The axial and transverse thermal expansion of unidirectionally reinforced HMS/7740 composites is presented in Figs. 51-54. In both cases a series of six thermal cycles was performed with the first three cycles going to a maximum temperature of approximately 725 K and the last three cycles extending the maximum temperature to 860 K. The initial axial thermal expansion curve, Fig. 51, presents several interesting features. First, the initial deformation of the specimen on heating is a contraction. The rate of contraction decreases with increasing temperature until, at about 510 K, the specimen reverses the direction of deformation and begins to expand. Thus, over a limited temperature range, the thermal expansion coefficient is approximately zero due to the reversal of deformation. Also of importance is the observation that the heating and cooling curves do not coincide, but instead there is evidence of a hysteresis effect. By comparison with cycle 2 it is clear that this hysteresis is transient and, for almost all of the second thermal cycle, has disappeared. A residual strain at room temperature remains, however. Because of the very small magnitude of the residual strain it was not clear whether this is an artifact, due to a failure of the system to return completely to the initial starting condition, or whether it is indeed a true residual contraction of the specimen.

By increasing the maximum temperature, Fig. 52, it can be seen that the hysteresis effect once again becomes prominent. Additional thermal cycles also tend to decrease the magnitude of this difference between heating and cooling, although it is still quite evident in the sixth cycle.

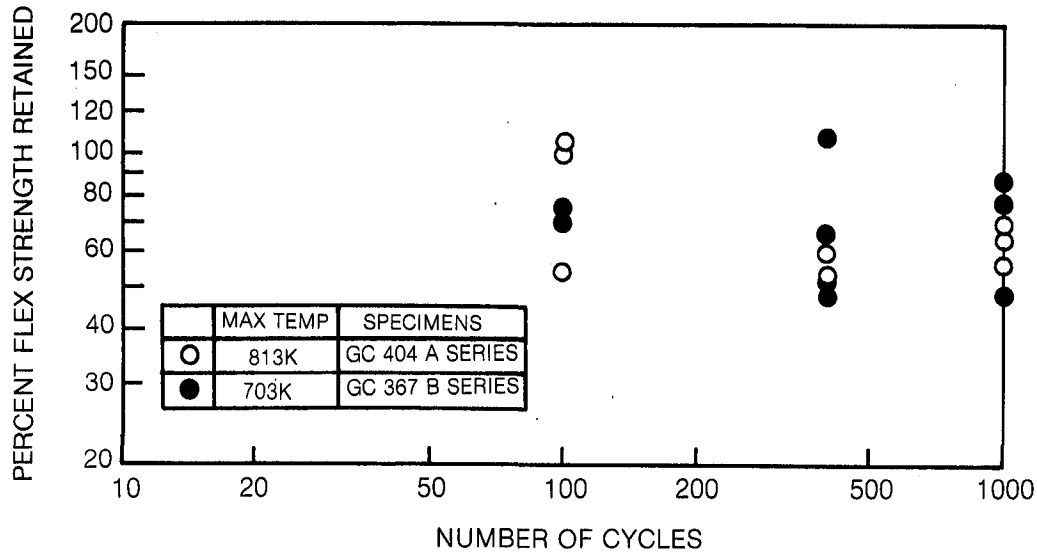

Fig. 48 Change in Flex Strength of HMS Fiber Reinforced 7740 Glass as a Function of Number of Thermal Cycles in Air

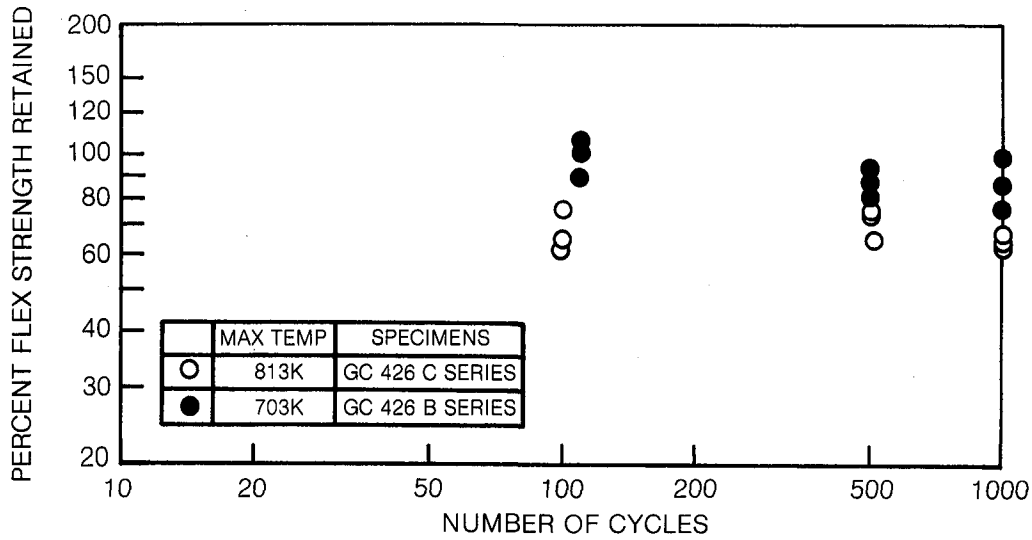

Fig. 49 Change in Flex Strength of GY70 Fiber Reinforced 7740 Glass as a Function of Number of Thermal Cycles in Air

80-5-82-15

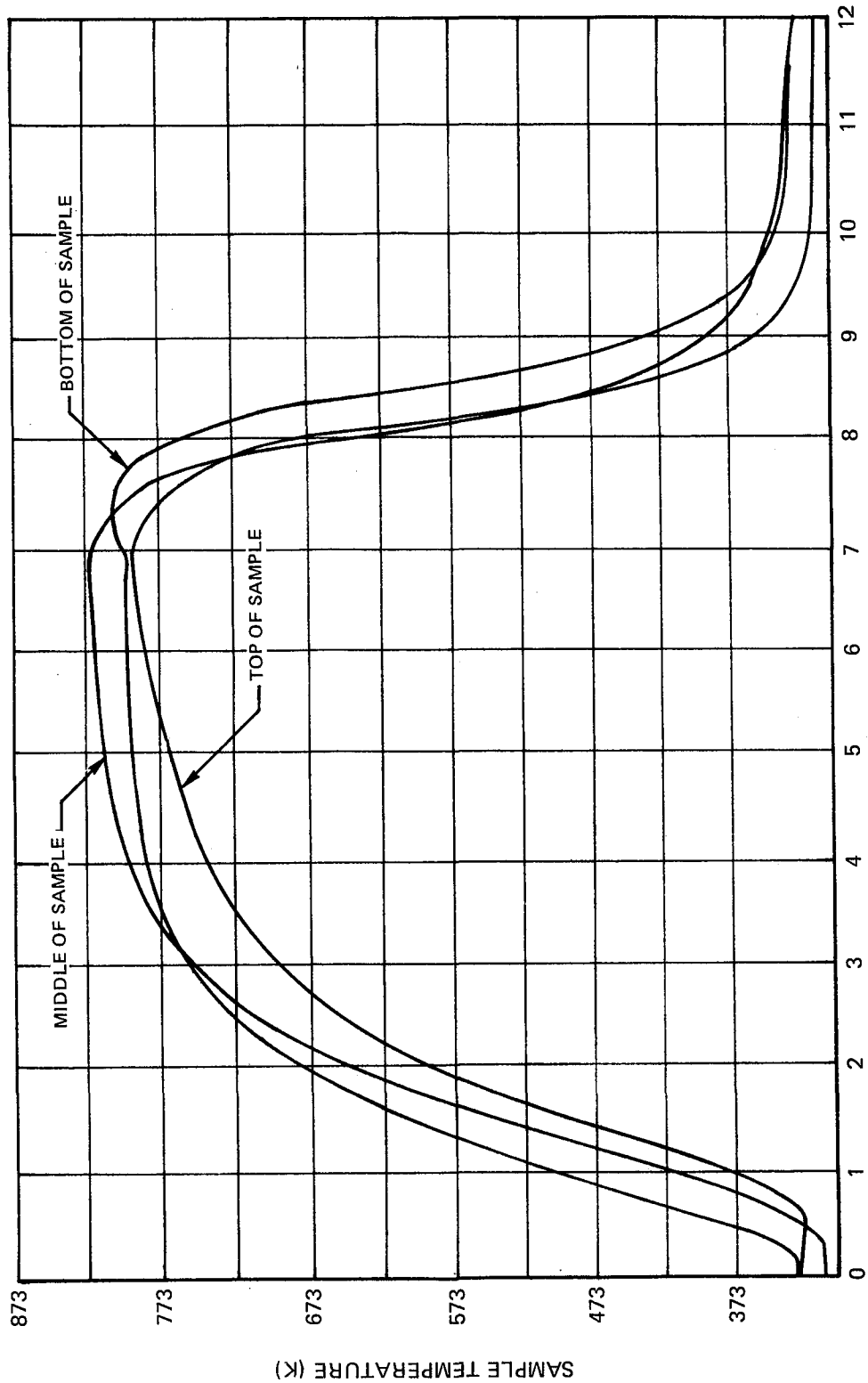

Fig. 50 Specimen Temperature as a Function of Time for Thermal Cycling in Air Between 323K and 813K

78–08–67–3

Table XII

Flexural Strength of 0/90 - GY70/7740 after Thermal Cycling in Air Between 323 K and 703 K

Number of Cycles	Three Point Flex. Strength (MPa)
0	207
0	145
0	248
0	213
500	210
500	209
500	210

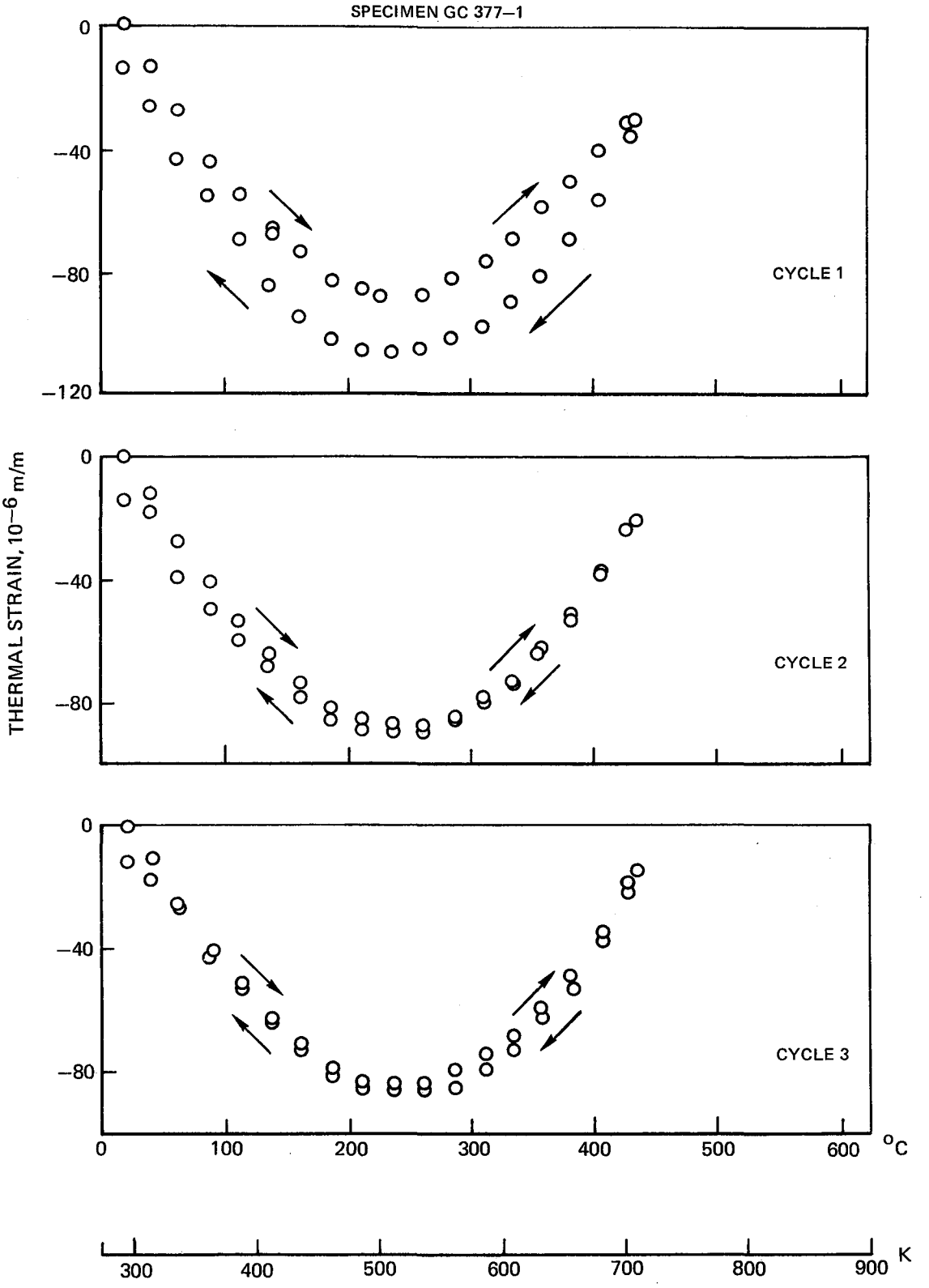

Fig. 51 Axial Thermal Expansion of Unidirectionally Reinforced HMS/7740 Cycles 1,2,3

79–04–144–1

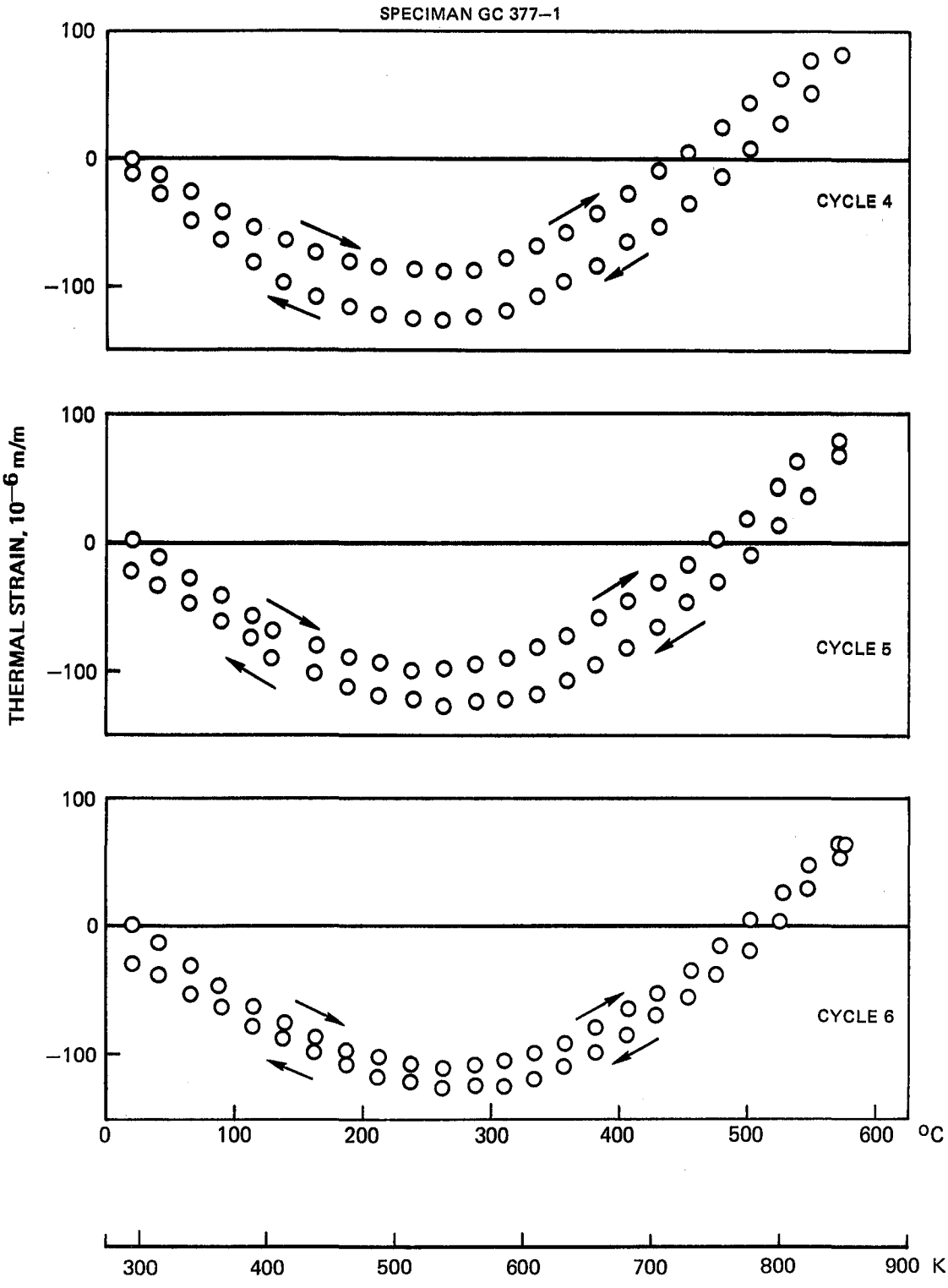

Fig. 52 Axial Thermal Expansion of Unidirectionally Reinforced HMS/7740 Cycles 4,5,6

79–04–144–2

To further examine the nature of this effect, this tested specimen GC 377-1 was allowed to "age" in the ambient laboratory environment for 60 days after which time it was placed once again in the dilatometer and cycled between 300 K and 680 K. No hysteresis effects were noted during this thermal excursion and the shape of the strain versus temperature curve agreed with that shown in Fig. 51. Thus the "precycling" treatment succeeded in substantially stabilizing composite thermal performance.

It is interesting to note that in all of the thermal cycles shown in Figs. 51 and 52, the cooling curve occurred at more negative strain values than the heating curve. Also, the residual strain was always negative. The reason for this probably relates to the fact that the graphite fiber has a highly negative axial thermal expansion coefficient (approximately-1 x 10^{-6} K^{-1}) while 7740 glass has a positive value of 3.2 x 10^{-6} K^{-1}. Thus, on heating the composite contracts and the matrix is loaded in compression. It is likely that the fibers may slip slightly along the fiber-matrix interface and some compressive matrix yield may also occur. On cooling the specimen attempts to return to its initial room temperature dimension; however, because of the above two postulated effects which occurred at the elevated temperature, it cannot. Thus the cooling curve occurs with more negative strain values and a residual negative strain remains after test. It should be noted, however, that this material was fabricated at elevated temperature and was subjected to one very large cooling cycle prior to the cycles herein reported. From the above data it would appear that if the composite were subjected to several thermal cycles prior to removal from the fabrication hot press almost all signs of hysteresis would be removed from subsequent tests. It should also be noted that the levels of strain which are being measured are extremely small, i.e. 20 x 10^{-6} m/m. For a 2.54 cm long specimen this corresponds to 5 x 10^{-5} cm.

The transversely oriented specimen thermal expansion behavior, Figs. 53,54 differs significantly from that of the axial material. The magnitude of strain measured is much larger and is everywhere positive. The first three cycles, run to a maximum temperature of 725 K, exhibit no evidence of hysteresis using the scales shown. In actual fact, however, there was some hysteresis which is observable on a higher resolution scale. As in the case of the axial specimens, however, it has not yet been demonstrated that the residual strain measured at room temperature is purely due to the composite and not an artifact of the experimental apparatus and procedure. Reheating to the higher temperature of 865 K, Fig. 54 cycle 4, caused a larger hysteresis effect which decreased with additional cycles. The reasons for this transverse hysteresis are less clear

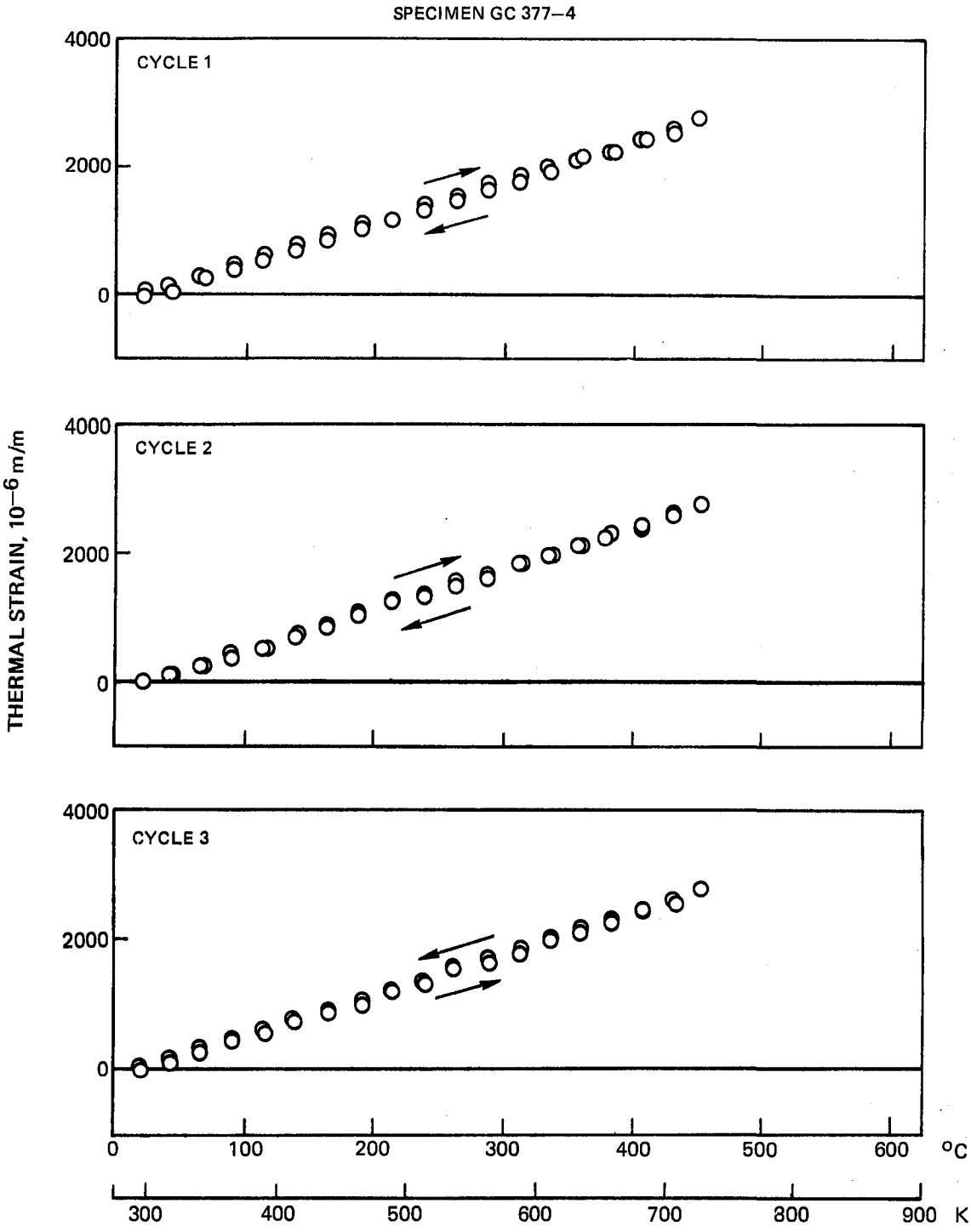

Fig. 53 Transverse Thermal Expansion of Unidirectionally Reinforced HMS/7740 Cycles 1,2,3

79–04–144–3

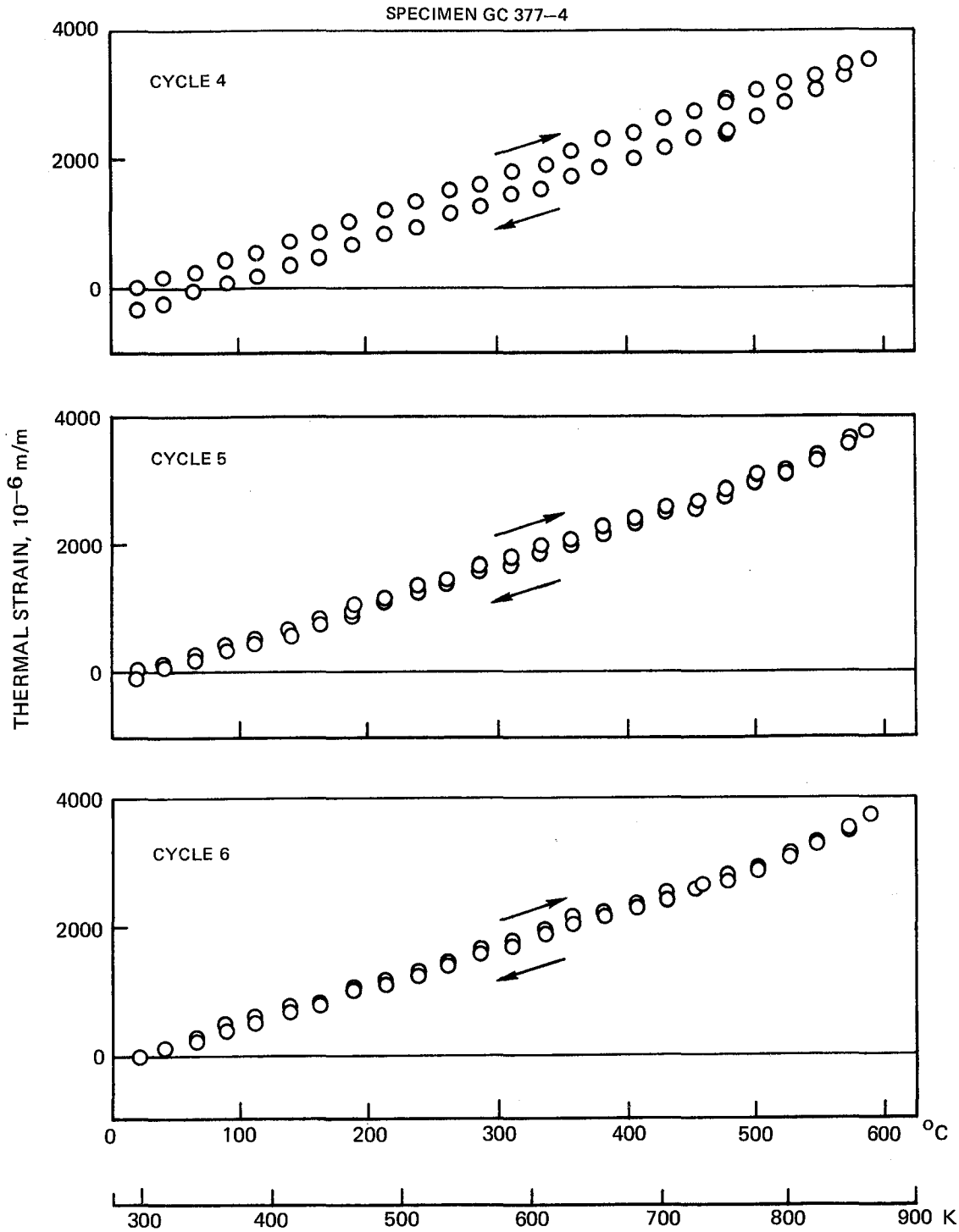

Fig. 54 Transverse Thermal Expansion of Unidirectionally Reinforced HMS/7740 Cycle 4,5,6

79–04–144–4

since the fiber transverse thermal expansion (α_f^t) is not well known. Values of α_f^t larger than that of the 7740 matrix, however, have been quoted in the literature and the overall composite transverse thermal expansion coefficient would agree with this.

Similar axial and transverse thermal strain vs temperature curves for unidirectional GY70 (Figs. 55,56), Thornel Pitch (Figs. 57,58), and Thornel 300 (Figs. 59,60) fiber reinforced composites are also presented for temperatures of up to 625 K. The general features of these materials' behavior agree with those of the above described HMS/7740. Two major differences, however, are the values of thermal expansion coefficient and location of the axial specimen inflection point ($\alpha = 0$). It appears that this point occurs at a higher temperature for the higher modulus Thornel pitch fiber than for either of the other materials. The thermal expansion coefficients for all of the fiber reinforced glass composites are listed in Table XIII. These values, taken from the figures at 300 K in both the axial and transverse directions, indicate the tendency for a more negative axial coefficient with increasing fiber elastic modulus. The following expression, which has been used successfully to calculate composite axial thermal expansion, illustrates how this can happen:

$$\alpha_{11}{}^c = \frac{E_m \alpha_m V_m + E_f \alpha_f^a V_f}{E_m V_m + E_f V_f}$$

E, V and α are the elastic modulus, volume percent and thermal expansion of fiber and matrix, and the α_f^a term refers to the axial component of fiber thermal expansion. Thus, even without altering the already negative value of α_f, an increase in fiber elastic modulus will result in a more negative value of composite axial thermal expansion, $\alpha_{11}{}^c$.

A recent tabulation of GY 70 fiber data (Ref. 5) permits an examination of the validity of the above expression. The fiber properties are E_f = 537 GPa, $\alpha_f^a = -1.08 \times 10^{-6}$ K^{-1} while 7740 matrix properties are E_m = 62.7 GPa and $\alpha_m = 3.25 \times 10^{-6}$ K^{-1}. Using these values and a fiber volume fraction of 75% obtained experimentally, a resultant value for $\alpha_{11}{}^c$ was calculated to be -0.92×10^{-6} K^{-1}. This is in excellent agreement with the value of -1.0×10^{-6} K^{-1} obtained experimentally.

The composite transverse thermal expansion coefficient $\alpha_{22}{}^c$ did not indicate a consistent trend with fiber elastic modulus. At present an accurate formulation for the calculation of $\alpha_{22}{}^c$ based on fiber and matrix properties is not available because of the extreme complexity introduced by the orthotropic nature of the fiber.

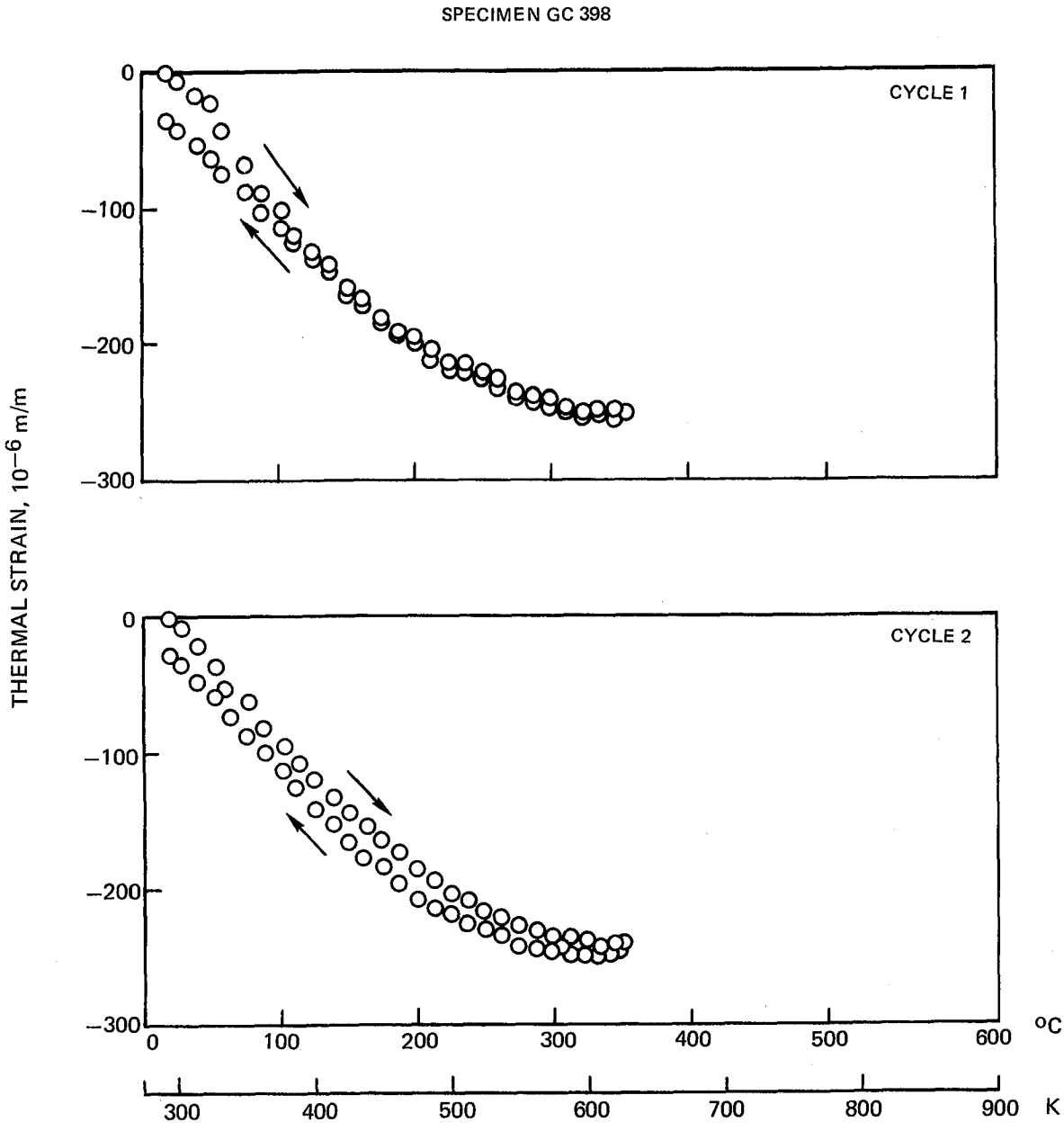

Fig. 55 Axial Thermal Expansion of Unidirectionally Reinforced GY70/7740 Cycles 1,2

79-04-144-5

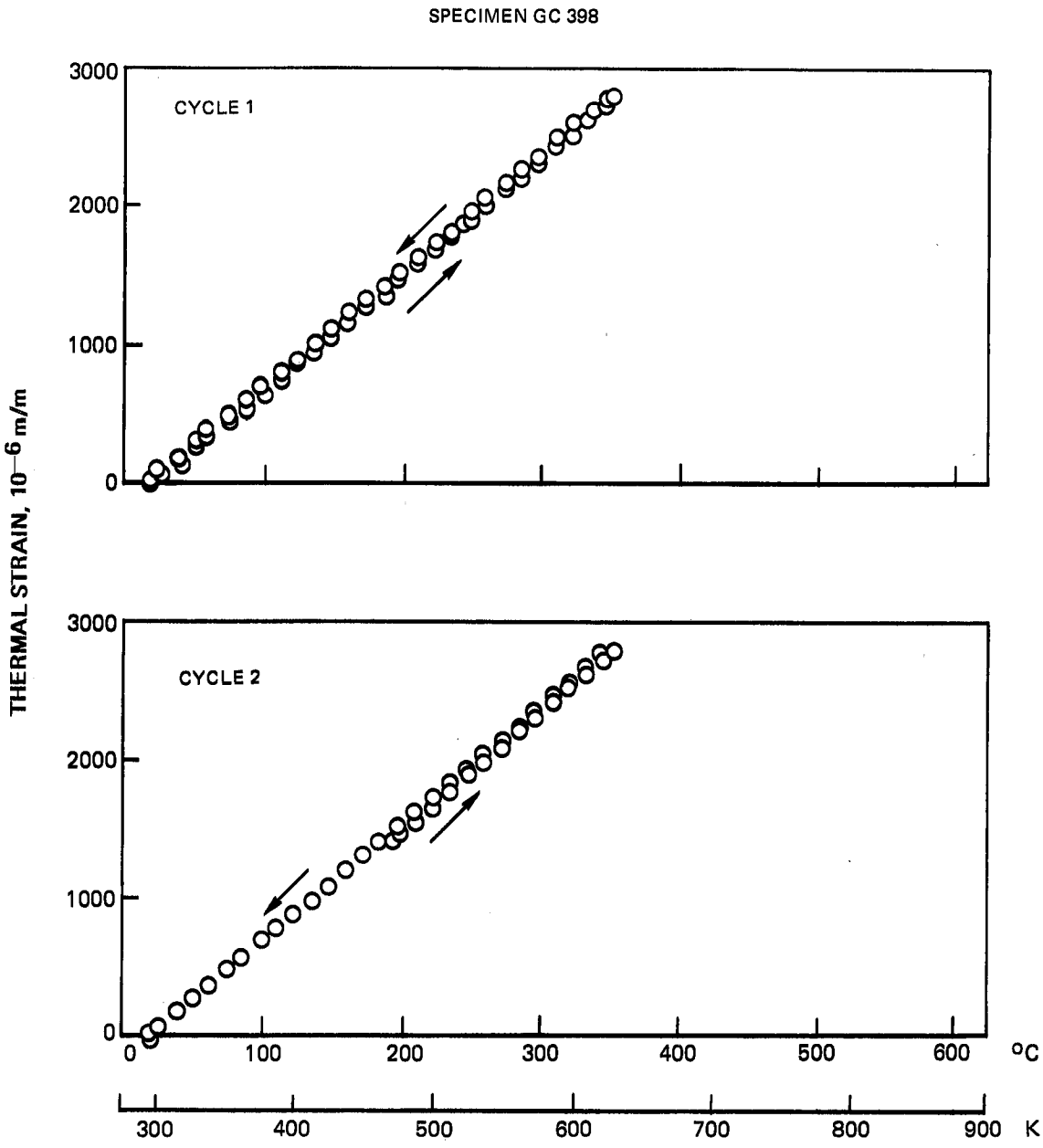

Fig. 56 Transverse Thermal Expansion of Unidirectionally Reinforced GY 70/7740 Cycles 1,2

79-04-144-6

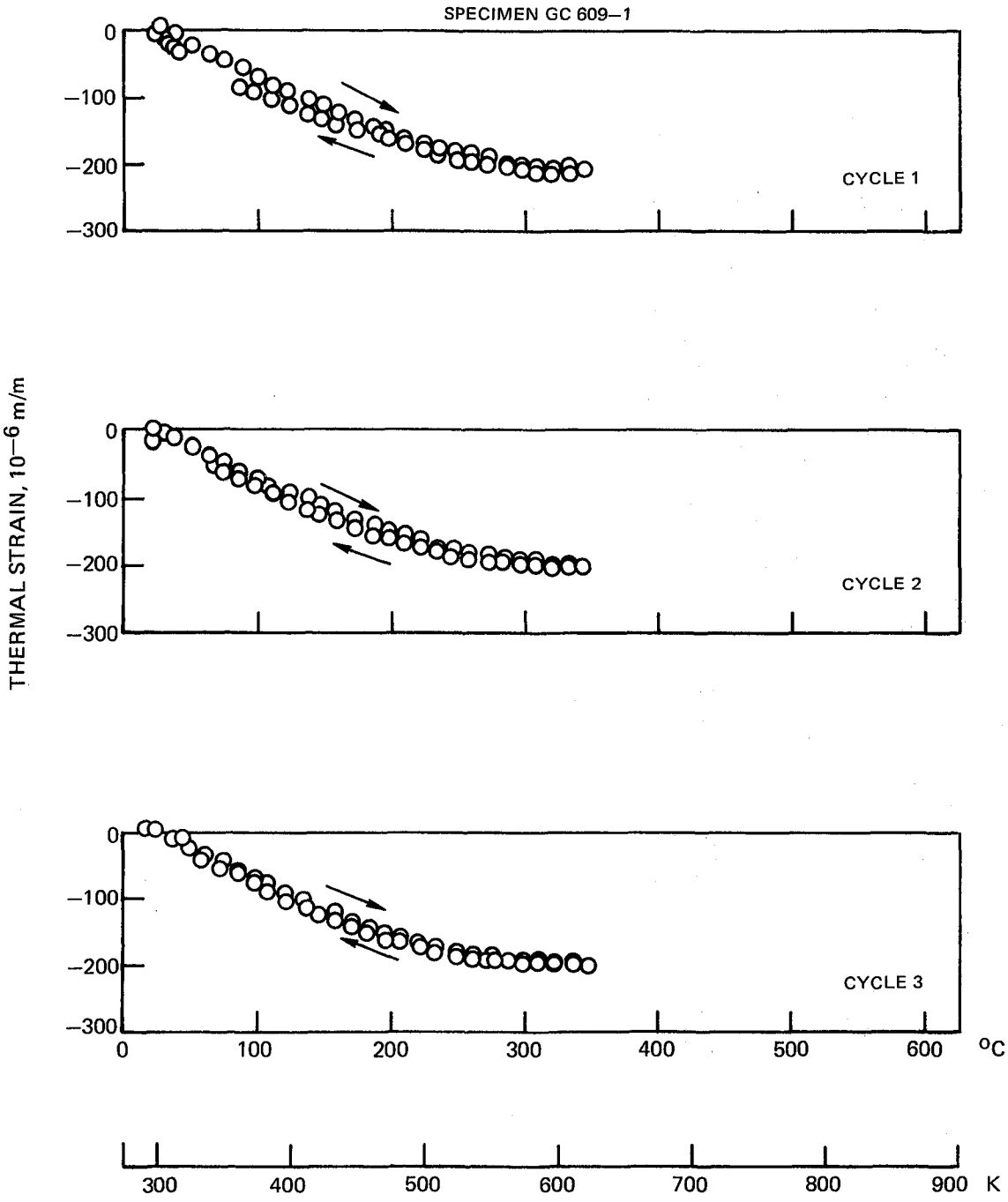

Fig. 57 Axial Thermal Expansion of Unidirectionally Reinforced Thornel Pitch (VS0054-0)7740, Cycles 1,2,3

79–06–70–3

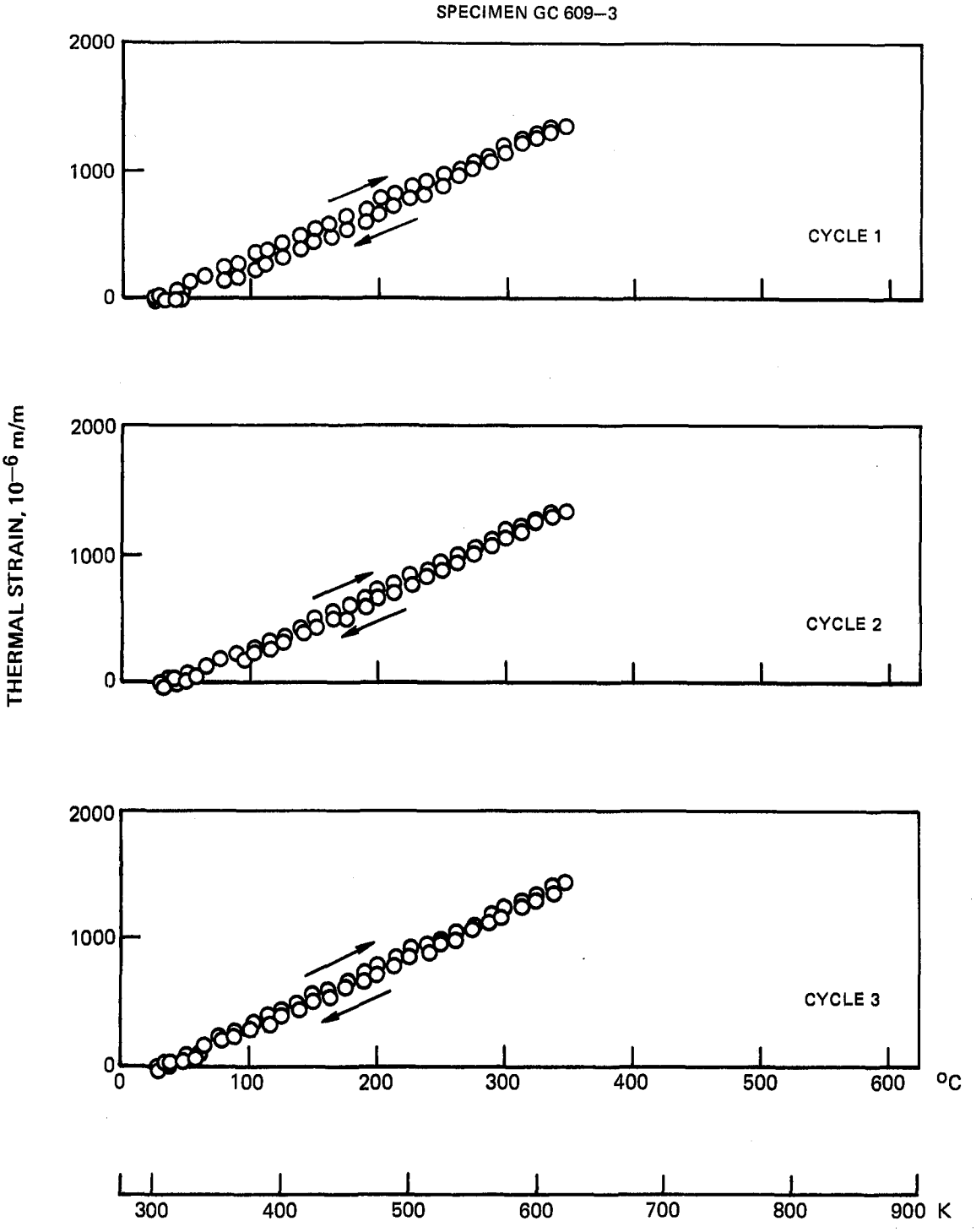

Fig. 58 Transverse Thermal Expansion of Unidirectionally Reinforced Thornel Pitch (VS0054-0) 7740, Cycles 1,2,3

79–06–70–2

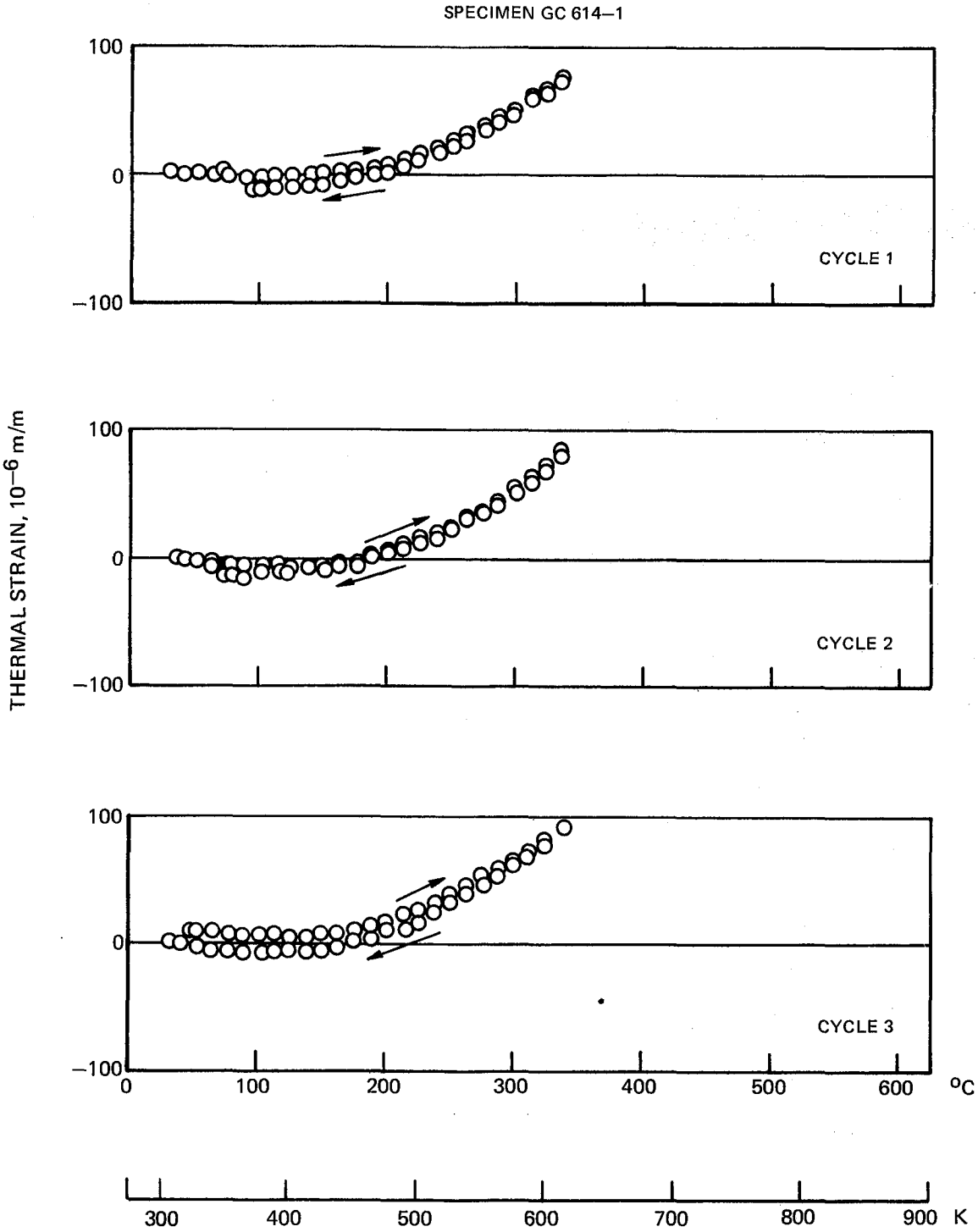

Fig. 59 Axial Thermal Expansion of Unidirectionally Reinforced Thornel 300/7740, Cycles 1,2,3

79–06–70–4

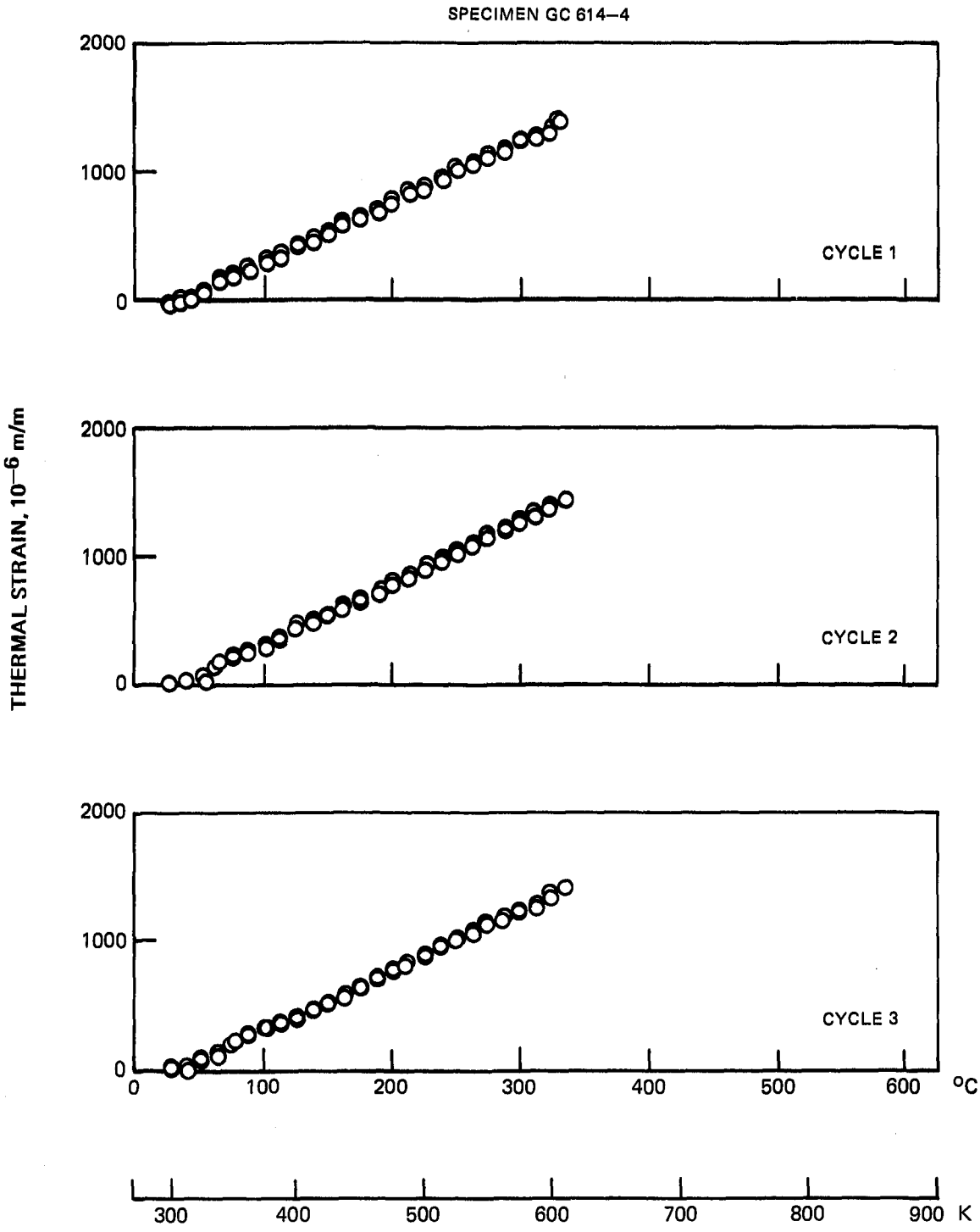

Fig. 60 Transverse Thermal Expansion of Unidirectionally Reinforced Thornel 300/7740, Cycles 1,2,3

79–06–70–5

Table XIII

Thermal Expansion at 300 K of Graphite Fiber Unidirectionally Reinforced 7740 + 2% SiO_2 Matrix Composites

Composite	Fiber Type	Fiber Elastic Modulus (GPa)	v/o Fiber	Thermal Expansion Coefficient (10^{-6} m m^{-1} K^{-1})	
				0°	90°
377	HMS	350	70	-0.50	+6.5
398	GY70	537	75	-1.0	+8.1
609	Pitch (VS0054-0)	654	50	-1.0	+4.4
614	Thornel 300	234	54	-0.10	+4.6

Table XIV

GY 70 Fiber Reinforced 7740 Composite Thermal Expansion Coefficients

Composite Lay-Up	$\alpha_{300\ K}$ (10^{-6} m m^{-1} K^{-1})	$\alpha_{300-550\ K}$ (10^{-6} m m^{-1} K^{-1})
Unidirectional @ 0°	-1.0	-0.95
@ 90°	+8.1	+8.1
0/90 Cross Ply	-0.8	-0.6

The thermal expansion of a 0/90 cross ply GY70 fiber reinforced 7740 composite is presented in Figs. 61 and 62. These curves bear a close resemblance to those obtained for the axial thermal expansion of unidirectionally reinforced GY 70/7740, Figs. 55,56. However, there are some differences. First, the slope of the curve is slightly less than that for the unidirectional case at 300 K and the overall specimen contraction up to 500-600 K is significantly less. The data are compared in Table XIV in terms of thermal expansion coefficients. Second, the apparent extent of hysteresis is less for the 0/90 composite. Within the resolvable limits of the experimental system, it does not appear that, after the first cycle, there is any residual specimen strain after thermal cycling. As can be seen in Figs. 61 and 62. the final specimen dimensions are equivalent to the starting dimensions.

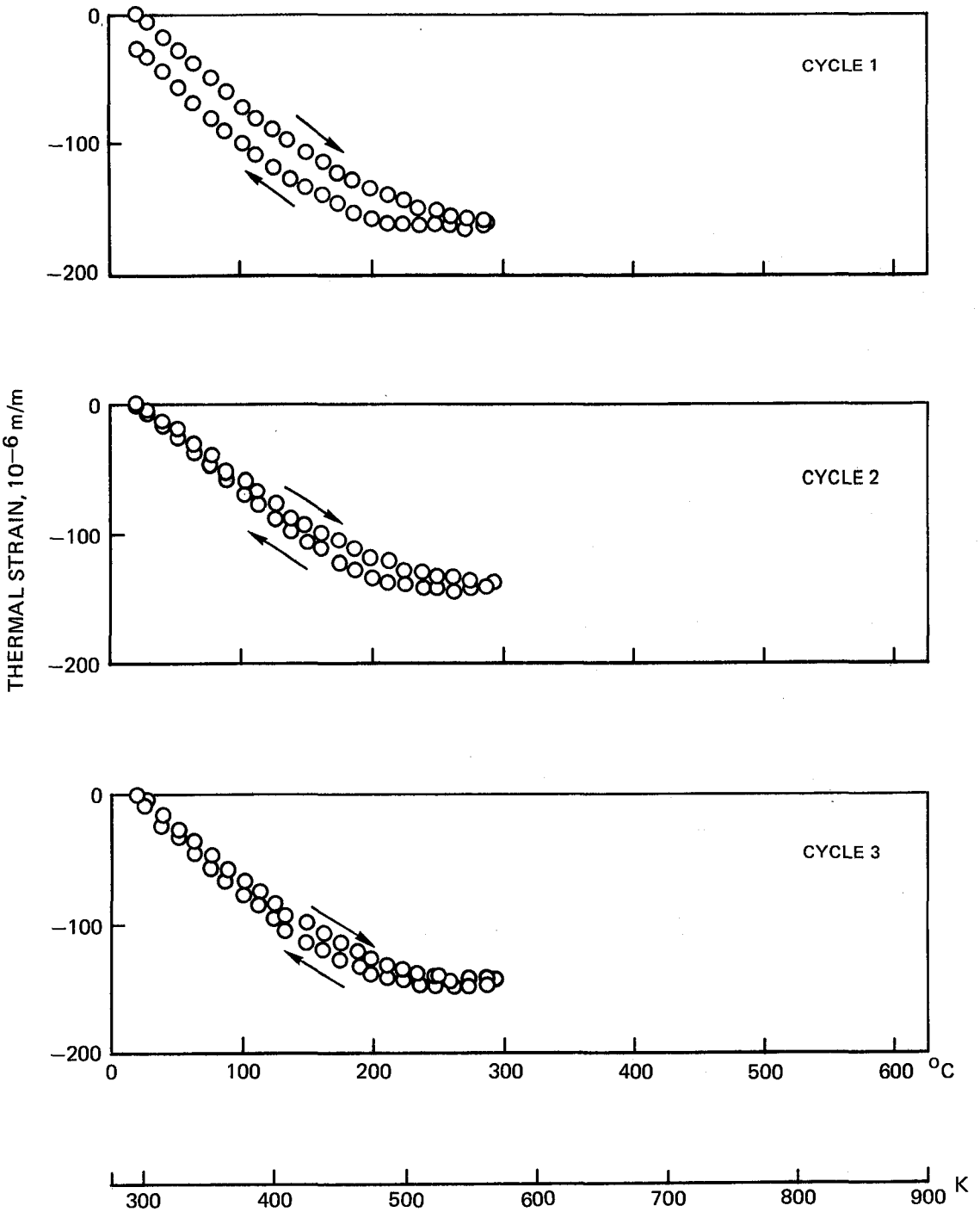

Fig. 61 0° Thermal Expansion of 0/90 Reinforced GY70/7740 Cycles 1,2,3

79-04-144-9

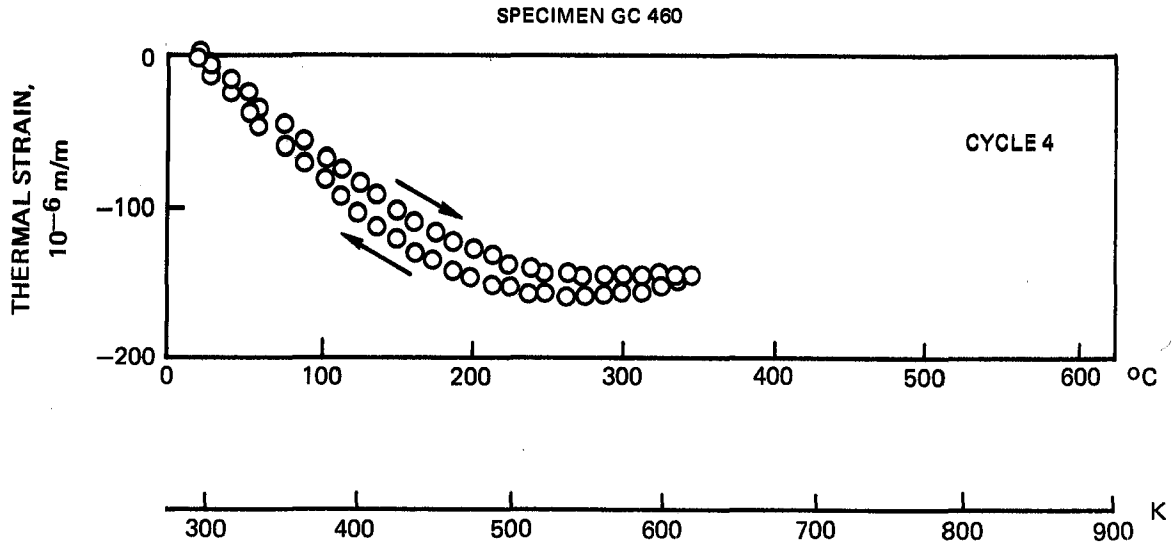

Fig. 62 0° Thermal Expansion of 0/90 Reinforced GY70/7740 Cycle 4

79-04-144-10

IV. SUMMARY AND CONCLUSIONS

In this most recent phase of the program a wide variety of unique aspects of graphite fiber reinforced glass have been demonstrated. It has been shown that shaped articles can be fabricated by two different procedures. The first is a simple extension of the previously developed hot press consolidation process while the second makes use of the exceptional thermoplastic nature of the glass matrix which permits it to be softened and shaped by reheating. Thus, as demonstrated by the fabrication of simple hat sections, low pressures and short time durations can be used to reshape preconsolidated composite plates. In addition to this ability to form shaped parts, it was also shown that sections of composite material can be joined together using glass solder and metal brazing techniques.

The use of chopped graphite fibers was demonstrated to be an effective way of achieving multidirectional composite reinforcement. The fibers, obtained in a two dimensional random array, were combined with glass powder and then consolidated into composites which contained approximately 30-45 v/o reinforcement. Average three point flexural strengths of as high as 315 MPa were obtained by this procedure when Celion 6000 fiber was used as the reinforcement while strengths of only 54 MPa resulted when a low cost pitch based fiber was used.

An extensive characterization of composite mechanical properties demonstrated that excellent performance can be achieved. These findings include the following.

- The selection of graphite fiber type determined the values of strength (flexural and tensile) and elastic modulus achieved. A high elastic modulus pitch based graphite fiber provided the highest level of composite tensile elastic modulus, 334 GPa, while an HTS graphite fiber reinforcement achieved the highest value of tensile strength, 614 MPa.

- Composite resistance to mechanical fatigue was found to be excellent for both unidirectional and 0/90 cross ply material. Composite 10^6 run out stresses were found to reach levels within the range of composite monotonic strength, and residual strength after fatigue was found to be equivalent to original "as fabricated" composite strength.

- Composite creep and stress rupture properties were found to be limited by the oxidative stability of the graphite fibers. At 703 K composites withstood stresses equivalent to their as fabricated flexural strength for over 200 hrs without rupture or degradation while at 813 K fiber oxidation limited composite life.

- Composite resistance to thermal cycles between 300-703 K and 300-813 K was also found to be limited only by fiber oxidation.

The thermal expansion characteristics of several different fiber-matrix combinations were measured over the temperature range of 300 K - 860 K and it was shown that exceptionally low values of axial and transverse thermal expansion coefficient (α) can be achieved. These low values are due to the low α values of the fiber and matrix materials themselves which also contribute to the very small amount of hysteresis observed on repeated thermal cycling. A unique form of axial composite thermal expansion was also noted to take place wherein, at room temperature, the initial composite thermal deformation is contraction upon heat up which is then followed by a gradual change to expansion at some elevated temperature. The magnitude and temperature range over which these effects take place were found to depend on the type of graphite fiber used; however, in each case this type of thermal contraction-expansion cycle was found to be exceptionally stable over repeated temperature excursions. It was thus possible to find both a temperature and a temperature range over which the composite thermal expansion coefficient was precisely zero.

When combined with the fact that the density of graphite fiber reinforced glass matrix composites is approximately 2000 kg/m^3, the above characteristics indicate that this system offers a unique combination of high specific mechanical properties and environmental stability not achievable in either resin or metal matrix systems.

REFERENCES

1. J. F. Bacon, K. M. Prewo: "Research on Graphite Reinforced Glass Matrix Composites", NASA Contract Report 145245, June 1977.

2. J. F. Bacon, K. M. Prewo and E. R. Thompson: "Research on Graphite Reinforced Glass Matrix Composites", NASA Contract Report 158946, June 1978.

3. K. M. Prewo, J. F. Bacon: "Glass Matrix Composites-I - Graphite Fiber Reinforced Glass", Proc. of the 1978 International Conference on Composite Materials, AIME, 1978.

4. K. M. Prewo, J. F. Bacon, D. L. Dicus: "Graphite Fiber Reinforced Glass Matrix Composites", SAMPE Quarterly, Vol. 10, No. 4, July 1979.

5. "Satellite Applications of Metal Matrix Composites", Interim Tech. Report LMSC-DG21612, May 1978, Contract F33615-77-C-5190.

1. Report No.	2. Government Accession No.	3. Recipient's Catalog No.
NASA CR-159312		

4. Title and Subtitle	5. Report Date
RESEARCH ON GRAPHITE REINFORCED GLASS MATRIX COMPOSITES	February 1980
	6. Performing Organization Code

7. Author(s)	8. Performing Organization Report No.
K. M. Prewo and E. R. Thompson	R80-912545-49
	10. Work Unit No.

9. Performing Organization Name and Address	11. Contract or Grant No.
United Technologies Research Center East Hartford, CT 06108	NAS1-14346
	13. Type of Report and Period Covered Interim Report June 1978 - February 1980

12. Sponsoring Agency Name and Address	14. Sponsoring Agency Code
National Aeronautics & Space Administration Washington, DC 20546	

15. Supplementary Notes

Project Manager, Dennis Dicus, NASA Langley Research Center, Hampton, VA 23665

16. Abstract The data compiled in this report demonstrate that graphite fiber reinforced glass matrix composites can exhibit high levels of mechanical performance in tension, flexure, fatigue, and creep loading situations. At test temperatures of up to 813 K it was found that the major limiting factor was the oxidative instability of the reinforcing graphite fibers. Particular points to note include the following:

- A wide variety of graphite fibers were found to be compatible with the glass matrix composite fabrication process.
- Choice of fiber, to a large extent, controlled resultant composite performance. Both continuous and chopped fibers provided effective reinforcement.
- Composite fatigue performance was found to be excellent at both 300 K and 703 K.
- Composite creep and stress rupture at temperatures of up to 813 K was limited by the oxidative stability of the fiber.
- Exceptionally low values of composite thermal expansion coefficient were attributable to the dimensional stability of both matrix and fiber.
- Component fabricability was demonstrated through the hot pressing of hot sections and brazing using glass and metal joining phases.

17. Key Words (Suggested by Author(s))		18. Distribution Statement
Composite	Ceramic Matrix Composite	Unclassified - unlimited
Fiber Reinforced Glass	Graphite-Glass	
Glass Matrix Composite	Graphite Fiber Reinforced	

19. Security Classif. (of this report)	20. Security Classif. (of this page)	21. No. of Pages	22. Price*
Unclassified	Unclassified	84	

* For sale by the National Technical Information Service, Springfield, Virginia 22161